

University of Windsor

Scholarship at UWindor

Electronic Theses and Dissertations

Theses, Dissertations, and Major Papers

2008

Modeling stretched methane-air flame growth

Pegah Ghanbari-Bavarsad
University of Windsor

Follow this and additional works at: <https://scholar.uwindsor.ca/etd>



Part of the [Mechanical Engineering Commons](#)

Recommended Citation

Ghanbari-Bavarsad, Pegah, "Modeling stretched methane-air flame growth" (2008). *Electronic Theses and Dissertations*. 5341.

<https://scholar.uwindsor.ca/etd/5341>

This online database contains the full-text of PhD dissertations and Masters' theses of University of Windsor students from 1954 forward. These documents are made available for personal study and research purposes only, in accordance with the Canadian Copyright Act and the Creative Commons license—CC BY-NC-ND (Attribution, Non-Commercial, No Derivative Works). Under this license, works must always be attributed to the copyright holder (original author), cannot be used for any commercial purposes, and may not be altered. Any other use would require the permission of the copyright holder. Students may inquire about withdrawing their dissertation and/or thesis from this database. For additional inquiries, please contact the repository administrator via email (scholarship@uwindsor.ca) or by telephone at 519-253-3000ext. 3208.

MODELING STRETCHED METHANE-AIR FLAME GROWTH

by

Pegah Ghanbari-Bavarsad

A Thesis

Submitted to the Faculty of Graduate Studies
through Mechanical, Automotive and Materials Engineering
in Partial Fulfillment of the Requirements for
the Degree of Master of Applied Science at the
University of Windsor

Windsor, Ontario, Canada

2008

© 2008 Pegah Ghanbari-Bavarsad



Library and
Archives Canada

Bibliothèque et
Archives Canada

Published Heritage
Branch

Direction du
Patrimoine de l'édition

395 Wellington Street
Ottawa ON K1A 0N4
Canada

395, rue Wellington
Ottawa ON K1A 0N4
Canada

Your file Votre référence
ISBN: 978-0-494-47012-1
Our file Notre référence
ISBN: 978-0-494-47012-1

NOTICE:

The author has granted a non-exclusive license allowing Library and Archives Canada to reproduce, publish, archive, preserve, conserve, communicate to the public by telecommunication or on the Internet, loan, distribute and sell theses worldwide, for commercial or non-commercial purposes, in microform, paper, electronic and/or any other formats.

The author retains copyright ownership and moral rights in this thesis. Neither the thesis nor substantial extracts from it may be printed or otherwise reproduced without the author's permission.

AVIS:

L'auteur a accordé une licence non exclusive permettant à la Bibliothèque et Archives Canada de reproduire, publier, archiver, sauvegarder, conserver, transmettre au public par télécommunication ou par l'Internet, prêter, distribuer et vendre des thèses partout dans le monde, à des fins commerciales ou autres, sur support microforme, papier, électronique et/ou autres formats.

L'auteur conserve la propriété du droit d'auteur et des droits moraux qui protègent cette thèse. Ni la thèse ni des extraits substantiels de celle-ci ne doivent être imprimés ou autrement reproduits sans son autorisation.

In compliance with the Canadian Privacy Act some supporting forms may have been removed from this thesis.

Conformément à la loi canadienne sur la protection de la vie privée, quelques formulaires secondaires ont été enlevés de cette thèse.

While these forms may be included in the document page count, their removal does not represent any loss of content from the thesis.

Bien que ces formulaires aient inclus dans la pagination, il n'y aura aucun contenu manquant.

■ ■ ■
Canada

Author's Declaration of Originality

I hereby certify that I am the sole author of this thesis and that no part of this thesis has been published or submitted for publication.

I certify that, to the best of my knowledge, my thesis does not infringe upon anyone's copyright nor violate any proprietary rights and that any ideas, techniques, quotations, or any other material from the work of other people included in my thesis, published or otherwise, are fully acknowledged in accordance with the standard referencing practices. Furthermore, to the extent that I have included copyrighted material that surpasses the bounds of fair dealing within the meaning of the Canada Copyright Act, I certify that I have obtained a written permission from the copyright owner(s) to include such material(s) in my thesis and have included copies of such copyright clearances to my appendix.

I declare that this is a true copy of my thesis, including any final revisions, as approved by my thesis committee and the Graduate Studies office, and that this thesis has not been submitted for a higher degree to any other University or Institution.

Abstract:

In this study, a one-dimensional, spherical, adiabatic, laminar, premixed flame is considered. Reactant conditions include methane-air mixture having fuel/air equivalence ratios of 0.6 to 1.4, pressures of 1 to 3 atm and temperatures of 300 to 500 K. The underlying unstretched laminar flame characteristics including the unstretched laminar flame speed, adiabatic flame temperature and gas density ratio are calculated using CHEMKIN 4.1 with GRI mechanism 3.0, dealing with 325 reactions and 53 species. Stretched flame speeds are then deduced by invoking Markstein theory. These results are extended to investigate the effect of confinement on flame propagation inside a closed chamber. For the methane-air mixture conditions considered, Stretch always decreases the flame speed, and the largest reduction occurs when the flame is the smallest. Increasing initial unburned gas temperature lessens the flame speed reduction due to stretch, while moderate changes in pressure do not influence the flame speed–flame stretch relationship in any significant manner.

Dedicated to

My Parents

ACKNOWLEDGEMENTS

Firstly, I would like to express my thanks to my parents for their enormous amount of faith, encouragement and support all the time.

I am deeply grateful to my supervisor, Dr. D. S-K Ting for not only giving me this opportunity but also for his generous help, valuable advice and encouragement in all the time of research and writing of this thesis.

I would like to express my sincere thanks to my thesis committee members, Dr N. Zamani, Dr. S. Cheng and Dr. A. Sobiesiak.

TABLE OF CONTENTS

AUTHOR'S DECLARATION OF ORIGINALITY	iii
ABSTRACT	iv
DEDICATION	v
ACKNOWLEDGEMENTS	vi
LIST OF TABLES	x
LIST OF FIGURES	xi
NOMENCLATURE	xv
CHAPTER	
1. INTRODUCTION	1
1.1 Motivation	1
1.2 Objective	2
1.3 Scope of Study	2
1.4 Contribution	2
2. BACKGROUND	3
2.1. Premixed Laminar Flame Structure	3
2.2. Flame Stretch	6
2.3. Planar Premixed Laminar Flame	7
2.3.1. Flame Propagation Rate	7
2.3.2. Unstretched Laminar Flame Speed	8

2.4. Spherical Premixed Laminar Flame in Open Atmosphere	9
2.4.1. Flame Growth Rate	9
2.4.2. Stretched Laminar Flame Speed	9
2.5. Spherical Premixed Laminar Flame in Confinement	10
3. LITERATURE REVIEW	11
3.1. Fundamental Deductions on Flame Stretch	11
3.2. Stretched Flame Speed Modeling	13
3.2. The State of Existing Stretched Flame Research	16
4. MODELING DETAILS	17
4.1. Planar Unstretched Laminar Flame Speed Calculation	17
4.2. Stretched Freely Propagating Spherical Laminar Flame Growth	19
4.3. Stretched Premixed Flame Model in a Confined Chamber	24
5. RESULTS AND DISCUSSION	29
5.1. Unstretched Planar Adiabatic Premixed Methane-Air Flame	29
5.1.1. Flame Temperature Profile	29
5.1.2. Effect of Pressure and Temperature on the Adiabatic Flame Temperature	30
5.1.3. Unstretched Flame Speed	32
5.1.4. Unburned/ Burned Gas Density Ratio	36
5.1.5. Zeldovich Number	38
5.1.6. Effective Lewis Number	40

5.1.7. Markstein Length	41
5.1.8. Markstein Number	43
5.1.9. Stretched Flame Speed	44
5.2. Confined Flame Results	51
5.2.1. Effect of Initial Mixture Temperature on Flame Propagation Inside the Chamber	51
5.2.2. Effect of Chamber Pressure on Flame Propagation inside the Chamber	56
5.2.3. Flame Speed for Different Mixture Conditions	57
5.3. Comparison of the Simulation Results with the Experiment	64
6. CONCLUSIONS AND RECOMMENDATIONS	68
6.1 Conclusions	68
6.2 Recommendations	69
7. REFERENCES	70
APPENDIX A: Stretched Freely Propagating Flame Calculations	77
APPENDIX B: Thermodynamic Equilibrium Flame Growth Model in Confinement	81
VITA AUCTORIS	89

LIST OF TABLES

Table 4.1: Thermal diffusivities and effective Lewis numbers of fuel and oxidizer at different unburned gas temperatures and pressures [Mills, 1995]	22
Table 4.2: Pressure and temperature exponents for different fuel air mixtures	25
Table 5.1: Pressure and temperature exponents for different methane-air mixtures	36
Table 5.2: Comparison of Markstein lengths at $P=1$ atm, $T_u=300$ K with the literature	43

LIST OF FIGURES

Figure 2.1:	Schematic diagram of the temperature variation across a typical laminar flame	4
Figure 2.2:	Schematic of flame thickness	5
Figure 2.3:	Flame under strain-imposed stretch	6
Figure 2.4:	Flame under curvature imposed stretch	7
Figure 2.5:	One-dimensional planar premixed laminar flame propagation	8
Figure 2.6:	One-dimensional, spherical laminar flame growth in open atmosphere	9
Figure 2.7:	One-dimensional spherical laminar flame growth in a confined chamber	10
Figure 4.1:	Flow chart showing the structure of the CHEMKIN package	19
Figure 4.2:	The structure of the stretched freely propagating flame code	24
Figure 4.3:	Confined stretched flame calculation flow chart	28
Figure 5.1:	Temperature profiles of unstretched laminar planar flames. Error bars: van Maaren et al [1994]	30
Figure 5.2:	Effect of unburned gas temperature on adiabatic flame temperature at P=1 atm	31
Figure 5.3:	Effect of pressure on adiabatic flame temperature at $T_u=300$ K	31
Figure 5.4:	Comparison of the simulated adiabatic flame temperatures of different methane-air mixtures at $T_u=300$ K, P=1atm with literature	32
Figure 5.5:	Effect of unburned mixture temperature on unstretched flame speed for different methane-air mixtures at P=1 atm	33
Figure 5.6:	Effect of pressure on unstretched flame speed for different methane-air mixtures at $T_u=300$ K	34

Figure 5.7:	Comparison of the unstretched flame speed results with literature	35
Figure 5.8:	The effects of temperature and pressure on unstretched flame speed for stoichiometric methane-air mixture	36
Figure 5.9:	Variation of unburned/ burned gas density ratio with temperature at P=1 atm	37
Figure 5.10:	Variation of unburned/ burned gas density ratio with pressure at $T_u=300$ K	38
Figure 5.11:	Effect of temperature on Zeldovich number for different equivalence ratios at P=1 atm	39
Figure 5.12:	Effect of temperature on Zeldovich number for different equivalence ratios at $T_u=300$ K	39
Figure 5.13:	Effect of temperature on Lewis number for different equivalence ratios at P=1 atm	40
Figure 5.14:	Effect of pressure on Lewis number for different equivalence ratios at $T_u=300$ K	41
Figure 5.15:	Effect of unburned gas temperature on Markstein lengths of different methane-air mixtures at P=1 atm	42
Figure 5.16:	Effect of temperature on Markstein numbers of different methane-air mixtures at P=1 atm	44
Figure 5.17:	Effect of pressure on Markstein numbers of different methane-air mixtures at $T_u=300$ K	44
Figure 5.18:	Stretched flame speed for different methane-air mixtures at $T_u=300$ K and P=1 atm	45

Figure 5.19:	Stretched/Unstretched flame speed as a function of flame radius for different methane-air mixtures at $T_u=300$ K and $P=1$ atm	46
Figure 5.20:	Stretched flame speed as a function of stretch rate for different methane-air mixtures at $T_u=300$ K and $P=1$ atm	47
Figure 5.21:	Stretch rate as a function of radius for different methane-air mixtures at $T_u=300$ K and $P=1$ atm	48
Figure 5.22:	Normalized flame speed versus Karlovitz number for different mixture compositions at $T_u=300$ K and $P=1$ atm	49
Figure 5.23:	Normalized flame speed versus flame radius at different pressures for stoichiometric methane-air mixture at $T_u=300$ K	50
Figure 5.24:	Normalized flame speed versus flame radius at different temperatures for stoichiometric methane-air mixture at $P=1$ atm	51
Figure 5.25:	Effect of initial mixture temperature on laminar stretched flame speed of the stoichiometric mixture in a confined chamber at $P_0=1$ atm	52
Figure 5.26:	Effect of initial mixture temperature of the stoichiometric mixture on flame stretch in a confined chamber at $P_0=1$ atm	53
Figure 5.27:	Effect of temperature exponent on flame speed in a confined chamber	54
Figure 5.28(a):	Equilibrium temperature of the stoichiometric mixture inside the chamber at $T_0=300$ K and $P=1$ atm	55
Figure 5.28(b):	Equilibrium pressure of the stoichiometric mixture inside the chamber at $T_0=300$ K, $P_0=1$ atm	55
Figure 5.29:	Effect of chamber pressure on laminar stretched flame speed of the stoichiometric mixture at $T_0=300$ K	56

Figure 5.30:	Effect of chamber pressure on flame stretch of the stoichiometric mixture at $T_0=300$ K	57
Figure 5.31:	Flame speed results with and without stretch for the stoichiometric mixture at $T_0=300$ K, $P_0=1$ atm	58
Figure 5.32:	Normalized flame speed versus flame radius for different methane-air mixtures at $T_0=300$ K, $P_0=1$ atm	59
Figure 5.33:	Stretch rate for different methane-air mixtures at $T_0=300$ K, $P_0=1$ atm	60
Figure 5.34:	Effect of stretch on flame speed for different mixture stoichiometries at $T_0=300$ K, $P_0=1$ atm	61
Figure 5.35:	Stretched/Unstretched flame speed versus stretch rate for different mixture stoichiometries at $T_0=300$ K, $P_0=1$ atm	62
Figure 5.36:	Flame radius versus time for different mixture stoichiometries at $T_0=300$ K, $P_0=1$ atm	63
Figure 5.37:	Effect of time step changes on the simulation results of flame propagation inside the chamber at $T_0=300$ K, $P_0=1$ atm	64
Figure 5.38:	Comparison of temperature profile inside the chamber with experiment for the stoichiometric mixture	65
Figure 5.39:	Comparison of the pressure profile inside the chamber with experiment for the stoichiometric mixture	66
Figure 5.40:	Comparison of stretched flame speed inside the chamber with experiment for the stoichiometric mixture	67

NOMENCLATURE

A	Flame surface area, [m ²]
C_p	Specific heat capacity at constant temperature
D_{CH_4}	Methane mass diffusivity, [m ² /s]
D_{O_2}	Oxidizer mass diffusivity, [m ² /s]
D_{th}	Thermal diffusivity of the mixture, [m ² /s]
dM_b	Mass of the burning element, [kg]
dr_u	Thickness of unburned gas mixture consumed over time dt, [m]
dt	Time step, [s]
dx_u	Thickness of unburned gas mixture consumed over time dt, [m]
dV_{bg}	Volume of the burning element, [m ³]
E	Overall activation energy, [kJ/ kmol]
Γ	Specific heat ratio
Ka	Karlovitz number
L	Markstein length, [mm]
Le_D	Lewis number of the deficient reactant
Le_E	Lewis number of the excess reactant
Le_{eff}	Effective Lewis number of the mixture
$Le_{eff, fuel}$	Effective Lewis number of the fuel
$Le_{eff, oxidizer}$	Effective Lewis number of the oxidizer
l_F	preheat zone thickness, [mm]
Ma	Markstein number
M_b	Burned mass, [kg]
mol_P	Moles of products/ mole of fuel
mol_R	Moles of reactants/ mole of fuel
P	Pressure of the mixture, [atm]

P_E	Pressure at thermodynamic equilibrium, [Pa]
P_{exp}	Pressure exponent
P_i	Initial Pressure, [Pa]
P_0	Reference pressure of the mixture, 1 atm
P_u	Pressure of the unburned mixture, [atm]
r	Flame radius, [m]
R_{bnow}	Radius of the burning element, [m]
R_0	Universal gas constant, 8.314 kJ/ kmol·K
R_{spark}	Spark radius, [m]
S_f	Flame propagation speed, [m/s]
\tilde{S}_L	Stretched laminar flame speed, [m/s]
$S_{L\infty}$	Unstretched laminar flame speed, [m/s]
S_{L0}	Laminar flame speed at reference condition, [m/s]
$\text{Sum}V$	Sum of the volumes, [m ³]
t	Time, [s]
T_a	Adiabatic flame temperature, [K]
T_b	Temperature of the burned mixture, [K]
T_{exp}	Temperature exponent
T_i	Intermediate temperature (Temperature at the inflection point), [K]
T_0	Initial temperature of the unburned mixture, [K]
T_r	Temperature at thermodynamic equilibrium, [K]
T_u	Temperature of the unburned mixture, [K]
V_{ba}	Volume of the burned side after the element burns, [m ³]
V_{bb}	Volume of the burned side before the element burns, [m ³]
V_E	Volume element at equilibrium, [m ³]
V_{tot}	Total volume of the chamber, [m ³]
V_{ua}	Volume of the unburned side after the element burns, [m ³]
V_{ub}	Volume of the unburned side before the element burns, [m ³]

W_k	Molecular weight of the k^{th} species, [kg/ kmol]
Y_k	Mass fraction of the k^{th} species

Greek Symbols

α	Thermal Diffusivity, [m^2/s]
β	Zeldovich number
δ	Characteristics flame thickness, [mm]
ϕ	Excess to deficient reactant mole ratio
φ	Fuel/ air equivalence ratio
κ	Stretch rate, [s^{-1}]
λ	Thermal conductivity of the mixture, [W/m·K]
ν_k	Stoichiometric coefficient of the k^{th} species
ρ_b	Density of burned gas mixture, [kg/m^3]
ρ_u	Density of unburned gas mixture, [kg/m^3]
σ	Thermal expansion coefficient (unburned/ burned gas density ratio)

Subscripts:

a:	Adiabatic
b:	Burned
u:	Unburned

CHAPTER 1

INTRODUCTION

The subject of this thesis is the modeling of spherical premixed methane-air flame propagating freely and in a confined chamber. The focus is on investigating the effect of initial conditions on flame characteristics, especially its response under varying amount of stretch. The following sections provide motivation, objectives and scope of this study.

1.1. Motivation

The spark ignition engine is a prime example of the use of premixed combustion. In a spark ignition engine, power is obtained from the chemical energy of the fuel via combustion. During the energy conversion process, the spark kernel propagates through the turbulent mixture in a complicated manner. The propagation process influences the efficiency of energy conversion, engine performance and pollutant formation. Accurate predictions of transient flame development and propagation are useful for relating alterations in SI engine design and operating variables to changes in engine performance [Heywood, 1988]. There have been many attempts to accurately model and/or predict this turbulent flame propagation, which detects the performance of the engine like burning rate and cycle to cycle variations to a large extent.

By and large, the premixed turbulent flame growth is in the 'laminar flamelet' regime in which the turbulent flame can be perceived as a sum of laminar flame elements of different sizes undergoing varying degrees of corrugation. As such, it is possible to model turbulent flame growth in terms of elements of laminar flamelets. It appears that a simple and fundamentally viable approach would be via the stretched flame modeling, which aims at accurately accounting for the stretching effect on the local laminar flame speed.

1.2. Objectives

The objective of this research is to model flame growth in a confinement and study the effect of stretch on flame propagation. Investigating the effects of initial mixture conditions on flame speed and other dependent parameters is a secondary objective.

1.3. Scope of Study

To accomplish our objectives, a premixed methane-air flame growth model is proposed. Fuel-air equivalence ratio is varied from 0.6 to 1.4 (with increment of 0.2) taking care not to exceed the lower and upper flammability limits of methane in standard air, which are 0.53 and 1.58, respectively [Borman and Ragland, 1998], while initial temperature and pressure are altered from 300 to 500 K and 1 to 3 atm, respectively.

First, a freely expanding laminar flame growth is modeled. To accomplish this, a numerical simulation is performed to obtain the underlying unstretched flame characteristics such as unstretched flame speed, flame thickness, Markstein length, Markstein number and gas density ratio via some chemical kinetics and thermo chemical relations. The software package used is CHEMKIN 4.1 [Kee et al., 2006] with GRI 3.0 kinetic mechanisms [Smith et al., 2004]. Based on CHEMKIN output data, the stretched flame speed is calculated via analytical expressions with the MATLAB programming language. The freely propagating flame is further extended to flame propagation model inside a confinement and the effect of different parameters are discussed systematically.

1.4. Contribution

Emami et al. [2005] and De et al. [2006] are two preliminary attempts in modeling laminar freely propagating flame. To the best of the author's knowledge, the method used for confined flame modeling based on analytical thermodynamic relations has not been attempted. It is a straightforward method and the results are found to be in agreement with the literature. The respective roles played by pressure and temperature are unveiled. The flame stretch is emphasized and the effect of stretch rate on different flame characteristics is studied in detail.

CHAPTER 2

BACKGROUND

This chapter provides basic background and definitions of premixed laminar flame. A premixed flame can be defined knowing the inner flame structure, the kinematics of the flame and flow, the stretching of the flame and the flame thickness. Here, the inner structure of a premixed flame is explained followed by the flame stretch concept and definitions of planar and spherical flame speed and propagation rates.

2.1. Premixed Laminar Flame Structure

The structure of the flame has been studied in great detail by some researchers such as Fristrom and Westerberg [1965] who suggested the flame to be consisted of four distinct regions. 1) Unburned; 2) Preheat; 3) Reaction; 4) Burned gas. These zones are shown in Figure 2.1. As the mixture approaches the flame front, it is heated by conduction and radiation from the flame zone upstream. Chemical reaction and heat release are negligible at this stage. The preheat zone can be considered to be chemically inert. Once temperatures are hot enough to sustain combustion, chemical reaction takes place in the reaction zone.

The reaction layer can be divided into the inner and oxidation layer. For hydrocarbon fuels, fuel is converted into hydrogen and carbon monoxide in the inner layer. The oxidation layer is located downstream of the reaction layer. In this part the oxidation of hydrogen and carbon monoxide to water and carbon dioxide takes place.

The gases emerging from the reaction zone enter the burned gas zone where their concentrations and temperatures approach the equilibrium values asymptotically. The flame propagation process influences the efficiency of energy conversion and pollutant formation. The nature and/or the rate of propagation depend on many factors including mixture composition, mixture state (pressure and temperature), fluid motion in the combustion chamber and combustion chamber shape [Gatowski et al., 1984].

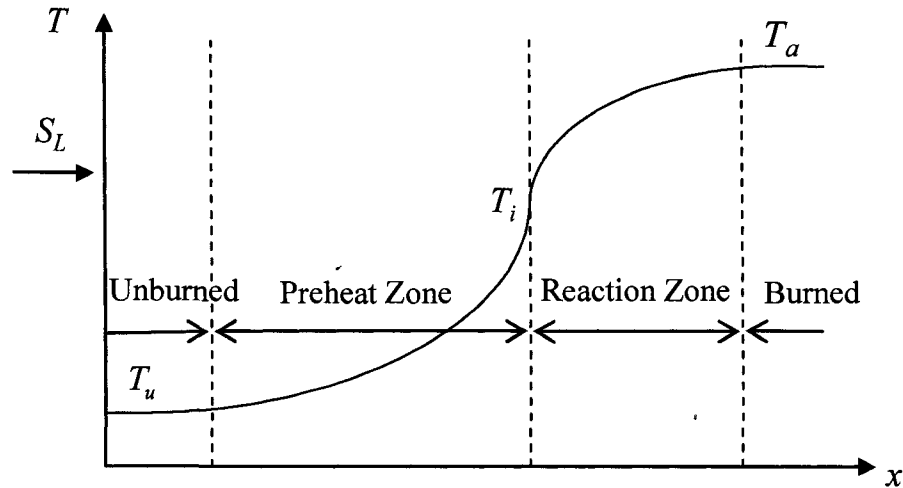


Figure 2.1: Schematic diagram of the temperature variation across a typical laminar flame

An important length scale in flame structure is the flame thickness. Different approaches exist in the literature to deduce this flame thickness. One approach relies on using the steepest tangent to the flame profile to find the interval distance of the intersection of that line with the horizontal axis between unburned and burned temperatures. Another approach is based on the definition of the preheat zone thickness in estimating the flame thickness [Gottgens et al., 1992].

In the former method, deriving temperature profile from CHEMKIN, the flame thickness is defined as the interval distance of the tangent passing through the inflection point which spans the temperature profile between T_u and T_a . This geometrical definition, according to Gottgens et al.'s report [1992], may lack a physical meaning. The second approach is based on the Gottgens et al.'s asymptotic structure of premixed flame which has been related to the geometrical definition described below.

With the assumption of an infinitely thin inner layer, two layers of finite thickness exist, the preheat zone and the oxidation layer. The temperature increases exponentially in the preheat zone up to the T_i (temperature at the inflection point) and then relaxes towards T_a (the adiabatic temperature of the burned gases) in the oxidation layer. The curvature of the temperature profile changes as we move from the preheat zone to the oxidation layer. The location of T_i would be the location of the steepest tangent, that is, the inflection point of the temperature profile [Gottgens et al., 1992]. The segmented

distance of the tangent line through the inflection point from T_i to T_u , is Δx_1 as is shown in Figure 2.2.

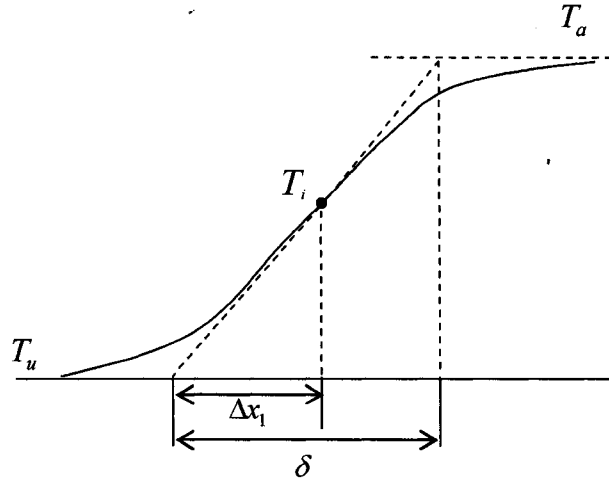


Figure 2.2: Schematic of flame thickness

If the preheat zone is considered to be chemically inert, Δx_1 would be equal to the preheat zone thickness (l_F). Gottgens et al. [1992] found the mean values of $\frac{\Delta x_1}{l_F}$ to be approximately 0.994 for methane, with a standard deviation of 0.118. In this thesis l_F is taken to be equal to Δx_1 . The entire flame thickness δ , can be computed from l_F using the following relation [Gottgens et al., 1992]:

$$\delta = \frac{T_a - T_u}{T_i - T_u} c \cdot l_F \quad (2.1)$$

Another definition for δ , which has been used in this investigation, considers the flame thickness to be a diffusive length scale:

$$\delta = 2 \frac{\alpha}{S_{L\infty}} = 2 \frac{\lambda}{S_{L\infty}} \quad (2.2)$$

where α is thermal diffusivity and $S_{L\infty}$ is the unstretched flame speed. According to Turns [1996], an appropriate mean temperature to define α is the average over the entire flame thickness, since conduction occurs over this interval.

2.2. Flame Stretch

In practical combustion systems, when a combustible gas mixture is ignited, the flame front always undergoes some amount of stretch. Stretch can result from strain and/or change of flame curvature and it can significantly affect the behavior of the premixed flame. Even in an idealized laminar flame, the flame is under the influence of some amount of stretch. Stretch rate κ , for a point on the flame surface, is defined as the time rate of the logarithmic area of an infinitesimal element, dA , surrounding that point, [Law, 1989]:

$$\kappa = \frac{d}{dt}(\ln A) = \frac{1}{A} \frac{dA}{dt} \quad (2.3)$$

Figure 2.3 depicts a premixed flame that is only subject to strain imposed stretch. Fuel and oxidizer mixture react ahead of the wall. Although the radius of curvature in this case is infinity, the imposed strain introduces stretch on the flame surface.

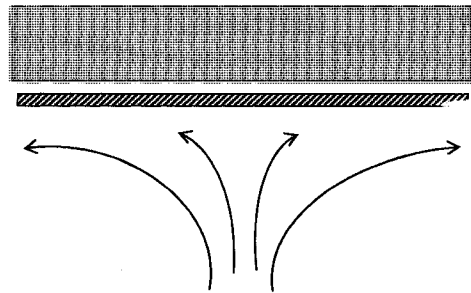


Figure 2.3: Flame under strain-imposed stretch

Figure 2.4 illustrates a flame which is propagating through a converging channel. States of one particular element on the flame front at two instants are shown as the initial and final positions. Although the elemental area remains approximately fixed, there is however appreciable changes in the flame curvature which imposes stretch on the flame surface.

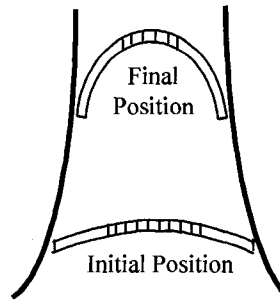


Figure 2.4: Flame under curvature imposed stretch

There is a third kind of stretch which is associated with dilation of the fluid. In this case, the flame is stretched by the effect of volume expansion of the fluid. This dilation imposed stretch is not considered in this study.

In practical systems such as spark ignition engines, the flame is always under some amount of stretch. This stretch effect can alter flame speed significantly and too much stretch may lead to flame extinction.

2.3. Planar Premixed Laminar Flame

A flame can be viewed as a combustion wave which propagates into a flammable mixture. Behind the flame are the hot products of combustion (burned gases). In general, there are two types of flames; premixed and nonpremixed (or diffusion). In a premixed flame, reactants are mixed at the molecular level before any chemical reaction takes place. The spark ignition engine is an example of this kind of flame. On the contrary, in a diffusion flame, the reactants are initially separated and diffuse into each other during the chemical reaction. An example of such a flame is a candle. Furthermore, flames could be identified as laminar and turbulent. The simplest flame is the laminar flame in which the fuel and oxidizer are premixed.

2.3.1. Flame Propagation Rate

Figure 2.5 shows a tube (one end closed and the other end open) with the premixed combustible gas mixture ignited at the closed end. A combustion wave spreads through the gas towards the open end. In the idealized situation, the combustion wave propagates as a one dimensional, planar wave at a constant speed relative to the tube. As is shown in

the figure, at time t , the location of the combustion wave or the flame front is the line before the crossed region. If the flame front propagates a horizontal distance of dx within time dt , the flame growth rate, S_f , is the rate of flame front propagation with respect to the tube:

$$S_f = \frac{dx}{dt} \quad (2.4)$$

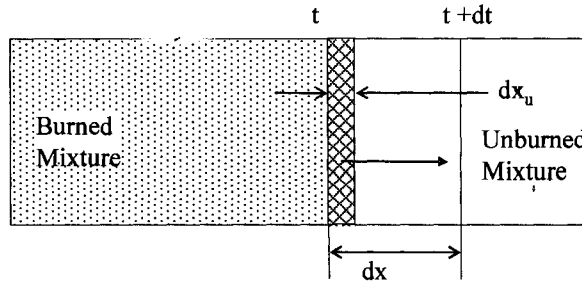


Figure 2.5: One-dimensional planar premixed laminar flame propagation

2.3.2. Unstretched Laminar Flame Speed

Laminar flame speed is the velocity of the combustion wave relative to the unburned gas ahead of the wave in the direction normal to the wave surface. In other words, it is the rate of unburned mixture thickness consumed by the flame. This laminar flame speed is also called laminar burning velocity, normal combustion velocity or flame velocity [Kuo, 2005]. For the idealized planar flame as portrayed in Figure 2.5, the laminar unstretched flame speed is:

$$S_{L\infty} = \frac{dx_u}{dt} \quad (2.5)$$

where dx_u is the amount of unburned gas consumed over time dt and the flame moves to $t+dt$ position due to thermal expansion.

2.4. Spherical Premixed Laminar Flame in Open Atmosphere

For a spark-ignited, radially expanding spherical flame in an open atmosphere, the flame growth rate and laminar flame speed are similar to those of the planar case. These definitions are explained subsequently.

2.4.1. Flame Growth Rate

As shown in Figure 2.6, for a radially expanding spherical flame, the element of unburned mixture is consumed as it burns and consequently, due to thermal expansion of this element, the flame front moves from $r(t)$ to $r(t + dt)$ over time dt . The flame growth rate is the rate of increase in flame radius with respect to the ignition point:

$$S_f = \frac{dr}{dt} \quad (2.6)$$

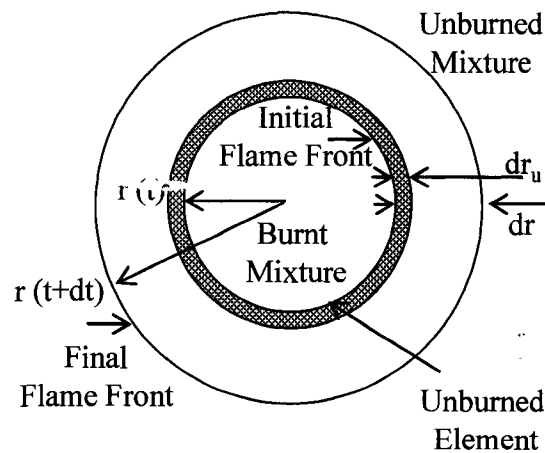


Figure 2.6: One-dimensional, spherical laminar flame growth in open atmosphere

2.4.2. Stretched Laminar Flame Speed

For the open atmospheric case shown in Figure 2.6, the laminar flame speed corresponds to the rate at which the thickness of the unburned mixture is consumed:

$$S_L = \frac{dr_u}{dt} \quad (2.7)$$

According to Strehlow and Savage [1978], the stretched laminar flame speed for this freely expanding case can be deduced from the flame growth rate as:

$$S_L = \left(\frac{\rho_b}{\rho_u}\right) \frac{dr}{dt} \quad (2.8)$$

2.5. Spherical Premixed Laminar Flame in Confinement

In a closed chamber, the confinement limits the free movement of the unburned mixture ahead of the flame. Under this condition the expanding spherical flame causes the combustion chamber pressure to rise. The laminar flame speed may be considered as the concentric shell thickness of the unburned mixture divided by the time taken to consume it. For modeling purpose the concentric shell thickness of the unburned mixture can be deduced as the volume of the unburned mixture divided by the mean flame surface area. The mean flame surface area is the surface area of the sphere of the geometric mean flame radius. The geometric mean flame radius is the root-mean-square of the 'compressed initial flame radius' and the final flame front radius $r(t+dt)$, as illustrated in Figure 2.7.

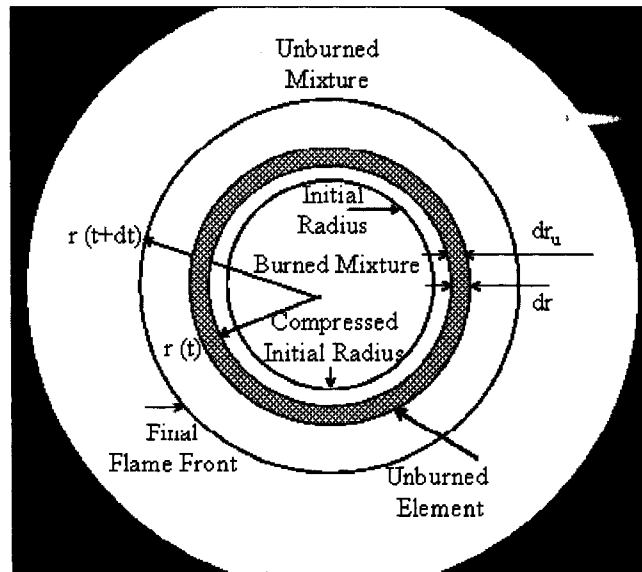


Figure 2.7: One-dimensional spherical laminar flame growth in a confined chamber

CHAPTER 3

Literature Review

This chapter goes through the literature of premixed laminar flame. The focus is mainly on the researches which have been carried out on flame stretch, flame speed and the related underlying parameters.

3.1. Fundamental Deductions on Flame Stretch

The concept of flame stretch was first introduced by Karlovitz et al. [1953]. Theoretical investigation of flame curvature aspect of stretch was established by Markstein [1964]. He postulated a linear relationship between flame speed and curvature-imposed flame stretch. Markstein theory has been found useful by experimentalists whose raw data from flame speed measurements correlate well as per the linear dependence of flame speed and flame stretch.

Since the late 1970s, significant progress has been made on the stretched flame modeling and quantifying its contribution to flame motion. Among others, Tseng et al. [1993], Bradley et al. [1996], Gu et al. [2000] and Davis et al. [2002] have measured the Markstein length to quantify the flame stretch considering the effects of strain and flame curvature, and/or attempt to incorporate these effects in numerical simulations of turbulent premixed flames. Numerous studies have been conducted to investigate stretch effects on flame behavior experimentally [Searby and Quinard, 1990; Deshaies and Cambay, 1990; Dowdy et al., 1991; Kwon et al., 1992] and numerically [Bradley et al., 1996; Lipatnikov, 1996; Muller et al., 1997; Sun et al., 1999].

Searby and Quinard [1990] reported experimental measurements of Markstein number (sensitivity to strain and curvature) of premixed diluted flames of hydrogen, methane, ethylene, and propane. Measurements were made on weakly stretched freely propagating quasi-planar flames. Three different methods of deducing the Markstein number were presented and compared—a direct method in which the stretch and the change in flame speed were measured locally, a global method based on the amplitude of the response of

the flame to a periodic shear flow, and a third method that related Markstein number to the flame speed at which an unperturbed flame spontaneously developed cellular structures. The direct method was found to give the least precise results.

Tseng et al. [1993] studied the effects of positive stretch on the laminar flame speeds of hydrocarbon-air mixtures experimentally using outwardly propagating spherical flames. The test conditions included propane, methane, ethane and ethylene- air flames at various fuel-air equivalence ratios at standard temperature and pressure. The experiments were carried out in a quasi-spherical test chamber. Direct observation of flame radius as a function of time and laminar flame speed as a function of flame radius was done. Their results showed that Markstein numbers varied linearly with fuel-air equivalence ratios over the range of measurements

Davis et al. [2002] proposed a method for measuring Markstein number, relative to both unburned and burned gases in flames with chemical zone of finite width. To accomplish this, numerical simulations of the counterflow flame were conducted. They used numerical simulations to compute Markstein numbers as a function of position through the flame zone. This procedure allowed the accurate estimation of the position of the flame surface. They showed that Markstein number calculated relative to the burned gases was almost identical to Markstein number based on the local mass flux which was measured in the expanding spherical flame. Furthermore, the difference between Markstein numbers measured relative to the burned and unburned gases was identified and quantified through numerical and theoretical comparisons. Temperatures, species mass fractions and density were functions of the axial direction. All calculations were carried out at one atmosphere and 300 K. The measurement was done for flame speed and stretch relative to the unburned and burned gases. They used the Sandia CHEMKIN-II and PREMIX code for the laminar flame simulation.

Frankel et al. [2007] studied the stretch-temperature dependency for flame-flow interaction numerically. This work is an extension of the higher-order models to incorporate effects due to the background flow-field based on a coupled system of second order dynamic equations. In their model, the problem of negative Markstein length instabilities was resolved using a geometrically-invariant extrapolation from the linear

analysis data which incorporated higher order effects. It is a mathematical model considering conventional reaction–diffusion–advection relations.

3.2. Stretched Flame Speed Modeling

Some basic theoretical studies showed that the local flame speed was proportional to the flame stretch rate which was expressed by Markstein number [Clavin and Williams, 1982; Matalon and Matkowsky, 1982; Frankel and Sivashinsky, 1983; Clavin, 1985]. For this reason, finding the value of Markstein number and the relation between flame speed and flame stretch became the objective of numerous experimental investigations [Deshaies and Cambray, 1990; Searby and Quinard, 1990; Dowdy et al., 1991; Kwon et al., 1992; Bechtold and Matalon, 2001].

Bechtold and Matalon [2001] predicted the linear relationship between flame speed and stretch, with both theory and experiment. They also determined the dependence of Markstein number on mixture strength for hydrogen-air, hydrocarbon-air, and alcohol-air mixtures over a range of equivalence ratio.

Dowdy et al. [1991] presented a new approach for expanding flames to determine flame speed and stretch effects in laminar flames. The stretch effect was quantified by deducing the Markstein length. In this analysis, the time variation of the radius of a one-dimensional spherical flame was derived considering the effect of stretch. Three types of flames were modeled: (a) one-dimensional planar; (b) stationary spherical; (c) expanding spherical.

Gottgens et al. [1992] provided accurate analytical expressions for the flame speed and flame thickness of lean hydrogen, methane, ethylene, ethane, acetylene and propane flames. Numerical computations were performed for pressures between 1 and 40 bar, unburned temperatures between 298 K and 800 K (500 K for H₂, C₂H₂ and C₂H₄), and fuel-air equivalence ratios between the lean flammability limit and stoichiometric mixture. A fitting function for the flame speed was derived that contains six parameters. This function predicts the flame speed for each fuel with a standard deviation of less than 7.6% for the entire data set. A definition for the flame thickness was derived for methane, propane, ethylene, and acetylene flames. This definition could readily be linked to the classical definition of the flame thickness that uses the x-interval spanned by the steepest

tangent to the temperature profile between the unburned and adiabatic temperature as the flame thickness.

Bradley et al. [1996] did the computation of spherical laminar flame propagation for a range of equivalence ratios at a pressure of 1 atm and an ambient temperature of 300 K, with flame propagation at constant pressure. Computations were done at three modes of flame propagation: outward propagation, inward propagation and stationary flame. Computed values of flame speeds were compared to Taylor's experimental results. For lean mixtures, the computed values were higher than those measured, while for rich mixtures the computed values were lower than those measured. Stretched values of flame speed were expressed as a function of flame radius and stretch rate. Two flame speeds were computed, one based on the rate of disappearance of unburned gas, the other on the rate of appearance of burned gas. Both cases resulted to the same laminar flame speed when extrapolated to zero stretch rate. The rate of burning was expressed as the rate of consumption of reactants at an initial unburned gas density and radius. They also suggested experimental procedures for the measurement of the stretch-free laminar flame speed and Markstein length.

Muller et al. [1997] numerically calculated flame speeds of n-heptane, iso-octane, methane, ethylene, ethane, acetylene and propane mixtures over a wide range of initial pressure and temperature. Markstein numbers were predicted for all these mixtures.

Gu et al. [2000] employed spherically expanding flames propagating at constant pressure to determine the unstretched laminar flame speed and the effect of flame stretch as quantified by the associated Markstein lengths. Methane-air mixtures at initial temperatures between 300 and 400 K, and pressures between 0.1 and 1.0 MPa were studied at equivalence ratios of 0.8, 1.0, and 1.2 by photographic observation of flames in a spherical vessel. They explored two definitions of stretched flame speed, one based on the disappearance of the unburned mixture, and another based on the appearance of the burned products. Two computer models were utilized to compute the laminar flame speed, one was of a one-dimensional flame using fully detailed kinetics and the other one was of a spherically expanding stretched flame with reduced scheme. The first model computed unstretched laminar flame speed of a freely propagating, one-dimensional, adiabatic premixed flame with Sandia PREMIX code. The CHEMKIN code evaluated the

thermodynamic properties of the reacting mixture and processed the chemical reaction mechanism. The chemical reaction mechanism of GRI-Mech 1.2 with 177 elementary reactions of 32 species was used. The second model was for a spherical flame subjected to changing flame stretch. They measured two different flame speeds, one based on the disappearance of the unburned mixture, and another based on the appearance of the burned products. These flame speeds had different values for a given stretch and different sensitivity to stretch. For both cases the associated Markstein numbers were measured. They also quantified flame stretch effects on the stretched flame speed. Markstein numbers were found to increase with equivalence ratio. They decrease with initial pressure, but only up to 0.5 MPa.

In a recent work by Shoshin and Jarosinski [2007] stretch rates and local flame speeds of lean methane-air flame propagating upward have been measured along the flame front in a standard flammability tube. The experiment was done in a transparent plastic tube of 1.8m length and 50mm inner diameter which was filled with mixture from its top. Velocity distributions were measured in the central plane located in the middle of the tube by PIV method. The measured local flame speed had a local minimum at the flame top where stretch rate was maximum. The extinction of flame was observed at methane concentrations ranging from 5.12% to 5.15%. It was observed to start from the flame tip. They proposed two hypothetical mechanisms for the limiting methane-air flame extinction behavior: first due to the radiation loss from combustion products and second due to depletion of oxygen near the reaction zone. Both mechanisms, individually or cumulatively, could reduce flame speed and lead to extinction at the flame tip. Normal to the flame front, component of the velocity of combustion products decreased faster in regions with higher stretch rate.

A number of studies focused on atmospheric pressures and temperatures for spherical flame with uniform flame stretch [Dowdy et al., 1991; Taylor, 1991; Bradley and Harper, 1994; Aung et al. 1995]. There are, however, much fewer studies considering higher pressures and temperatures which relate to internal combustion engine conditions. Rozenchan et al. [2002] determined stretch-free laminar flame speeds for methane-air flames up to 20 atm and methane-oxygen-helium flames up to 60 atm. Computational

simulation carried out using GRI-MECH 3.0 showed satisfactory agreement with the experimental data up to 20 atm, and moderate deviation for pressure above 40 atm.

3.3. The State of Existing Stretched Flame Research

It is clear from the literature review that rather intensive effort has been invested both in deducing the fundamental effect of stretch on flame speed and in modeling stretched flame growth. The various approaches utilized by different researchers, however, do not lead to agreeable results. In other words, there remains much discrepancy from one study to another. This is even true when it comes to relatively simple, experimental and analytical stretch effect deductions; the results of which are typically expressed in Markstein length or number.

A plausible route to resolving the outstanding issue is to systematically evaluate the underlying parameters which detect the value of Markstein length or number. To do so a simple, one-dimensional, spherically expanding, premixed methane-air flame appears to be an ideal candidate. The chemical kinetics of methane-air flame is among the most studied and verified. Laminar methane-air flame growth is also well documented. Apparently, stretched flame modeling has not been verified for the constrained flame growth in a constant volume combustion chamber, presumably the most commonly employed premixed laminar flame research methodology.

CHAPTER 4

MODELING DETAILS

This chapter describes the analytical and numerical modeling of flame growth. First, the planar unstretched laminar flame model is described. The unstretched laminar premixed flame is modeled using CHEMKIN software package. The results are used to model the stretched, freely propagating, spherical flame growth. This model is further extended to the model of a flame in a confined chamber.

4.1. Planar Unstretched Laminar Flame Speed Calculation

Numerical simulation of planar laminar premixed flame is carried out to predict unstretched flame speed, unburned to burned gas density ratio and adiabatic flame temperature. Corresponding calculations are performed with the one-dimensional laminar premixed flame computer code, CHEMKIN 4.1. Thermo chemical, gas-phase kinetics and transport properties in the default library are replaced with the GRI files [Smith et al., 2004]. GRI mechanism version 3.0, which deals with 325 reactions and 53 species, is a well-accepted comprehensive mechanism for methane-air combustion.

The premixed flame model solves a set of governing differential equations that describe the flame dynamics using implicit finite difference methods, as well as, a combination of time dependent and steady state methods. In this case, there are no heat losses, so the temperatures are computed from the energy equation. Flame speed depends, in part, on the transport of heat and predicts the temperature distribution as an integral part of the flame speed calculation.

To use the CHEMKIN package, three more components are needed: (1) A model input file to describe the system parameters and the combustible mixture properties; (2) A thermo-chemistry input file including thermodynamic properties of each component; (3) A transport properties input file. In Figure 4.1, a block diagram of the structure of CHEMKIN package is shown.

The problem environment is defined by setting initial and boundary conditions. As an initial guess, the mass flow rate of the mixture is set to be $40 \text{ mg/cm}^2\cdot\text{s}$. Initial temperature and pressure for the first simulation are set to be 300 K and 1 atm and are used as an estimation for the higher initial pressures and temperatures. Temperature profile is assumed based on the zone of 1 cm thick and in the subsequent iteration it is modified using the output obtained from the last iteration. Mass flow rate is determined as a part of the solution. Therefore, an additional constraint is required, or alternatively, one degree of freedom must be removed from the problem. This is done by fixing the temperature at one point. This selection must be done in such a way to ensure that the temperature and species gradients nearly vanish at the cold boundary [CHEMKIN collection III, 1998].

.CHEMKIN package is capable of a wide range of thermodynamic properties. These properties are expressed in terms of either polynomial fits or integrals of the specific heats at constant pressure [Kuo, 2005]

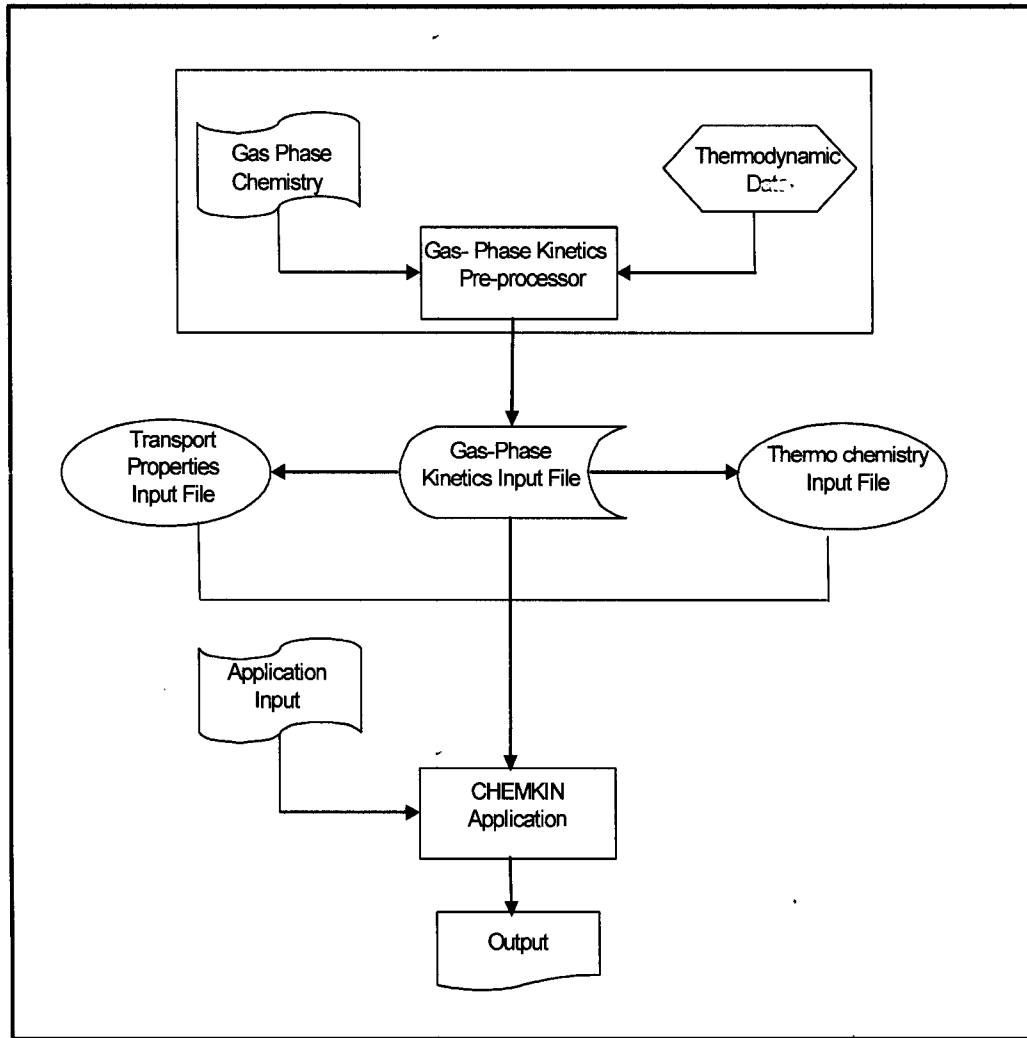


Figure 4.1: Flow chart showing the structure of the CHEMKIN package

4.2. Stretched Freely Propagating Spherical Laminar Flame Growth

The results of the previous section such as unstretched flame speed, adiabatic flame temperature and unburned-burned gas density ratio are implemented in this section to find the stretched flame speed. The influence of flame stretch on the laminar flame speed also depends on the amount of stretch. Sensitivity of flame speed changes to the flame stretch rate is expressed by Markstein length, L . It is usually determined as the slope of the linear relationship between the stretched laminar flame speed, S_L and stretch rate κ , by applying Equation (4.1) to the measured S_L and κ during the explosion.

$$S_L = S_{L\infty} - L\kappa \quad (4.1)$$

where $S_{L\infty}$ is the unstretched flame speed which is determined from gas-phase kinetics. For the case of outwardly propagating spherical flame, flame stretch can be defined as:

$$\kappa = \frac{2}{r} \frac{dr}{dt} \quad (4.2)$$

Substituting Equation (2.7) into (4.2) yields:

$$\kappa = \frac{\rho_u}{\rho_b} \frac{2}{r} S_L = \frac{2}{r} \sigma S_L \quad (4.3)$$

where $\sigma = \frac{\rho_u}{\rho_b}$ is the thermal expansion coefficient or unburned–burnt gas density ratio.

Substituting κ from Equation (4.3) into Equation (4.1) gives:

$$S_L = \frac{S_{L\infty}}{1 + (2\sigma L/r)} \quad (4.4)$$

The next step of getting the stretched flame speed is to find the Markstein length using the Bechtold and Matalon's [2001] analytical expression as illustrated below:

$$L = \delta[\alpha_1 - (\sigma - 1)\gamma_1 / \sigma] \quad (4.5)$$

where constants α , γ_1 and γ_2 are respectively:

$$\alpha_1 = \gamma_1 + \frac{1}{2} \beta (Le_{eff} - 1) \gamma_2 \quad (4.6)$$

$$\gamma_1 = \frac{\sigma}{\sigma - 1} \int_1^\sigma \frac{\lambda(x)}{x} dx \quad (4.7)$$

$$\gamma_2 = \frac{1}{\sigma - 1} \int_1^\sigma \frac{\lambda(x)}{x} \ln\left(\frac{\sigma - 1}{x - 1}\right) dx \quad (4.8)$$

The Zeldovich number β is defined as:

$$\beta = E(T_a - T_u) / R_0 T_a^2 \quad (4.9)$$

where R_0 is the gas constant and $E=47.435$ Kcal/mol is the overall activation energy for methane–air combustion. According to Bechtold and Matalon [2001], E is assumed to be unchanged for all the cases. The effective Lewis number, Le_{eff} , is the weighted average of the Lewis numbers of the reactants:

$$Le_{eff} = 1 + \frac{(Le_E - 1) + (Le_D - 1)A}{1 + A} \quad (4.10)$$

where

$$A = 1 + \beta(\phi - 1) \quad (4.11)$$

Le_E and Le_D are Lewis numbers of excess and deficient reactants, respectively, which are the ratio of thermal diffusivity to mass diffusivity. The diffusivity coefficients are taken to be functions of temperature only.

Equivalence ratio is defined by:

$$\phi = \frac{Y_F / \nu_F W_F}{Y_O / \nu_O W_O} \quad (4.12)$$

Based on the above formula, Matalon and Matkowsky [1982] took the ratio of mass of excess to deficient reactants, ϕ to avoid the need of discussing lean and rich mixtures separately. i.e.:

$$\phi = \frac{Y_E / \nu_E W_E}{Y_D / \nu_D W_D} \quad (4.13)$$

where Y is the mass fraction, ν is the corresponding stoichiometric coefficient and W is the molecular weight. Note that ϕ is always larger than one. It is equal to ϕ for fuel-rich mixtures and $\frac{1}{\phi}$ for fuel lean mixtures. The corresponding diffusivity coefficients can be

found in Table 4.1 [Mills, 1995].

Table 4.1: Thermal diffusivities and effective Lewis numbers of fuel and oxidizer at different unburned gas temperatures and pressures [Mills, 1995]

T_0	P	D_{th}	D_{O_2}	D_{CH_4}	$Le_{eff, fuel}$	$Le_{eff, oxidizer}$
K	atm	cm ² /s	cm ² /s	cm ² /s	D_{th}/D_{CH_4}	D_{th}/D_{O_2}
300	1	0.225	0.188	0.219	1.027	1.197
400	1	0.371	0.325	0.375	0.989	1.142
500	1	0.542	0.477	0.562	0.964	1.136
300	2	0.116	0.097	0.113	1.027	1.196
400	2	0.185	0.162	0.187	0.989	1.142
500	2	0.271	0.239	0.277	0.978	1.134
300	3	0.077	0.064	0.075	1.027	1.203
400	3	0.124	0.109	0.125	0.992	1.138
500	3	0.18	0.159	0.184	0.978	1.132

Bechtold and Matalon [2001] evaluated three most common assumptions, $\lambda = 1$, $\lambda = T^{1/2}$ and $\lambda = T$ to evaluate the integrals in Equations (4.7) and (4.8) and found $\lambda = T^{1/2}$ to agree best with the experimental data. Hence, final expression for γ_1 and γ_2 are:

$$\gamma_1 = \frac{2\sigma}{\sqrt{\sigma} + 1} \quad (4.14)$$

$$\gamma_2 = \frac{4}{\sigma - 1} \left\{ \sqrt{\sigma} - 1 - \ln \frac{1}{2} (\sqrt{\sigma} + 1) \right\} \quad (4.15)$$

Kwon et al. [1992] postulated that Markstein length is proportional to the local characteristic flame thickness, δ as both are representative of the scale of distances over which the diffusion of mass and heat occur in the flame. This assumption leads to the dimensionless Markstein number, Ma , defined as:

$$Ma = \frac{L}{\delta} \quad (4.16)$$

The corresponding parameter defined as a nondimensional stretch factor is the Karlovitz number, Ka , which is the ratio of the residence time for crossing an unstretched

flame ($\frac{\delta}{S_{L\infty}}$) over the characteristic time for flame stretching (κ^{-1}). So it can be defined

as:

$$Ka = \frac{\delta}{S_{L\infty}} \kappa \quad (4.17)$$

Substituting Equations (4.16) and (4.17) into (4.1) results in the following dimensionless relationship between the flame speed and the flame stretch:

$$S_{L\infty} = S_L (1 + Ma \cdot Ka) \quad (4.18)$$

As the flame grows, the flame speed is influenced by the varying stretch rate. So it should be adjusted according to the underlying stretch at each radius. Figure 4.2 shows the structure of the program which is implemented to find the corresponding flame speed at each flame size. Inputting the initial pressure and temperature, the flame speed is found at each flame size. The MATLAB code is given in Appendix A.

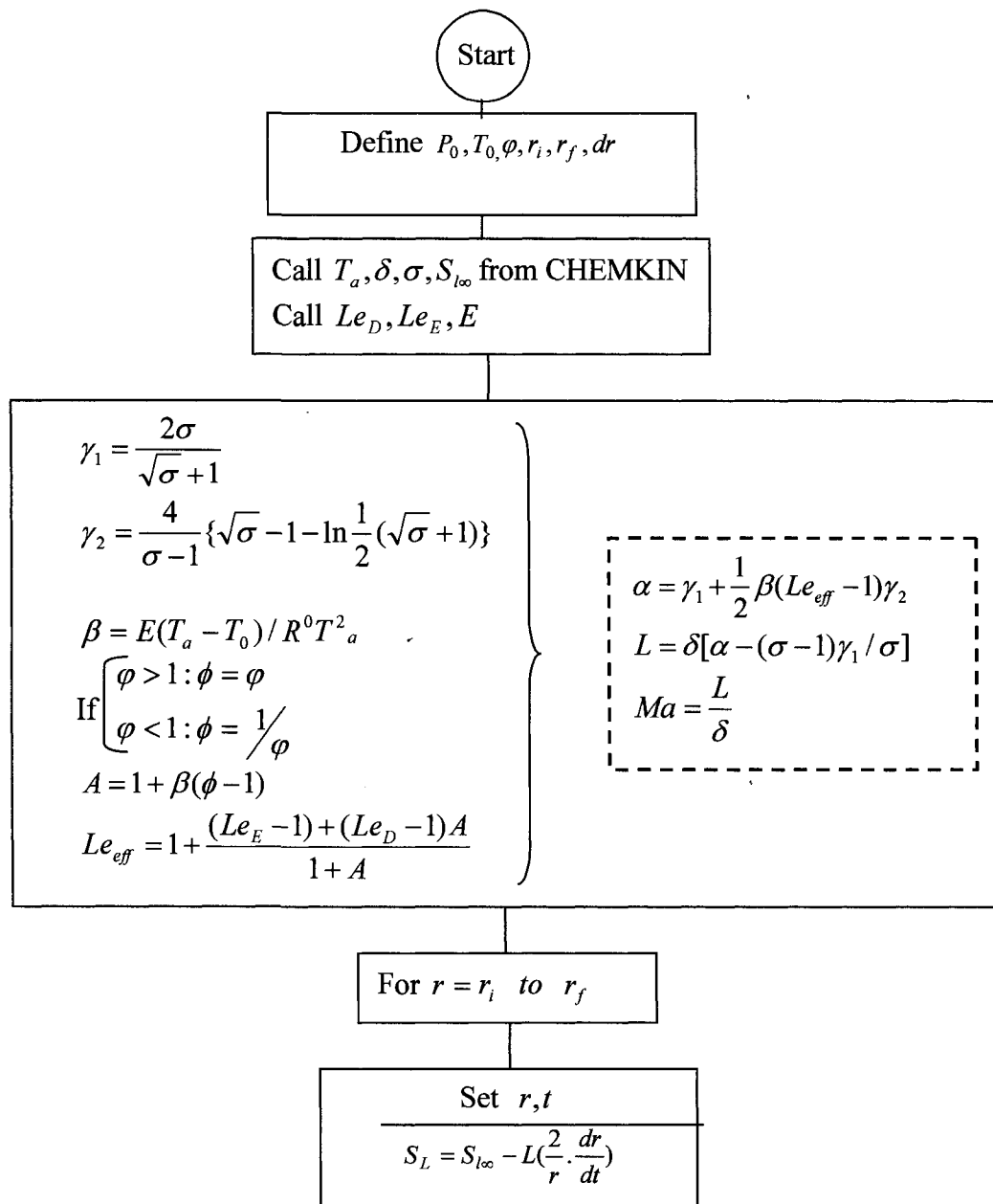


Figure 4.2: The structure of the stretched freely propagating flame code

4.3. Stretched Premixed Flame Model in a Confined Chamber

Closed vessel combustion causes the chamber pressure to rise. As a result, the burned and unburned mixtures are compressed and this restrains the flame growth. The indirect

effect of this pressure rise is to raise the unburned mixture temperature which tends to increase the flame speed.

The effect of pressure and temperature changes on the laminar flame speed can be expressed by the power law relation [Metghalchi and Keck, 1982]:

$$S_L = S_{L0} \left(\frac{P}{P_0}\right)^{P_{\text{exp}}} \left(\frac{T}{T_0}\right)^{T_{\text{exp}}} \quad (4.19)$$

where S_{L0} is the reference laminar flame speed at the reference pressure, P_0 , of 1 atm and the reference temperature, T_0 , of 300 K, P_{exp} and T_{exp} are the pressure and temperature exponents respectively. Liao et al. [2004] proposed functions to determine pressure and temperature exponents that are:

$$P_{\text{exp}} = 5.75\phi^2 - 12.15\phi + 7.98 \quad (4.20)$$

$$T_{\text{exp}} = -0.925\phi^2 + 2\phi - 1.473 \quad (4.21)$$

Following the above functions, the corresponding values of P_{exp} and T_{exp} for different equivalence ratios are calculated and tabulated in Table 4.2.

Table 4.2- Pressure and temperature exponents for different fuel air mixtures

ϕ	T_{exp}	P_{exp}
0.6	2.76	0.606
0.8	1.94	0.465
1	1.58	0.398
1.2	1.68	0.405
1.4	2.24	0.486

Figure 4.3 schematically shows the procedure to model the flame propagation inside a chamber. This simulation is based on using thermodynamic equilibrium for the flame growth model assuming adiabatic thin flame front propagation. The program is written in MATLAB (see Appendix B) and simulates flame growth starting from a specified kernel size. The kernel burns at the laminar flame speed with the pressure and temperature effects accounted for. Here, the reference unstretched laminar flame speed of CHEMKIN is used for the predetermined mixture. The whole program simulates a pressure trace of a laminar flame speed based on the mixture stoichiometry; spark kernel size, pressure and temperature effects in terms of pressure and temperature exponents and initial pressure and temperature.

The combustion chamber considered, is a spherical chamber of 0.001882 m^3 volume. Time step, spark kernel radius, pressure and temperature exponents are inputs. Thermal expansion coefficients are considered to be only temperature dependent. Initial flame speed is obtained from CHEMKIN based on the equivalence ratio, initial pressure and temperature of the mixture. However, the effects of pressure and temperature changes on flame speed are accounted via Equation (4.19). Having the time increment, the corresponding burning volume is calculated. It is worth mentioning that at each time step an element of dm mass is considered to burn completely. So, this mass is added to the burned side which leads to a new equilibrium condition with new equilibrium pressure and temperature. Also, the adiabatic flame temperature for the burning element is taken from CHEMKIN based on the fuel-air equivalence ratio. As, the burning process of each element is considered to be adiabatic, there is no heat transfer between the burned and

unburned side. The algorithm is based on guessing the new equilibrium pressure after each element burns.

The criterion for the accuracy of this guess is based on the equality of the total volume of the chamber with the sum of the burned and unburned volumes. The volume of the remaining unburned before and after combustion of the burning element is calculated. Based on these volumes and the guessed pressure, the volume of the burned side before and after combustion of the burning element is calculated. The volume of this element when is burned to temperature T_b and pressure P_E is compared to the left over volume of all the previously burned elements and volume left over from unburned gas will give the error which arises from the equilibrium pressure estimation. Positive error means that the pressure has been extrapolated. So the new guess will be:

$$P_E = P_i + 1.2(P_E - P_i) \quad (4.22)$$

and for the negative error:

$$P_E = P_i + (P_E - P_i)/1.2 \quad (4.23)$$

The calculation is repeated until this error is less than the desired accuracy.

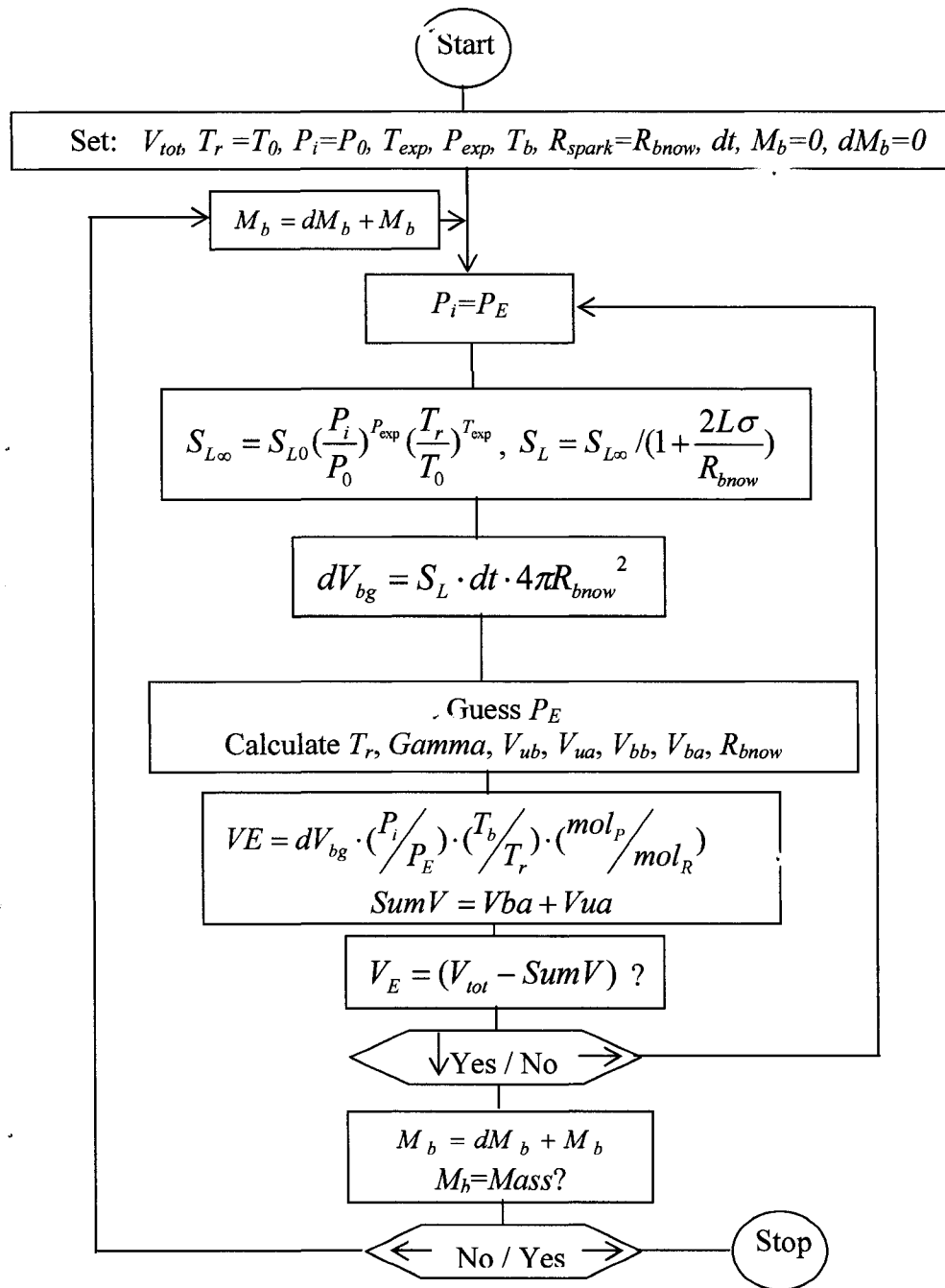


Figure 4.3 Confined stretched flame calculation flow chart

CHAPTER 5

RESULTS AND DISCUSSION

The numerical simulations are performed in order to predict values of adiabatic flame temperature, unburned/burned gas density ratio, stretched flame speed, Zeldovich, Lewis and Markstein numbers of a premixed, laminar, freely propagating, one-dimensional spherical flame. A parametric study is accomplished to see the effect of changing input pressure and temperature on flame characteristics for different methane-air mixtures. Subsequently, these results are used to predict flame growth inside a confinement and the effect of initial mixture condition on flame speed and flame stretch is investigated.

5.1. Unstretched Planar Adiabatic Premixed Methane-Air Flame

The underlying planar flame calculation is done with CHEMKIN 4.1 and the results are verified with the literature. Values of adiabatic flame temperature, unburned-burned gas density ratio, fuel and oxidizer Lewis numbers and thermal coefficients are used to compute the flame thickness, Markstein length, Markstein number and consequently the stretched flame speed.

5.1.1. Flame Temperature Profile

Flame temperature profiles of different methane-air mixtures at initial pressure and temperature of 1 atm and 300 K, respectively, are plotted in Figure 5.1. Temperature increases rapidly within the flame as we move from the unburned to the burned side. In fact most of the temperature changes occur within the preheat zone. It is worth mentioning that the flame speed is very sensitive to temperature and hence a correct estimation of temperature profile is vital [van Maaren et al., 1994]. The steepest temperature profile is for the stoichiometric mixture ($\phi \approx 1.1$ in reality) and decreases as we move away toward the lean or rich mixtures. The temperature at the end of the computational domain is considered as the adiabatic flame temperature. Figure 5.1 shows that the highest adiabatic flame temperature is somewhere around the stoichiometric

mixture ($\phi \approx 1.1$ to be accurate). Temperature profile of the stoichiometric mixture is also compared to the experimental results of van Maaren et al. [1994]. A good agreement is seen between the simulation results and the experimental measurements from the burner stabilized flame. The effect of the initial mixture temperature and pressure on the adiabatic flame temperature is shown in the following section.

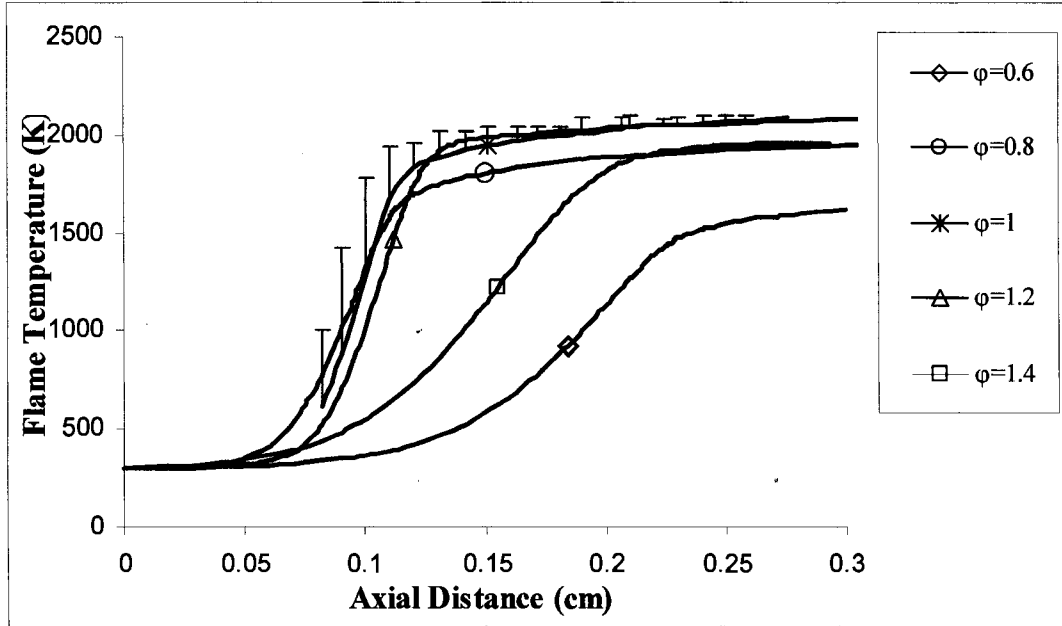


Figure 5.1: Temperature profiles of unstretched laminar planar flames.

Error bars: van Maaren et al [1994]

5.1.2. Effect of Pressure and Temperature on the Adiabatic Flame Temperature

The effect of unburned gas temperature on adiabatic flame temperature at 1 atm is plotted in Figures 5.2. The maximum adiabatic flame temperature is observed for the near stoichiometric mixture ($\phi \approx 1.1$ in reality). By increasing the equivalence ratio the adiabatic flame temperature is increased up to the stoichiometric mixture and then decreases moving toward the rich side. This effect is because of the fuel richness of the mixture that prevents the temperature to go far away. Also, increasing the initial mixture temperature from 300 K to 500 K results an up to 10% increase in adiabatic flame temperature.

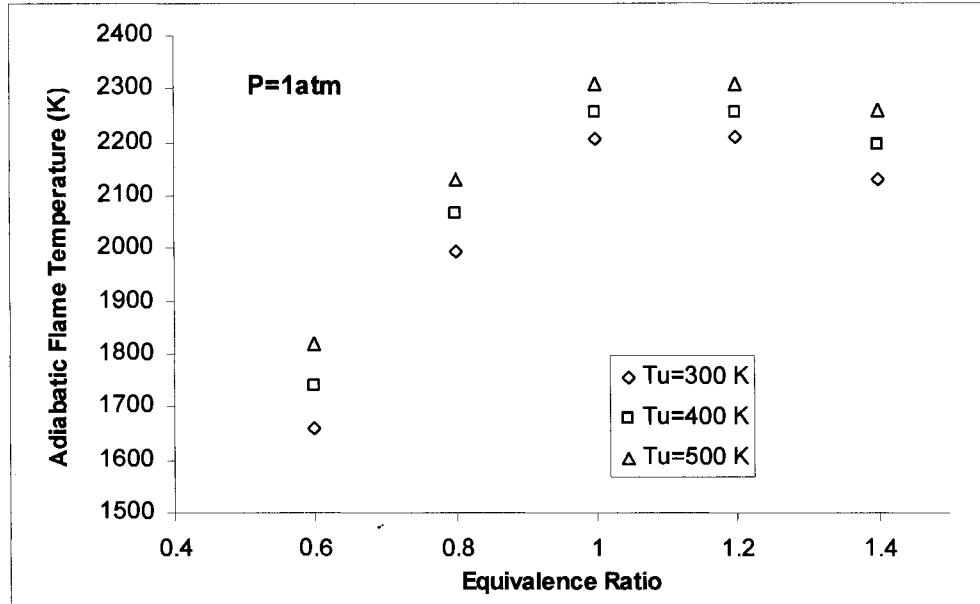


Figure 5.2: Effect of unburned gas temperature on adiabatic flame temperature at P=1 atm

The Effect of unburned mixture pressure on the adiabatic flame temperature is shown in Figure 5.3. These results show that moderate changes in pressure lead to negligible changes in adiabatic flame temperature.

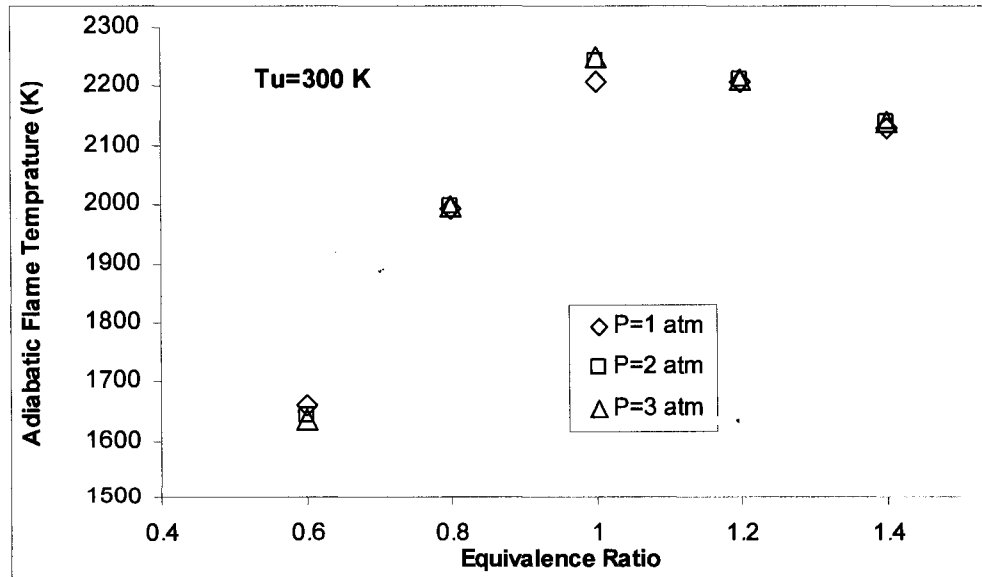


Figure 5.3: Effect of pressure on adiabatic flame temperature at Tu=300 K

Accurate calculation of the adiabatic flame temperature is very important as the other parameters like flame speed significantly changes with the adiabatic flame temperature. The comparison of the simulation results with the experimental results of van Maaren et al. [1994] and analytic approximations of Gottgens et al. [1992] is shown in Figure 5.4. These results are for the adiabatic flame temperature of stoichiometric mixture of 300 K unburned temperature and 1 atm pressure.

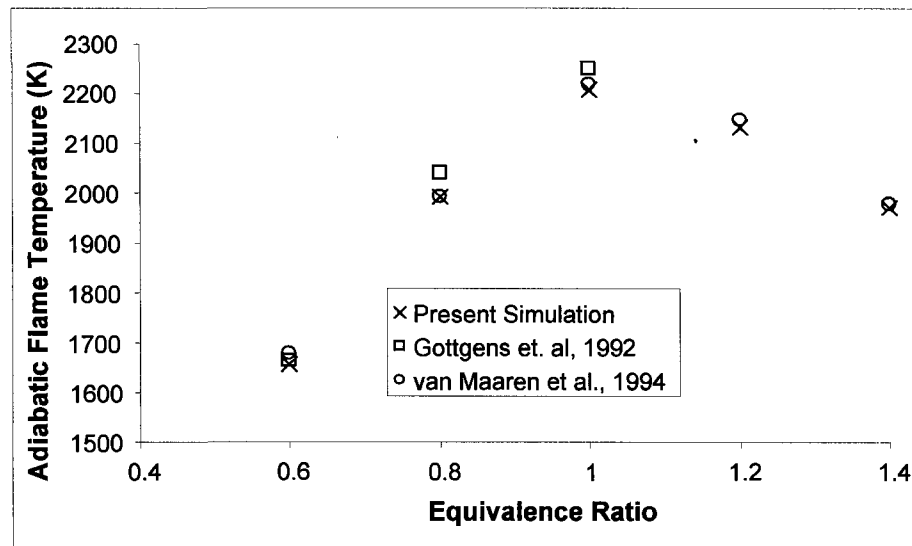


Figure 5.4: Comparison of the simulated adiabatic flame temperatures of different methane-air mixtures at $T_u=300$ K, $P=1$ atm with literature

5.1.3. Unstretched Flame Speed

Accurate measurement of unstretched flame speed has always been the key objective in combustion research. Figure 5.5 illustrates unstretched laminar flame speed as a function of methane-air equivalence ratio for different unburned mixture temperatures. Increasing the unburned mixture temperature results in faster flame propagation and higher burning rates. Increasing the unburned mixture temperature from 300 K to 500 K leads to almost 3 times faster flame speed for $\phi=1.2$.

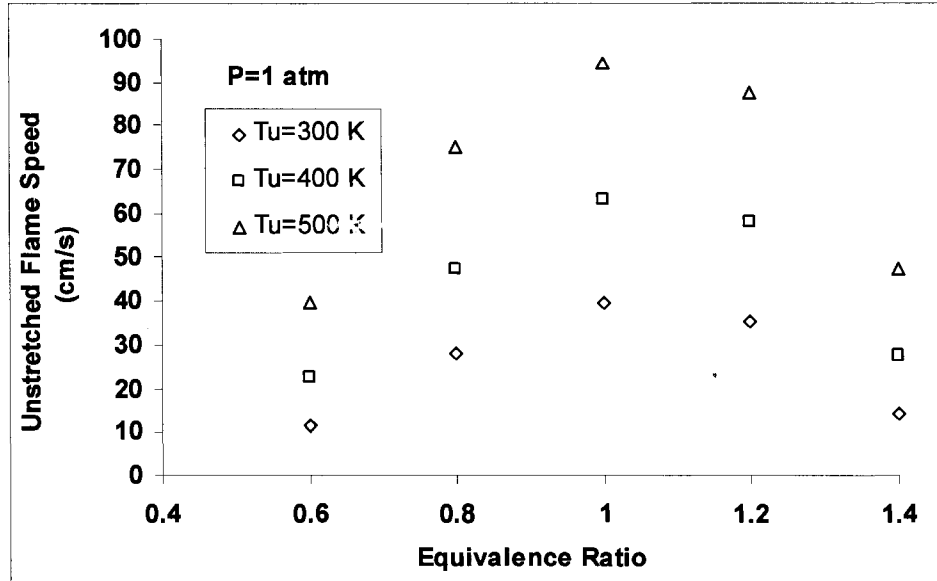


Figure 5.5: Effect of unburned mixture temperature on unstretched flame speed for different methane-air mixtures at P=1 atm

In Figures 5.6, the effect of pressure on the unstretched laminar flame speed is shown. Increasing the pressure reduces the flame speed. This effect is more pronounced when the pressure is changed from 2 to 3 atm rather than 1 to 2 atm. Quick comparisons between Figures 5.5 and 5.6 show that the effect of changing unburned mixture temperature on the unstretched flame speed is much more than the pressure.

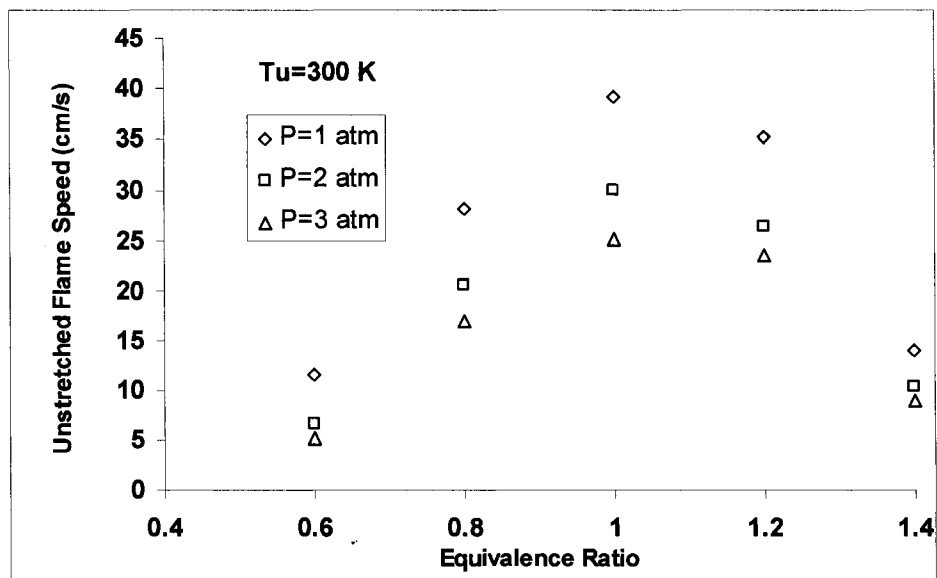


Figure 5.6: Effect of pressure on unstretched flame speed for different methane-air mixtures at $T_u=300$ K

The maximum unstretched laminar flame speed occurs near stoichiometric composition ($\phi \approx 1.1$). In Figure 5.7 simulation results are compared to the literature. The scatter in the data is due to the fact that no experiment can generate the one-dimensional, planar, adiabatic, steady, unstrained, laminar flame. All the data are for $T_u=300$ K and $P=1$ atm. The simulation results are in good agreement with Gu et al. [2000] on the lean side but about 15% higher on the rich side. The rich side results are in good agreement with van Maaren et al. [1994]. The underlying reason is the stretch level of different flame speeds and the strong relation between them. In Gu et al.'s combustion vessel, the stretch level is finite and positive. Therefore, for the fuel-rich mixtures (which has larger Markstein numbers and hence larger stretch level) the stretched methane-air flames combust slower than the unstretched counterparts [De et al., 2006]. They assumed the unstretched flame speed to be the flame speed measured for the largest flame ball in their limited size vessel, where the flame curvature and stretch rate are not negligible. Also, in the 380 mm diameter vessel, the chamber pressure and temperature will change from the initial condition during combustion, which causes additional variation in the measurements [Emami et al., 2005]. The results of van Maaren et al. [1994] were obtained using an adiabatic flat flame burner. The higher flame speed of the lean side was attributed to be as a result of the higher amount of uncertainty in the experiment for those mixtures.

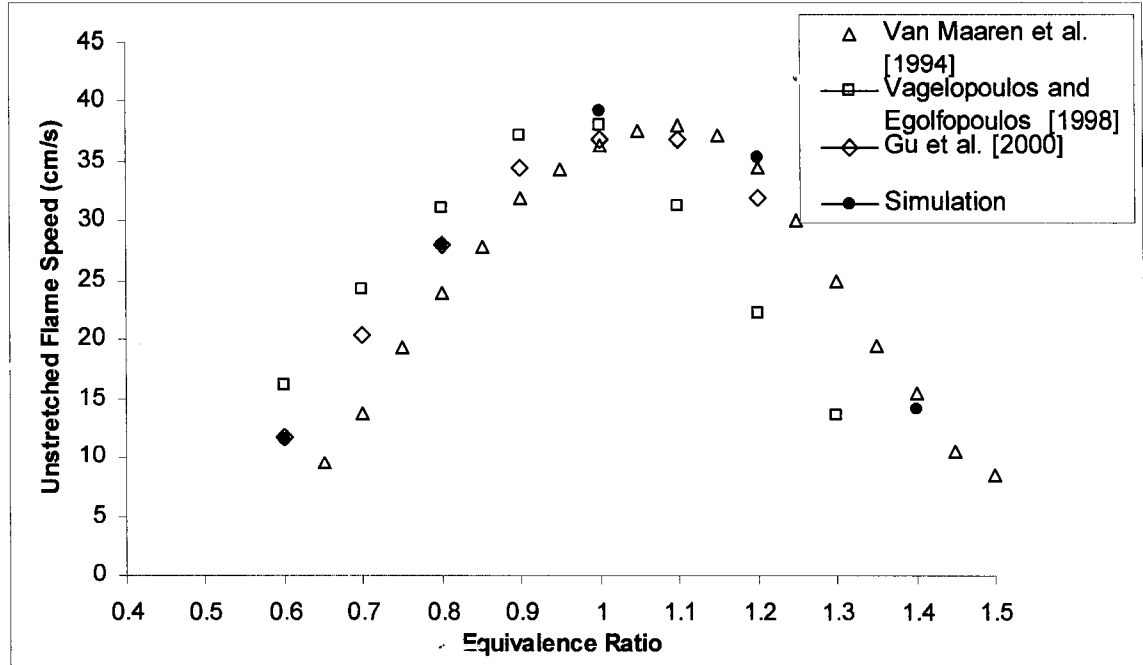


Figure 5.7: Comparison of the unstretched flame speed results with literature

The unstretched flame speed of stoichiometric mixture is plotted against unburned gas temperature for different pressures in Figure 5.8. The empirical equation, (3.19) expresses the effects of pressure and unburned gas temperature on the unstretched flame speed. The temperature and pressure exponents of this equation are taken from the functions introduced by Liao et al. [2004] in Equations (3.20) and (3.21), which are represented in Table 4.1. These values are also optimized by Gu et al. [2000] for the range of 300 K to 400 K and 0.1 MPa to 1 MPa, and at $\phi = 0.8, 1, 1.2$ which are also tabulated in Table 5.1.

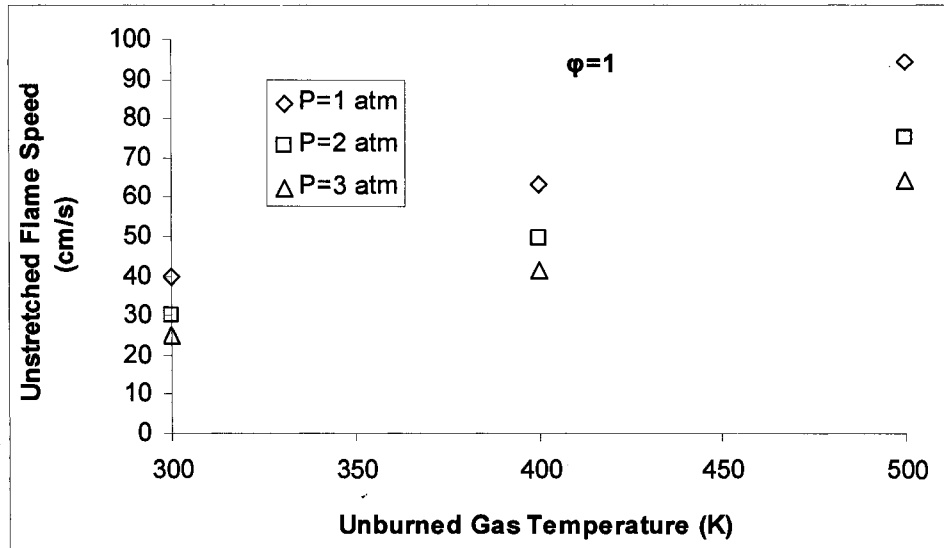


Figure 5.8: The effects of temperature and pressure on unstretched flame speed for stoichiometric methane-air mixture

Table 5.1: Pressure and temperature exponents for different methane-air mixtures

ϕ	Liao et al. [2004]		Gu et al. [2000]	
	T_{exp}	P_{exp}	T_{exp}	P_{exp}
0.6	2.76	-0.606	-	-
0.8	1.94	-0.465	2.105	-0.504
1	1.58	-0.398	1.612	-0.374
1.2	1.68	-0.405	2	-0.438
1.4	2.24	-0.486	-	-

5.1.4. Unburned/ Burned Gas Density Ratio

Another important parameter in laminar flame speed calculations is unburned/burned gas density ratio. It is a key parameter in stretched flame modeling. The variation of this parameter with respect to the equivalence ratio is shown in Figures 5.9 and 5.10 for

different initial mixture conditions. The trend is similar to the unstretched flame speed, which implies the direct dependency of flame speed on unburned/burned gas density ratio. As is shown in Figure 5.9, the computational results are in good agreement with the experimental values obtained by Gu et al. [2000]. Unburned /burned gas density ratio has strong dependency on mixture temperature and decreases significantly with increasing temperature but it is hardly affected by pressure changes between 1 atm to 3 atm.

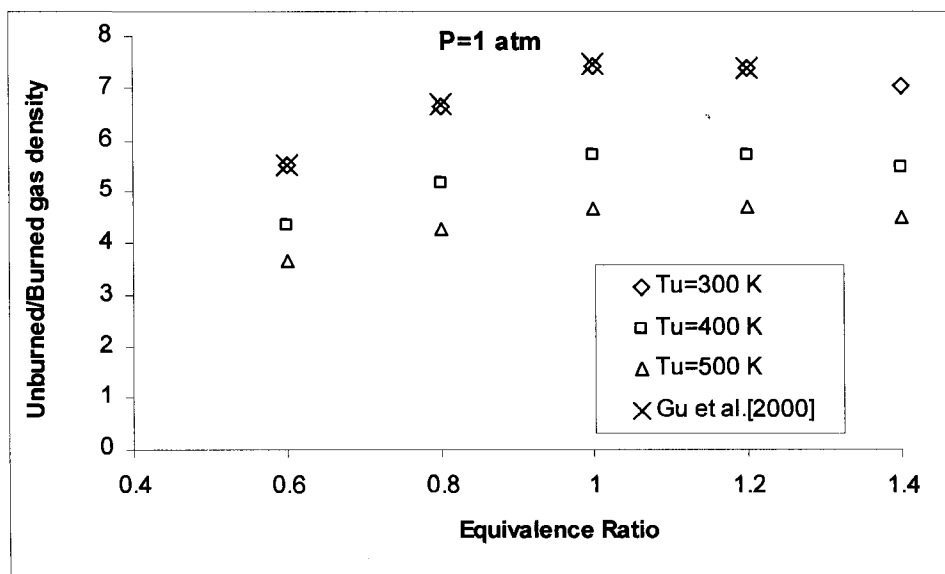


Figure 5.9: Variation of unburned/ burned gas density ratio with temperature at P=1 atm

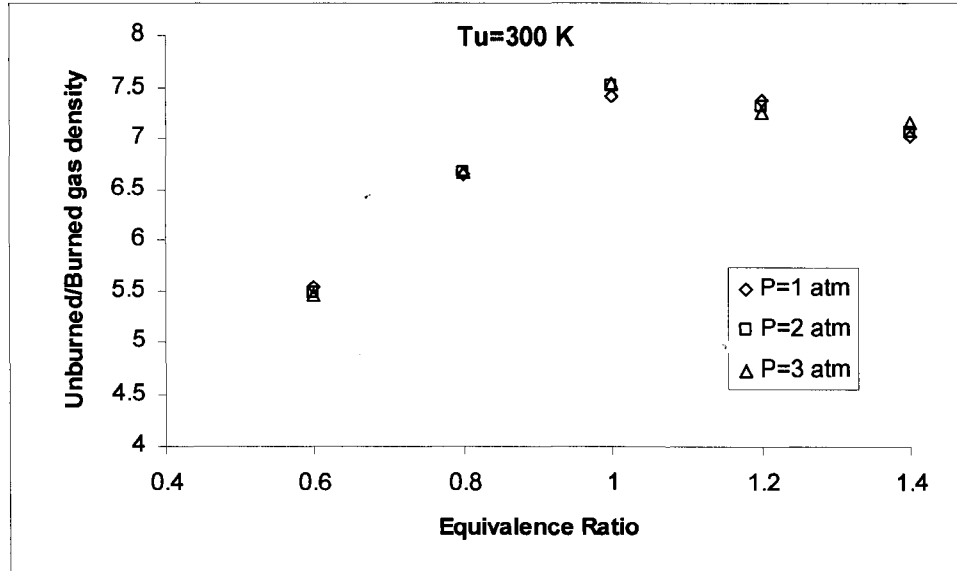


Figure 5.10: Variation of unburned/ burned gas density ratio with pressure at $T_u=300$ K

5.1.5. Zeldovich Number

Zeldovich number represents the sensitivity of chemical reactions to the variation of the adiabatic flame temperature. In other words it is the non-dimensional activation energy of the fuel mixture defined as the ratio of the diffusion temperature scale $T_a - T_u$ to the reaction temperature scale $\frac{RT_a^2}{E}$. The minimum Zeldovich number is for near stoichiometric composition ($\phi \approx 1.1$) as is shown in Figure 5.11. Increased temperature reduces the flame sensitivity to stretch and this is in consistent with the reduced Zeldovich number.

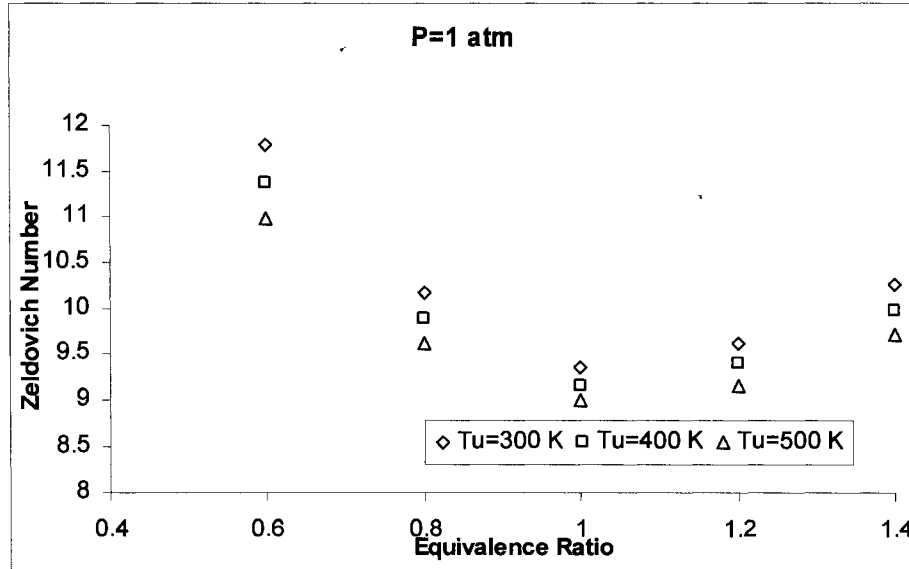


Figure 5.11: Effect of temperature on Zeldovich number for different equivalence ratios at P=1 atm

The effect of pressure on Zeldovich number is shown in Figure 5.12. It can be understood that moderate pressure changes do not have significant effect on Zeldovich number. It is reasonable as Zeldovich number is a function of unburned and adiabatic flame temperatures which do not vary considerably with pressure.

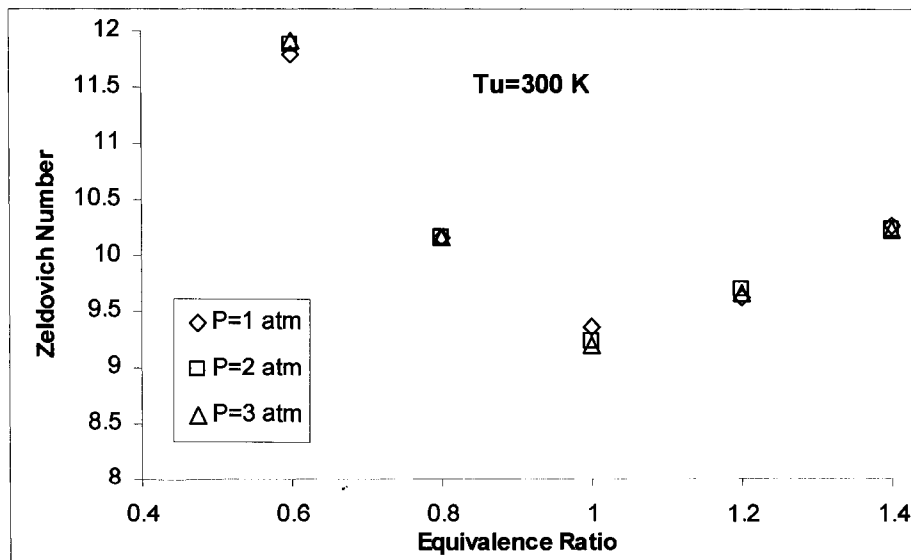


Figure 5.12: Effect of temperature on Zeldovich number for different equivalence ratios at $T_u=300$ K

5.1.6. Effective Lewis Number

Lewis number indicates the rate of energy transport with respect to the rate of mass transport. From Figure 5.13, it can be concluded that the effect of temperature changes from 300 K to 400 K has more prominent effect on Lewis number than from 400K to 500 K. This can be interpreted from the effect of temperature changes on the diffusion coefficients (Table 3.1), which indicates the same trend. Also, for each unburned mixture temperature, the effective Lewis number increases with increasing equivalence ratio which clearly shows that the unity Lewis number is not a good assumption in flame speed calculations.

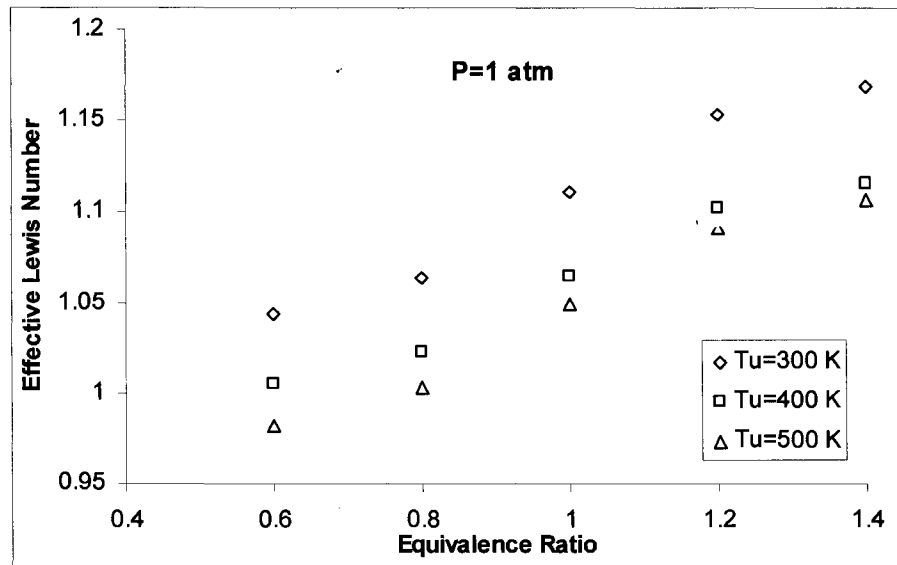


Figure 5.13: Effect of temperature on Lewis number for different equivalence ratios at P=1 atm

Figure 5.14 shows the effect of initial mixture pressure on the Lewis number. Pressure changes do not have significant effect on Lewis number as each reactant's Lewis number does not change with pressure significantly.

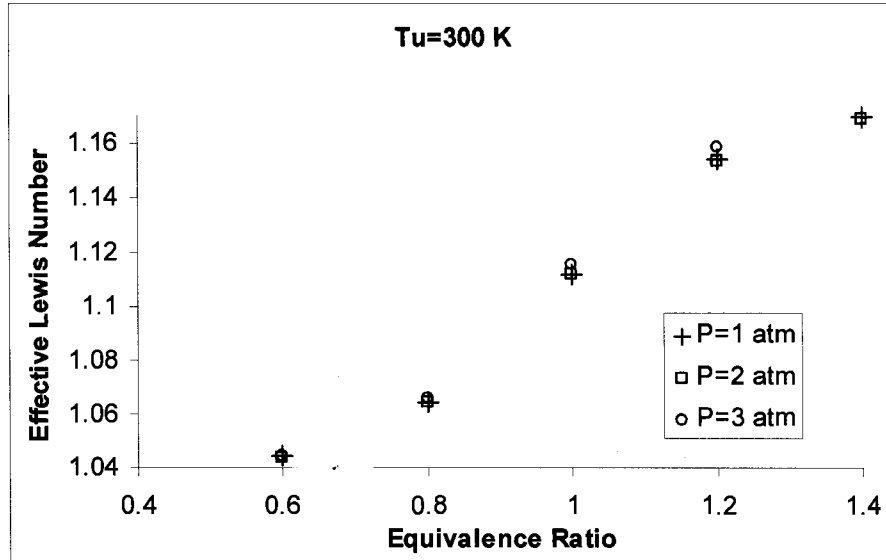


Figure 5.14: Effect of pressure on Lewis number for different equivalence ratios at $T_u=300$ K

5.1.7. Markstein Length

In Figure 5.15 Markstein lengths of different unburned gas temperatures at $P=1$ atm are compared. Since Markstein length characterizes the flame response to stretch, Figure 5.15 confirms stretch reduction at higher temperatures. With increasing temperature, Markstein length is decreased which implies stretch sensitivity reduction at higher temperatures. A quick comparison between Markstein lengths of the plotted range shows that the lowest Markstein length corresponds to approximately stoichiometric composition and the value increases as we move away from the stoichiometric mixture. The values of Markstein length indicate that the stretch influence is at its minimum around equivalence ratio of unity which means that the stoichiometric mixture has the least sensitivity to stretch.

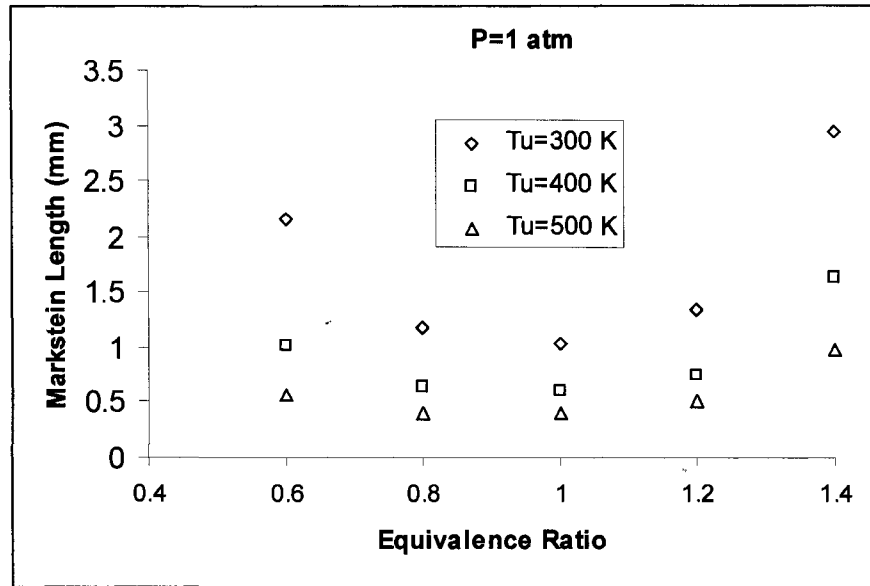


Figure 5.15: Effect of unburned gas temperature on Markstein lengths of different methane-air mixtures at P=1 atm

Table 5.2 compares the result of current research with experimentally and numerically determined Markstein lengths at unburned gas temperature of 300 K and pressure of 1 atm. It can be understood that the measured values in the literature differ considerably among themselves. Rozenchan et al. [2002] compared their experimental result of Markstein length for methane-air at 300 K and 1 atm with Gu et al. [2000] and found a good agreement. They examined flame growth in a spherical combustion chamber at constant pressure. Our results are in good agreement with Gu et al. [2000] in the lean side. The reason of such difference in the rich side was the same as explained for the unstretched flame speed. Because of the finite stretch level in their 380 mm spherical chamber the derived Markstein length are large especially in the rich side where the Markstein length has larger absolute value.

**Table 5.2: Comparison of Markstein lengths at P=1 atm, T_u=300 K
with the literature**

ϕ	Gu et al. [2000]	Rozenchan et al. [2002]	Bradley et al. [1996]	Present Simulation
0.8	0.78	0.91	0.65	1.18
1	1	1.29	0.85	1.04
1.2	2.56	2.63	1.08	1.34
1.4	-	-	2.24	2.94

5.1.8. Markstein Number

Markstein number is the nondimensional form of the Markstein length which shows the sensitivity of the flame to stretch. As Figure 5.16 shows, all calculated Markstein numbers are positive indicating the stability of the flame, i.e., stretch tends to reduce the flame speed and hence stabilizes the propagating flame. Markstein numbers increase with increasing initial mixture temperature. As Figure 5.17 shows, no significant changes are observed when pressure is altered from 1 to 3 atm. Zero Markstein length signifies stretch insensitive flame, the corresponding stretch-insensitive Markstein number for stretch insensitive flame should be zero in theory. However, comparing Figures 5.15 and 5.16 suggests that the least stretch sensitive flame (the one with the least Markstein length) does not correspond to the mixture with the least Markstein number. This is mainly because of the flame thickness changes for different mixture stoichiometries.

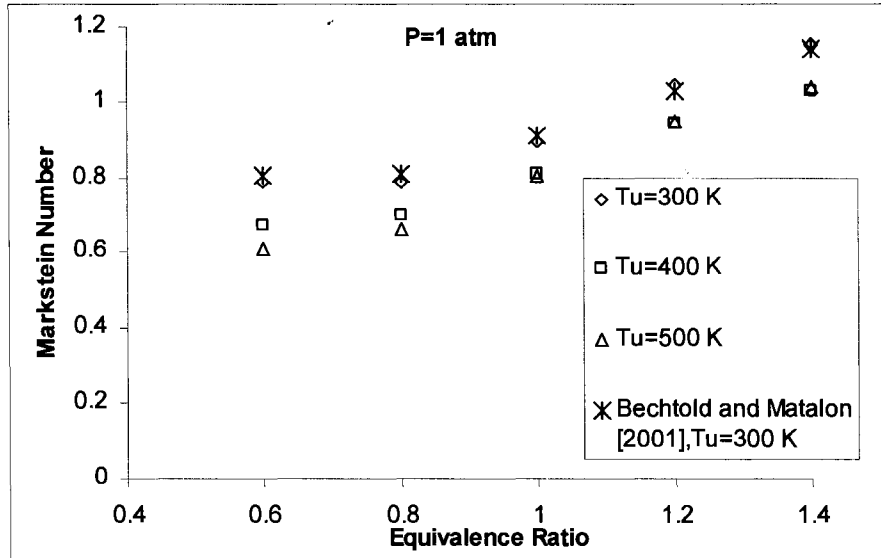


Figure 5.16: Effect of temperature on Markstein numbers of different methane-air mixtures at P=1 atm

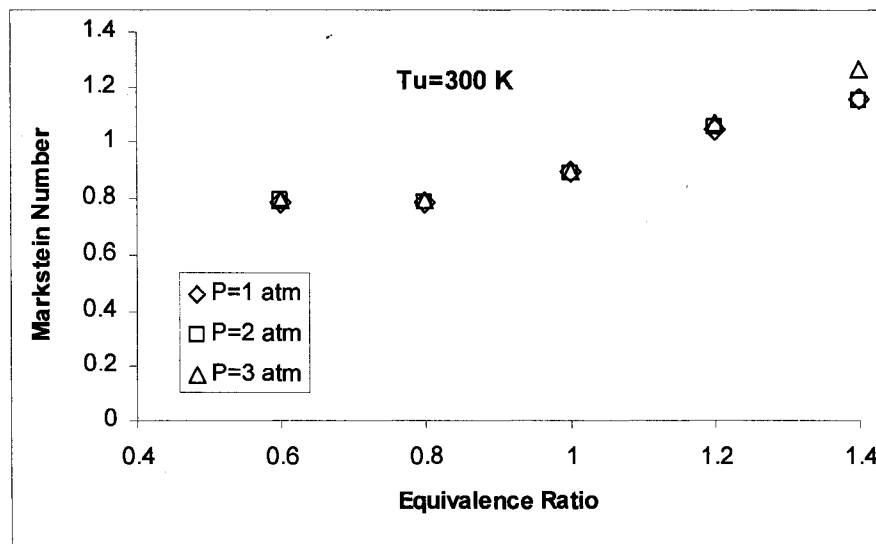


Figure 5.17: Effect of pressure on Markstein numbers of different methane-air mixtures at $T_u=300$ K

5.1.9. Stretched Flame Speed

In Figure 5.18 the variation of flame speed of different methane-air mixtures is plotted as the flame grows. The general trend for all the curves is that the stretched flame speed approaches the unstretched value asymptotically which shows decreasing effect of stretch. For all the cases the largest changes occur right after ignition. The absolute reduction from the stretched case is largest for the fastest burning mixture, $\phi \approx 1$. Also

note that for $\phi=0.6$ the flame seems to reach its asymptotic unstretched flame speed sooner than $\phi=1.4$ mixture.

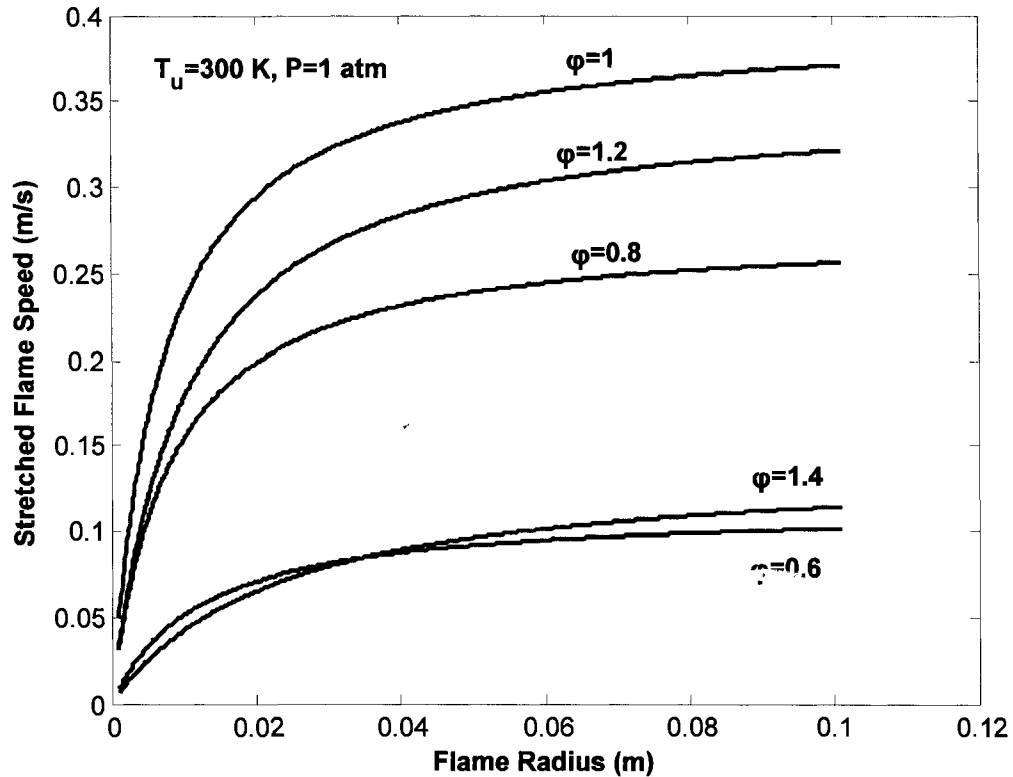


Figure 5.18: Stretched flame speed for different methane-air mixtures at $T_u=300$ K and $P=1$ atm

It is clear from the previous figure that flame speed is very low near the leanest and richest side and any reduction in flame speed may lead to serious cycle to cycle variations and combustion instabilities. To better illustrate the relative changes in flame speed as the flame grows, the stretched flame speed is normalized by the corresponding unstretched value and plotted as a function of flame radius in Figure 5.19. It is interesting to note that for $\phi=1.4$, it takes the longest time to approach its asymptotic value. For example when the flame radius is 0.1 m the stretched flame speed is still at 70% of the unstretched speed while for the other mixtures this ratio is more than 85%.

For a typical spark kernel size of 5mm radius, a near stoichiometric methane-air flame speed is reduced by no more than 50% from its unstretched value, while $\phi=0.6$ value is

about 33% and for $\phi=1.4$ is even less (about 20%). This is due to the effect of increasing stretch sensitivity away from stoichiometric mixture which is an important issue especially in lean burn engines.

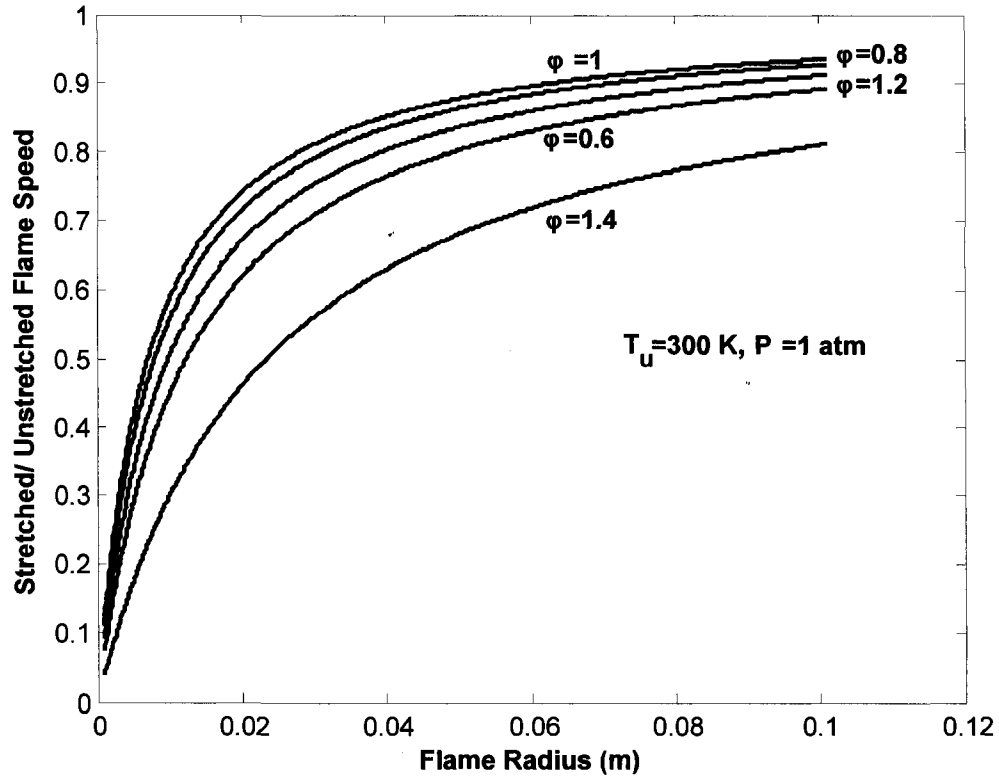


Figure 5.19: Stretched/Unstretched flame speed as a function of flame radius for different methane-air mixtures at $T_u=300$ K and $P=1$ atm

The stretched flame speed as a function of stretch rate is shown in Figure 5.20. It confirms the linear relationship between stretched flame speed and stretch rate. The rate of decrease in flame speed is largest for the richest and leanest mixtures ($\phi=1.4$ and $\phi=0.6$). As these mixtures have the steepest profile, they are most sensitive to stretch. Stretched methane-air flame speed always decreases when the flame stretch is increased due to the fact that Markstein lengths are always positive.

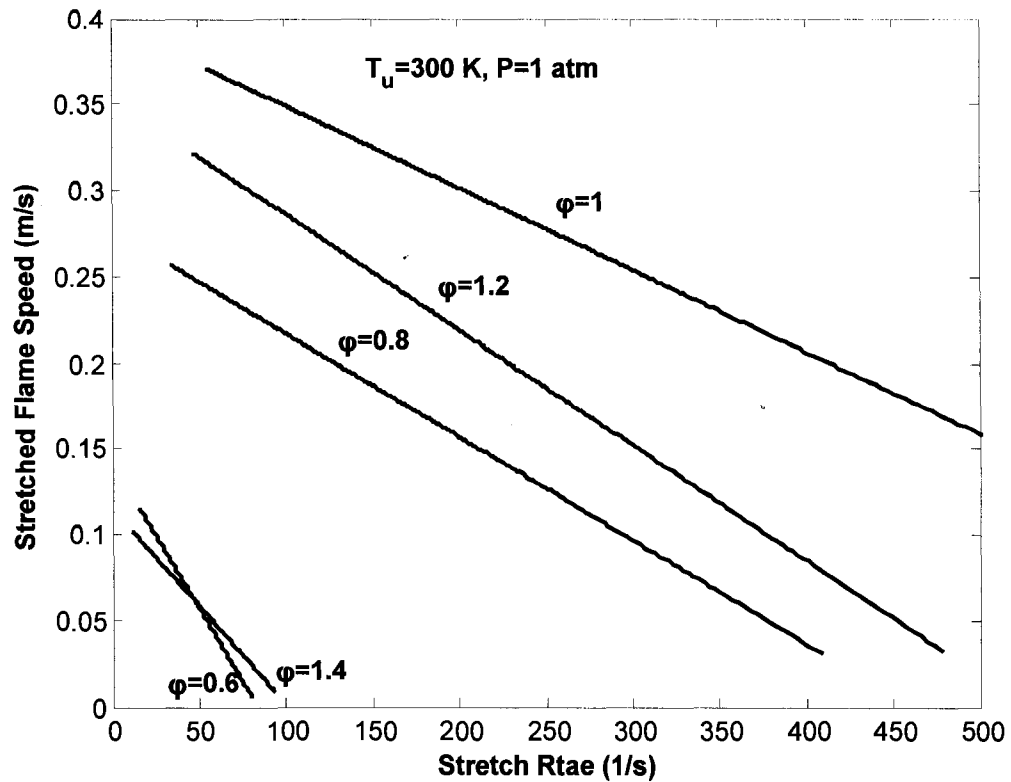


Figure 5.20: Stretched flame speed as a function of stretch rate for different methane-air mixtures at $T_u=300 \text{ K}$ and $P=1 \text{ atm}$

The stretch rates of different methane-air mixtures are compared in Figure 5.21. As it is shown the highest stretch levels is for the stoichiometric mixture and reduces notably for the lean and rich mixtures. This is due to the fact that near stoichiometric mixture burns the fastest. The largest flame speeds imply largest curvature and straining changes per unit time.

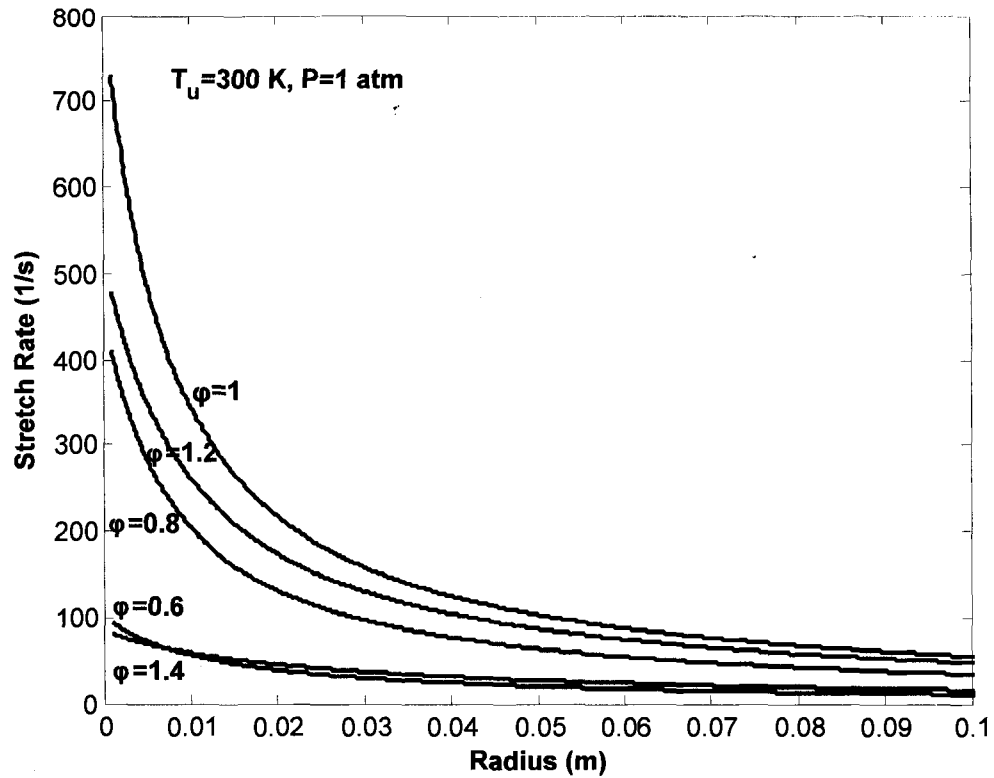


Figure 5.21: Stretch rate as a function of radius for different methane-air mixtures at $T_u=300 \text{ K}$ and $P=1 \text{ atm}$

The corresponding dimensionless parameter describing flame stretch is Karlovitz number. The mathematical relation between Karlovitz number and flame speed is expressed by Equation (4.18). So, the slope of the plot of stretched/unstretched flame speed versus Karlovitz number is Markstein number. As Figure 5.22 shows, the slope of these plots is constant over the range of Karlovitz number, portraying the independency of Markstein number on Karlovitz number over the illustrated range, as assumed in the model. The largest slope is for $\phi = 1.4$ which shows the largest Markstein number.

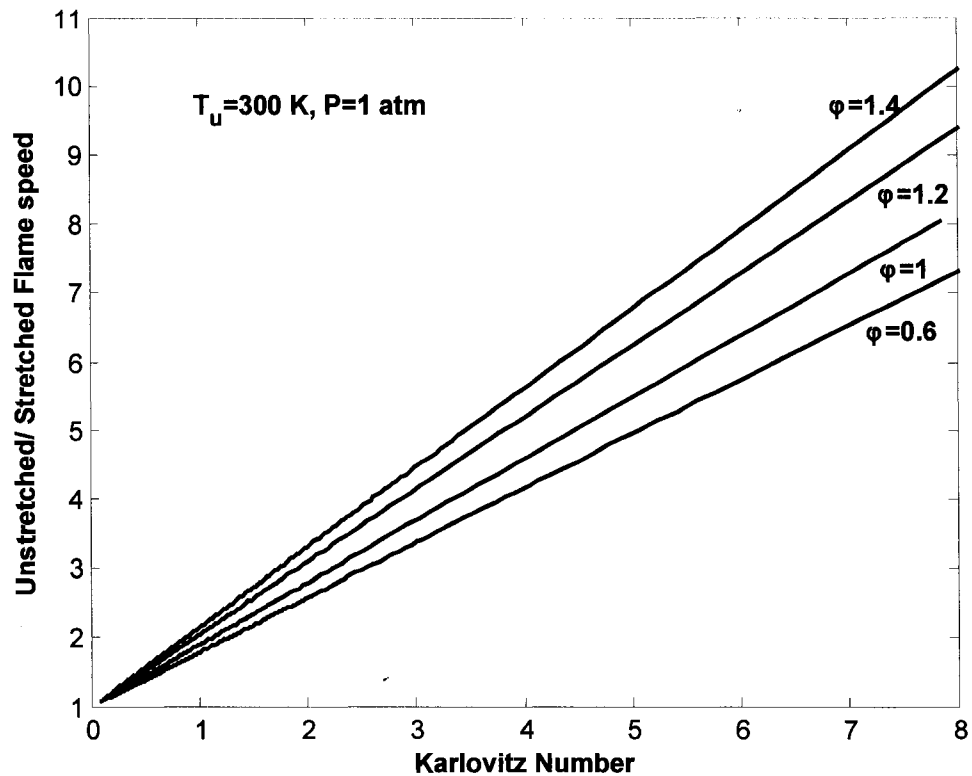


Figure 5.22: Normalized flame speed versus Karlovitz number for different mixture compositions at $T_u=300$ K and $P=1$ atm

Effects of unburned mixture pressure and temperature on the stretched flame speed for the stoichiometric mixture are shown in Figures 5.23 and 5.24 respectively. It can be understood that the flame burns slower as the pressure is increased at constant temperature. However, by increasing temperature at a constant pressure the flame propagates faster. This is primarily due to the fact that the underlying unstretched flame speed increases with increasing unburned mixture temperature and decreases with increasing pressure.

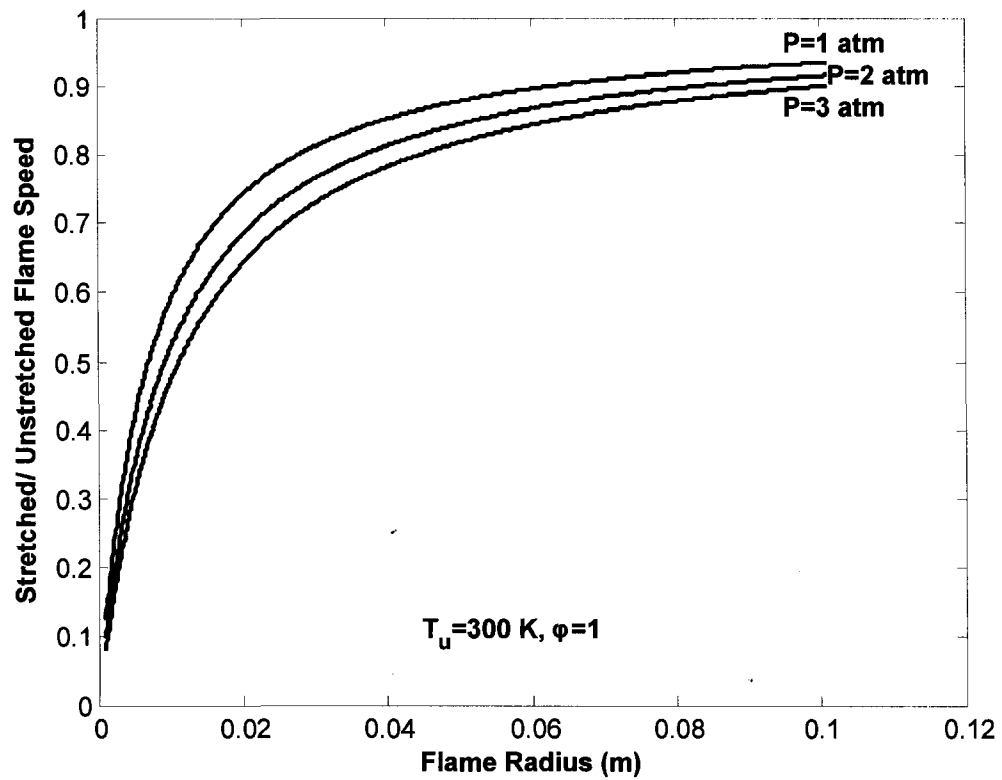


Figure 5.23: Normalized flame speed versus flame radius at different pressures for stoichiometric methane-air mixture at $T_u=300\text{ K}$

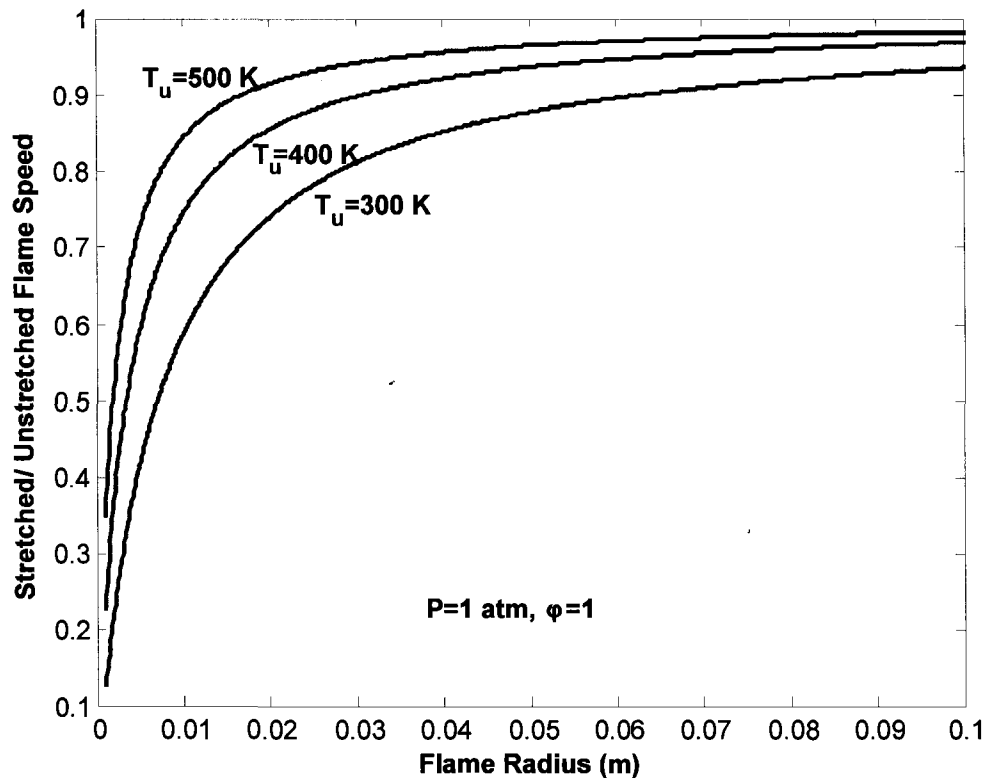


Figure 5.24: Normalized flame speed versus flame radius at different temperatures for stoichiometric methane-air mixture at P=1 atm

5.2. Confined Flame Results

5.2.1. Effect of Initial Mixture Temperature on Flame Propagation Inside the Chamber

In Figure 5.25, the effect of initial mixture temperature on flame speed of the stoichiometric mixtures is shown. Increasing the initial mixture temperature leads to faster burning. The absolute increase in stretched flame speed from 400 K to 500 K is larger than that from 300 K to 400 K. Note that as the stretched flame speed is increasing the stretch rate also increases, nevertheless, at higher temperatures the stretched flame speed even for the stretched small flame kernel (relative radius < 0.2) is larger than that of the less stretched flame at the same size at lower temperatures. In other words, in a warmer environment such as that in a spark ignition engine cylinder, the overall effect of stretch on the corresponding flame speed is less than that at room temperature flame.

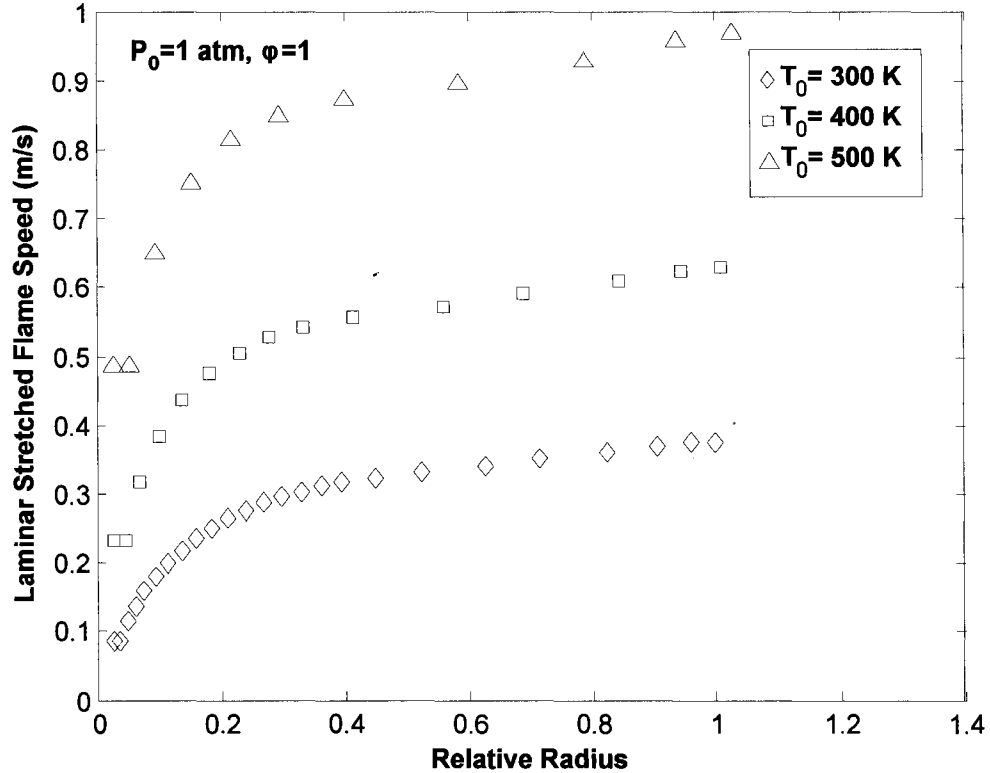


Figure 5.25: Effect of initial mixture temperature on laminar stretched flame speed of the stoichiometric mixture in a confined chamber at $P_0=1$ atm

A key underlying parameter which detects the flame speed is the flame stretch rate. The effect of initial mixture temperature on the flame stretch rate of the stoichiometric mixture is shown in Figure 5.26. The figure shows that the flame stretch rate is increased as the initial mixture temperature increases. The rate of increase is larger at the initial stages of flame growth when the stretch rate is the largest and has the most significant influence on flame propagation. However, at larger radii the difference between the stretch rates of different methane-air mixtures is not appreciable.

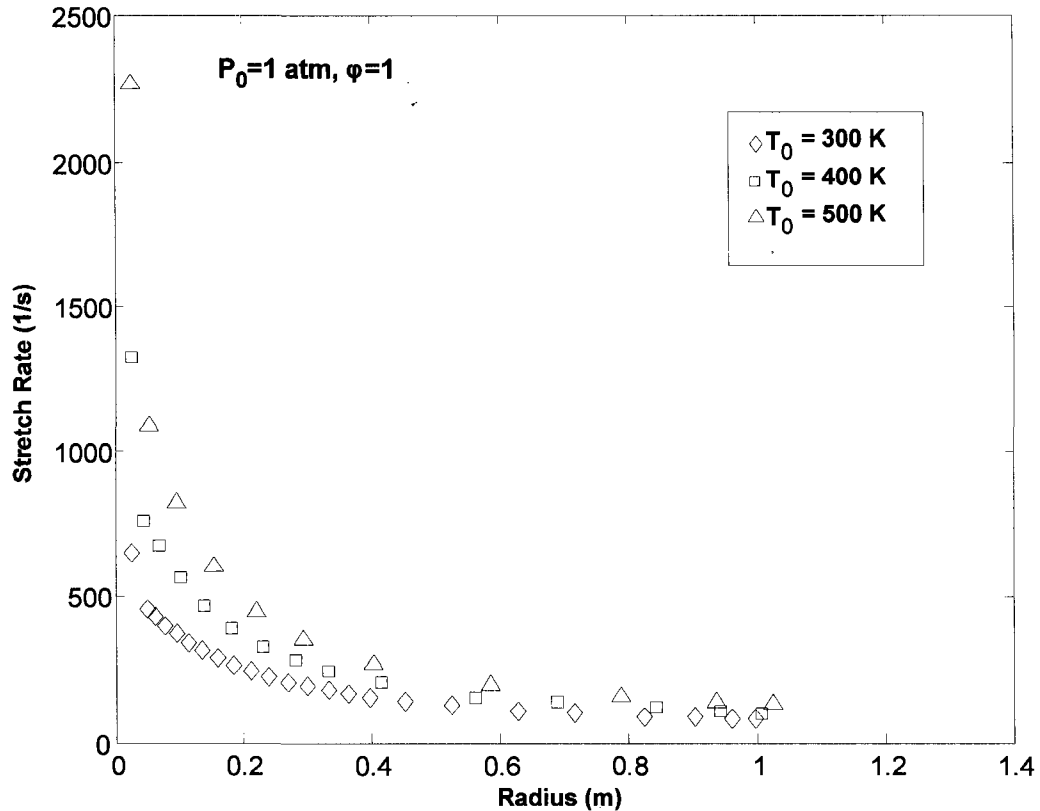


Figure 5.26: Effect of initial mixture temperature on flame stretch of the stoichiometric mixture in a confined chamber at $P_0=1$ atm

As it is explained before, unburned gas temperature is subject to change as the flame grows inside the chamber. This effect is accounted for via the temperature exponent in Equation (3.19). Setting the temperature exponent to zero nullifies the augmentation of flame speed with increasing chamber temperature. Figure 5.27 shows the effect of this factor on flame speed inside the chamber. As it can be seen, at moderately small radii up to approximately half of the chamber radius, whether to consider the effect of temperature changes or not, the stretched flame speed does not vary significantly from one another. However, this effect becomes important at larger flame sizes. This is due to the fact that when the flame is relatively small the stretch is substantial while the chamber pressure rise and hence the increase in unburned gas temperature, which enhances the flame speed is small. On the other hand at larger radii the effect of stretch becomes weaker and the increased pressure inside the chamber lessens the flame speed.

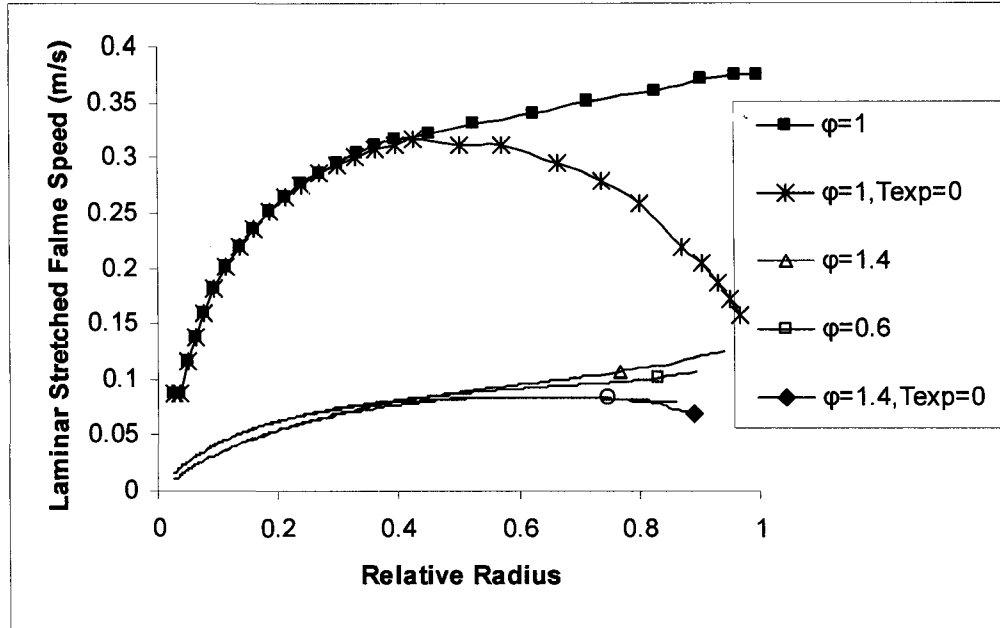


Figure 5.27: Effect of temperature exponent on flame speed in a confined chamber

Figure 5.28 shows how unburned gas temperature is changing as the flame is growing for three methane-air mixtures. As we have discussed regarding to the results in the previous figure (Figure 5.27), Figure 5.28(a) depicts that at small to moderate radii temperature changes are small and most of the changes occur at larger radii. Also, among the three equivalence ratios plotted, the highest temperature is for the stoichiometric mixture. This largest increase in unburned gas temperature, caused by the largest pressure rise shown in Figure 5.28(b), results in the substantial difference in the stretched flame speed of the stoichiometric mixture with $T_{exp}=0$ versus $T_{exp} \neq 0$.

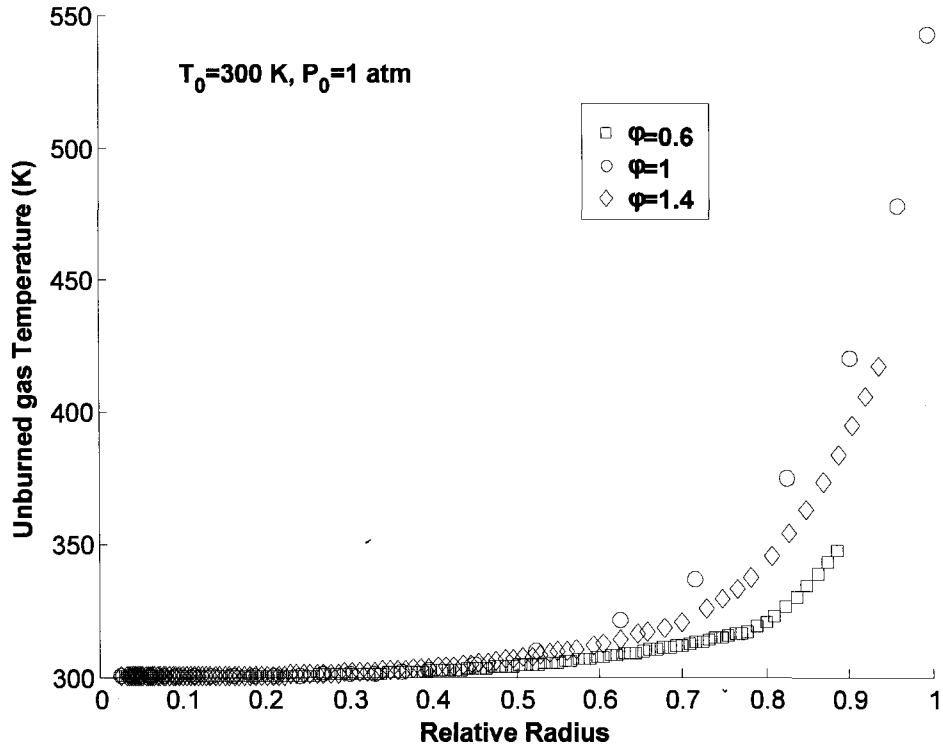


Figure 5.28(a): Equilibrium temperature of the stoichiometric mixture inside the chamber at $T_0=300 \text{ K}$, $P_0=1 \text{ atm}$

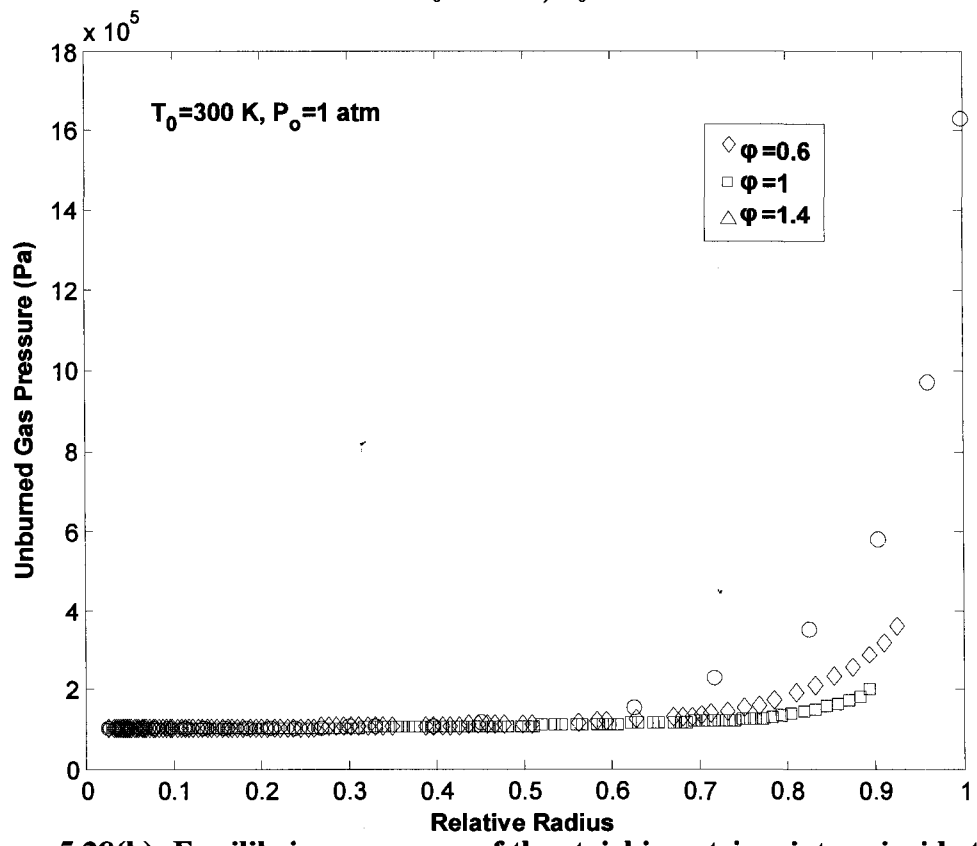


Figure 5.28(b): Equilibrium pressure of the stoichiometric mixture inside the chamber at $T_0=300 \text{ K}$, $P_0=1 \text{ atm}$

5.2.2. Effect of Chamber Pressure on Flame Propagation inside the Chamber

In Figure 5.29 the effect of chamber mixture pressure on the stretched flame speed is shown. It can be seen that decreasing the initial pressure enhances the flame speed. However this effect is not as much as the temperature effect. Increasing the initial mixture pressure from 2 atm to 3 atm has larger influence on the flame speed than that from 1 atm to 2 atm.

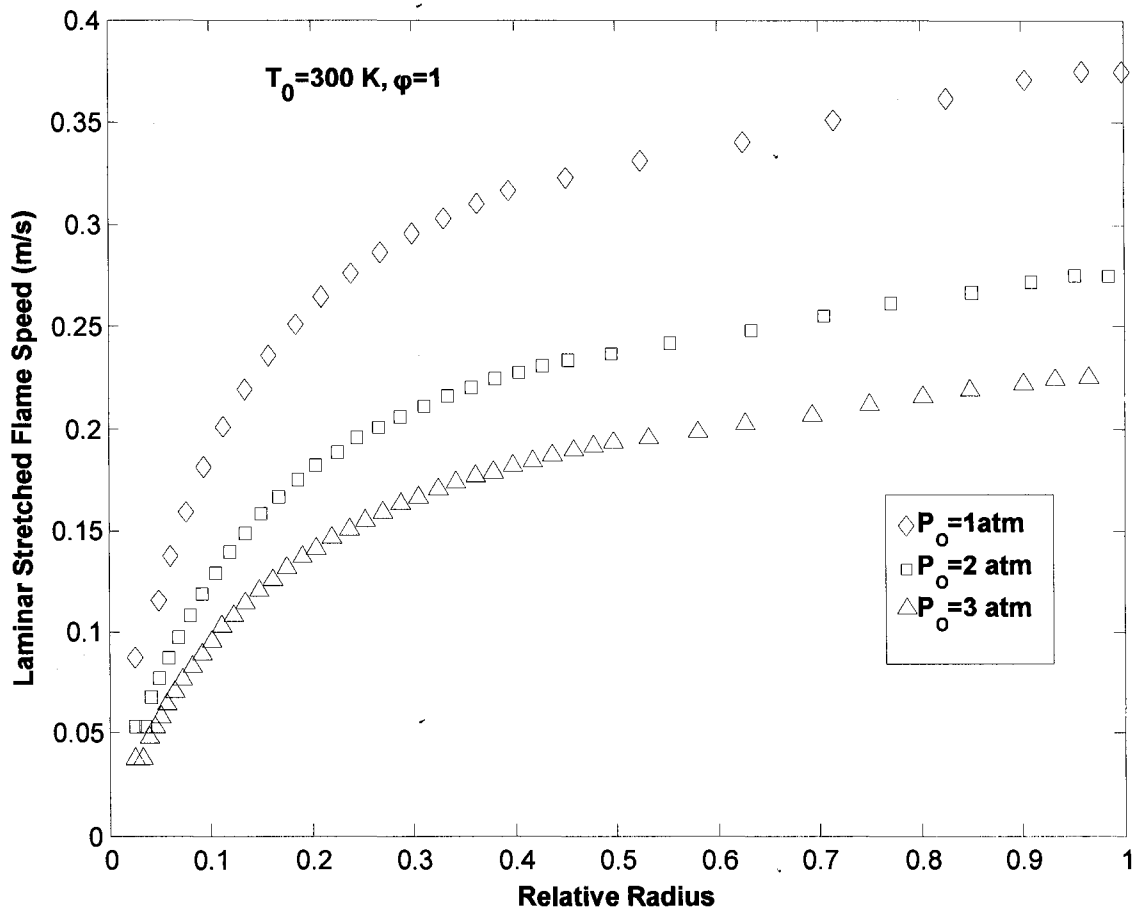


Figure 5.29: Effect of chamber pressure on laminar stretched flame speed of the stoichiometric mixture at $T_0=300\text{ K}$

The effect of chamber pressure on the stretch rate of the stoichiometric mixture is shown in Figure 5.30. As the initial chamber pressure is increased, the flame speed is reduced (negative pressure exponents as is introduced in Table 5.1). Consequently, the flame grows slower and thus, the rate of flame stretching decreases accordingly.

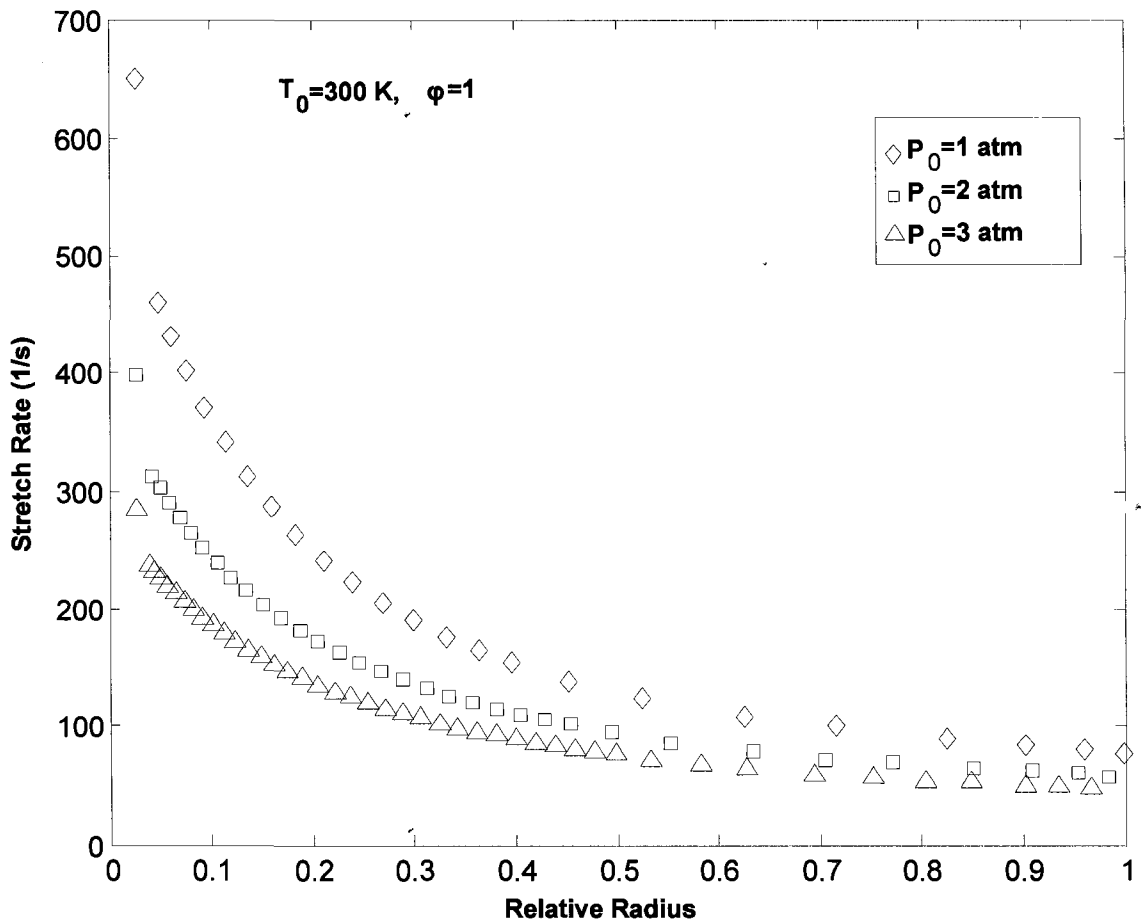


Figure 5.30: Effect of chamber pressure on flame stretch of the stoichiometric mixture at $T_0=300\text{ K}$

5.2.3. Flame Speed for Different Mixture Conditions

A quick comparison between Figures 5.25 and 5.29 shows that as the flame grows inside the chamber, the effect of pressure increase tends to lessen the laminar flame speed while the increase in mixture temperature due to compression has a positive effect. The overall pressure and temperature effects tend to increase the laminar flame speed moderately as the flame grows. It means that the temperature effect is more dominant than that of pressure.

Another comparison is done to highlight the effect of stretch on flame propagation. Three cases are shown in Figure 5.31; the speed of confined flame with and without stretch and the speed of freely propagating flame with stretch. For the unstretched

confined case, the small changes of flame speed at each flame size are simply due to the temperature and pressure changes. Because of the great effect of stretch at small radii, the stretched flame speed is lessened at the beginning compared to the unstretched confined case. However, there is not a significant difference between the confined and unconfined case when the stretch is imposed. The reason is that in the confined scenario there is a combined effect of stretch, chamber pressure and unburned gas temperature changes; but for the freely propagating case, there is only stretch which diminishes asymptotically as the flame grows (that is, the unburned gas temperature and pressure remains unchanged). The confined stretched flame speed is slightly less than that of the unconfined stretched flame for flames less than approximately 0.05 m which is attributed to restriction to freely propagation in the chamber. The overtaking for larger flame sizes is caused by the progressive augmentation caused by the appreciable rise in unburned gas temperature.

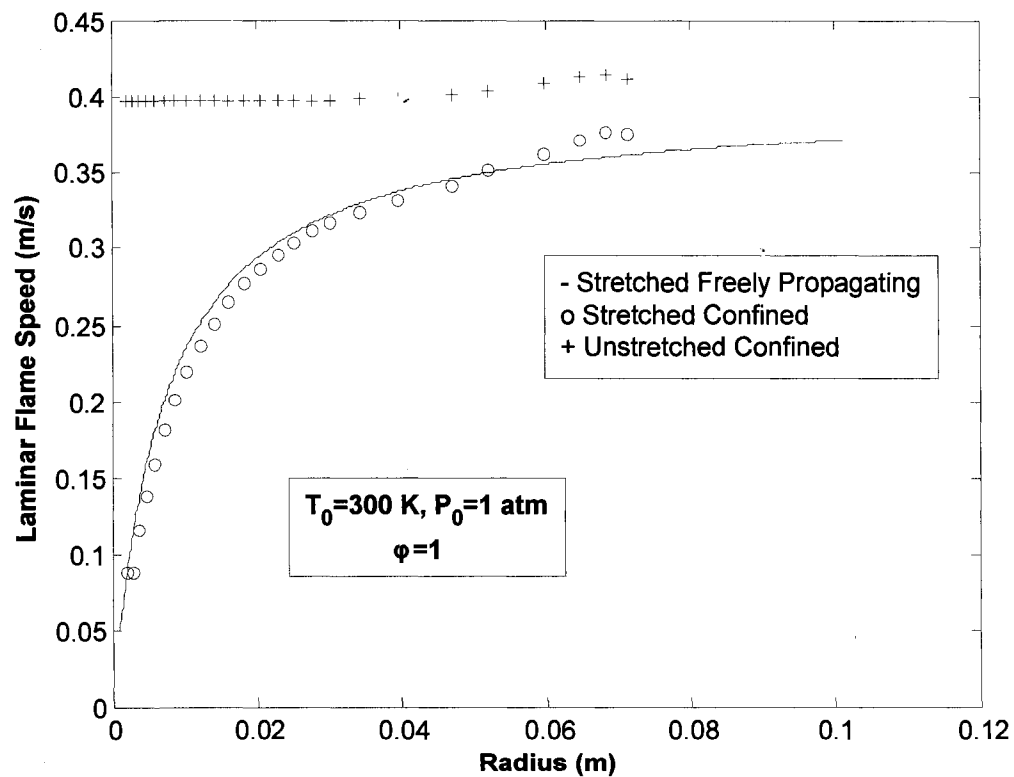


Figure 5.31: Flame speed results with and without stretch for the stoichiometric mixture at $T_0=300$ K, $P_0=1$ atm

In Figure 5.32 normalized flame speed of different methane-air mixtures are compared. It is evident that this ratio is highest for the stoichiometric mixture for any flame size and has the lowest value for the richest mixture considered. For leaner or richer flames, the flame growth rate becomes smaller compared to the stoichiometric condition and it takes longer time to burn. In addition, stretch sensitivity is least around the stoichiometric composition and thus stoichiometric flame reaches the corresponding asymptotic (unstretched) flame speed faster.

The underlying stretch rate which causes these differences is portrayed in Figure 5.33. The stretch level is the highest value for the stoichiometric mixture and reduces as we move toward the lean or rich side. Even though the fastest near stoichiometric flame is undergoing the lightest level of stretch, it is nonetheless, least stretch sensitive (smallest Markstein length as is portrayed in Figure 5.15). The combined effect as shown in Figure 5.32 is that stoichiometric flame is still favored for fastest burning.

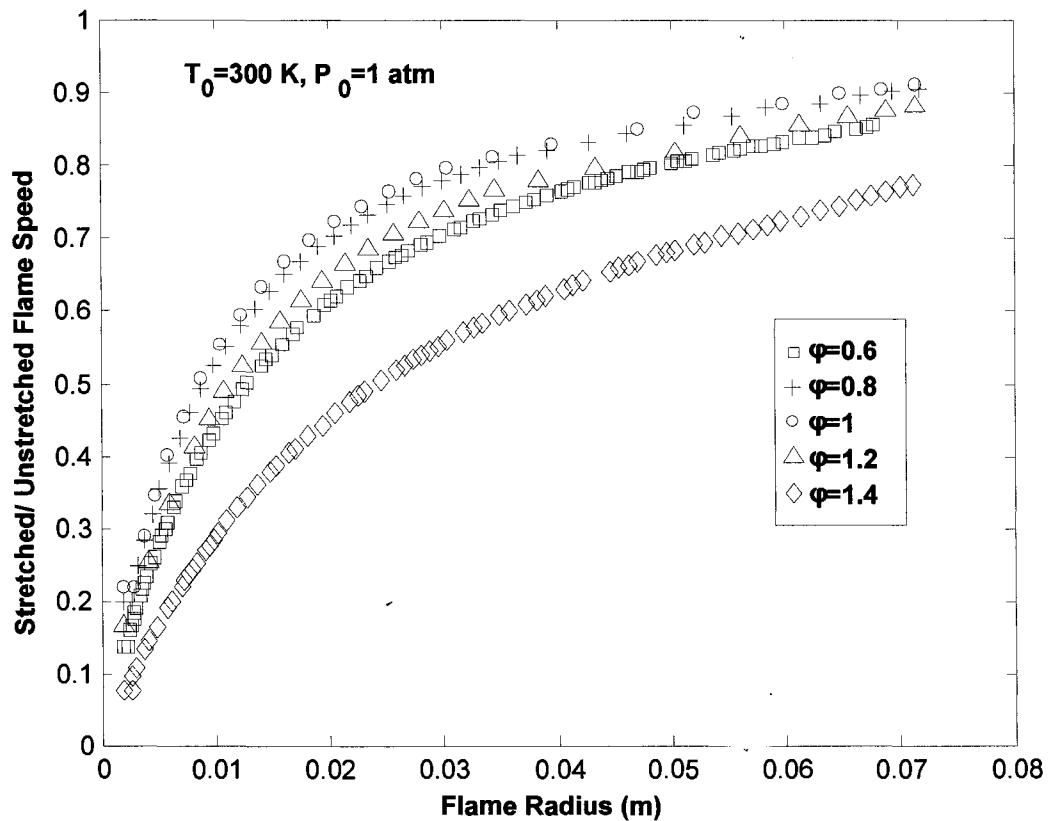
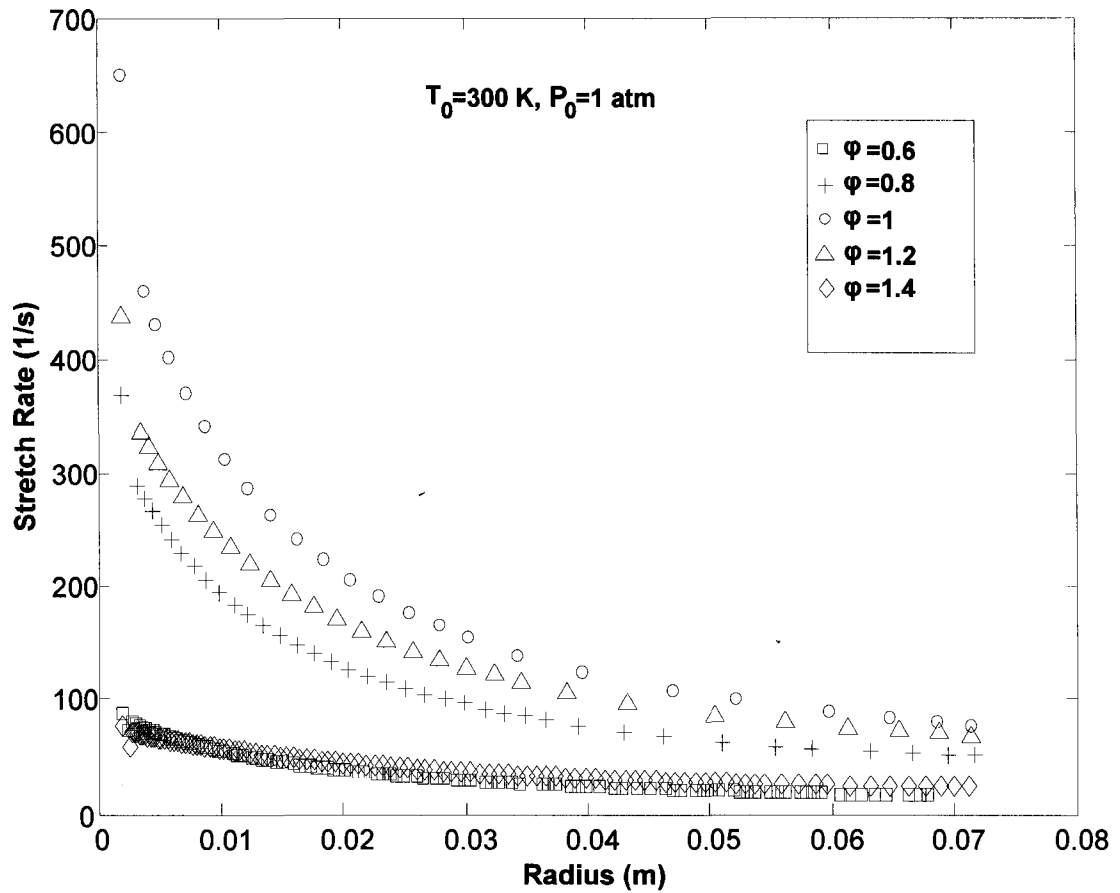


Figure 5.32: Normalized flame speed versus flame radius for different methane-air mixtures at $T_0=300$ K, $P_0=1$ atm



**Figure 5.33: Stretch rate for different methane-air mixtures
at $T_0=300 \text{ K}, P_0=1 \text{ atm}$**

In Figure 5.34 the effects of stretch on flame speed is shown for the lean, stoichiometric and rich mixtures. As the stretch is predominant at the initial flame growth stage, there is a significant difference between the stretched and unstretched speed. However, the stretched and unstretched curves of each mixture merge asymptotically indicating progressively reduced stretch effect as the flame grows.

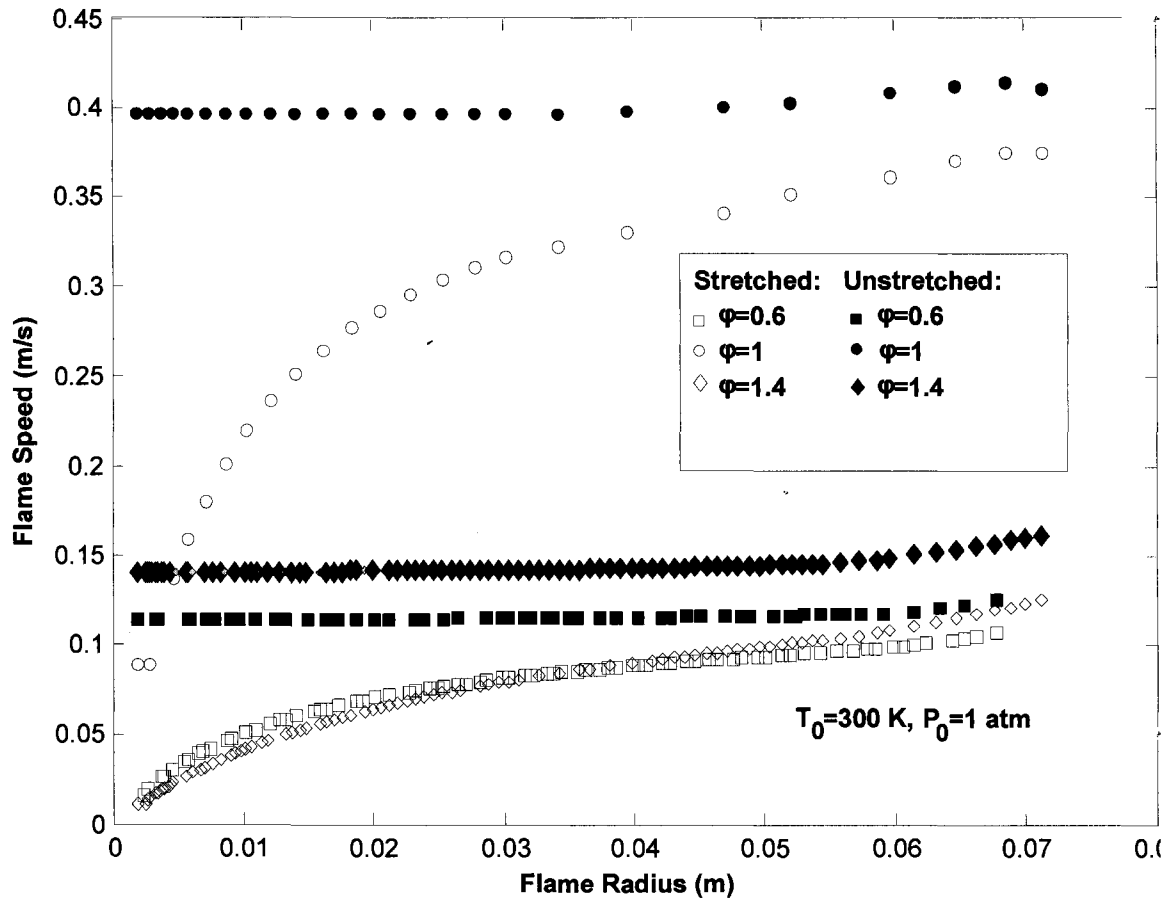


Figure 5.34: Effect of stretch on flame speed for different mixture stoichiometries at $T_0=300\text{ K}, P_0=1\text{ atm}$

To better illustrate the influence of stretch on flame speed, the plot of normalized flame speed versus stretch rate is shown in Figure 5.35. Flame sensitivity to stretch is increased as we move from the stoichiometric mixture toward the lean or rich side. It is an important issue especially in practical cases. Similar to the freely propagating case, though stretch rate lowers as the flame grows, however, the slope of the plots of the confined cases are not fixed due to temperature and pressure changes during the flame propagation.

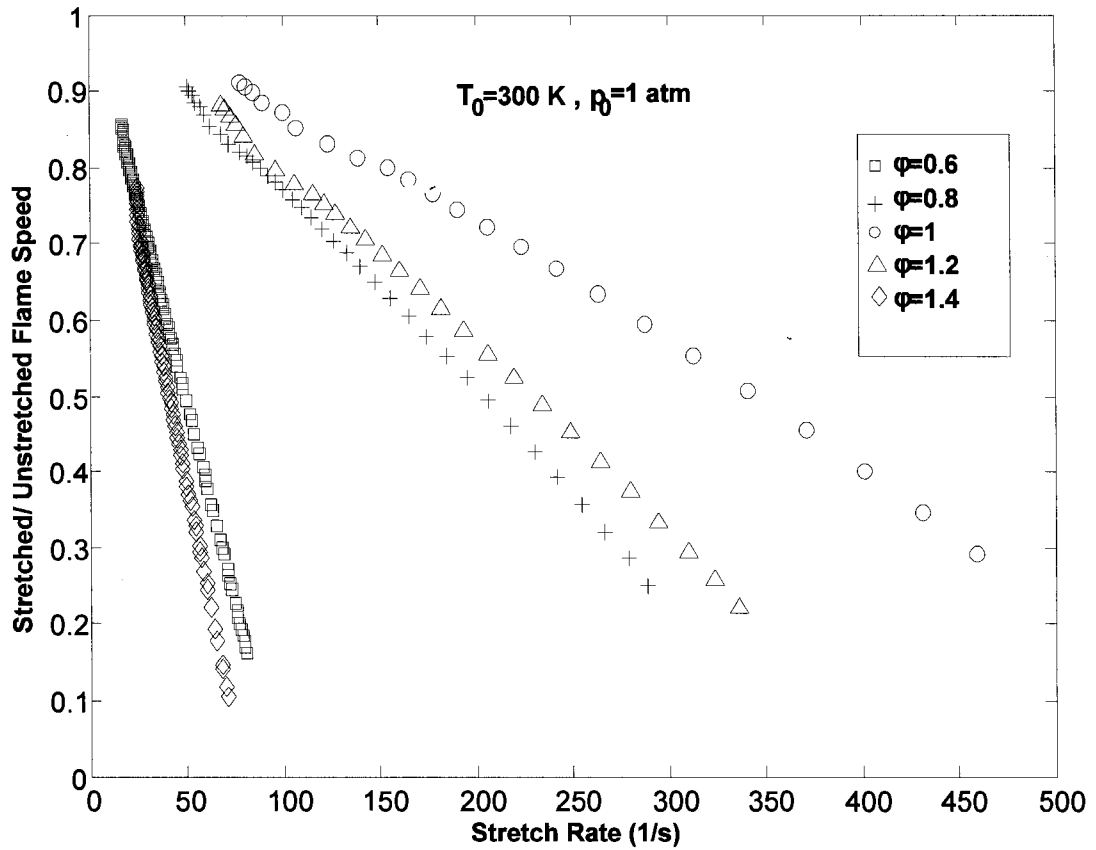


Figure 5.35: Stretched/Unstretched flame speed versus stretch rate for different mixture stoichiometries at $T_0=300 \text{ K}$, $P_0=1 \text{ atm}$

Flame propagation inside the chamber is plotted in Figure 5.36 for different methane-air mixtures. As expected, the fastest propagation rate is for the stoichiometric mixture where the flame radius increases rapidly after ignition. The slope decreases moving away toward the lean or rich mixtures, lowest being for the leanest mixture ($\phi=0.6$).

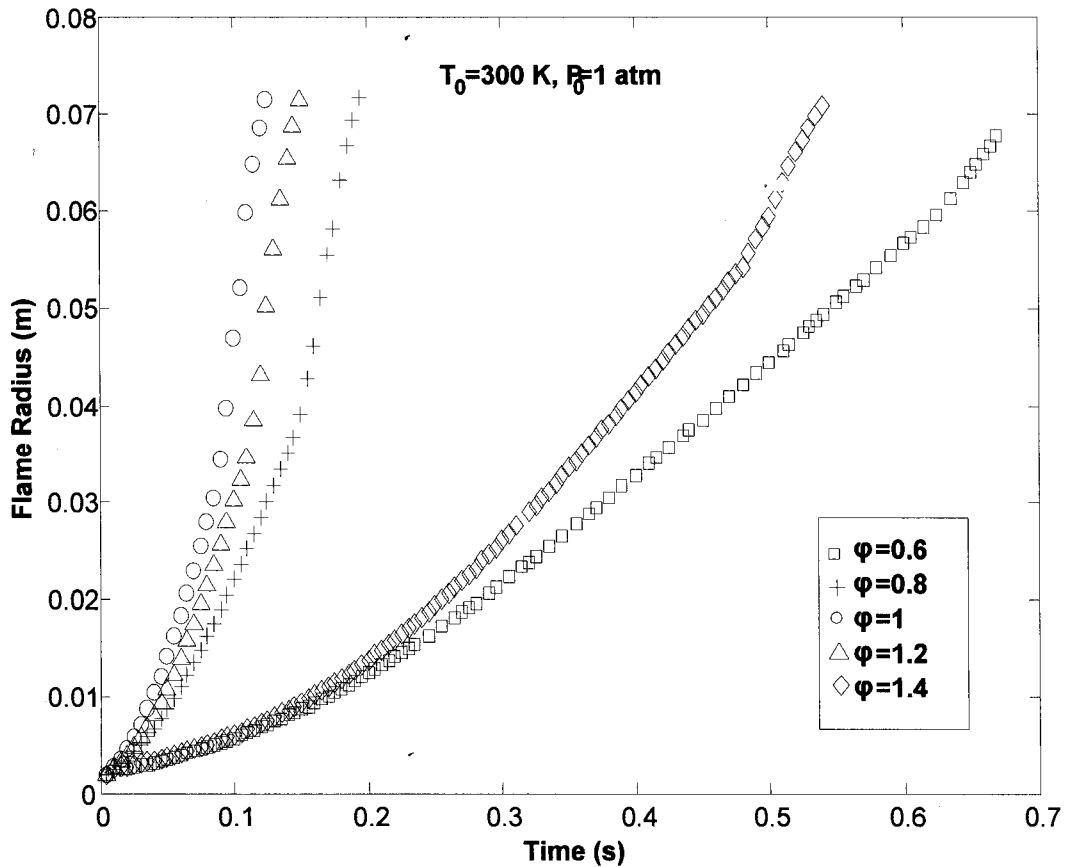


Figure 5.36: Flame radius versus time for different mixture stoichiometries at $T_0=300 \text{ K}, P_0=1 \text{ atm}$

It is worth mentioning that the input time step is an important parameter in our calculations. The domain should be divided into enough number of elements to be able to predict the flame behavior accurately. For all the results presented in this thesis, a time step of 0.005 second is chosen. It is found that a time step of 0.005 is adequate for all the cases considered in this thesis. The sensitivity of the model to the time step is shown in Figure 5.37 by investigating the effect of time step changes on flame radius for the stoichiometric mixture. Reducing the time step from 0.005 second to 0.0005 second does not affect the calculated flame growth. On the other hand, decreasing the time step to 0.05 second leads to incorrect results as the required accuracy is not met.

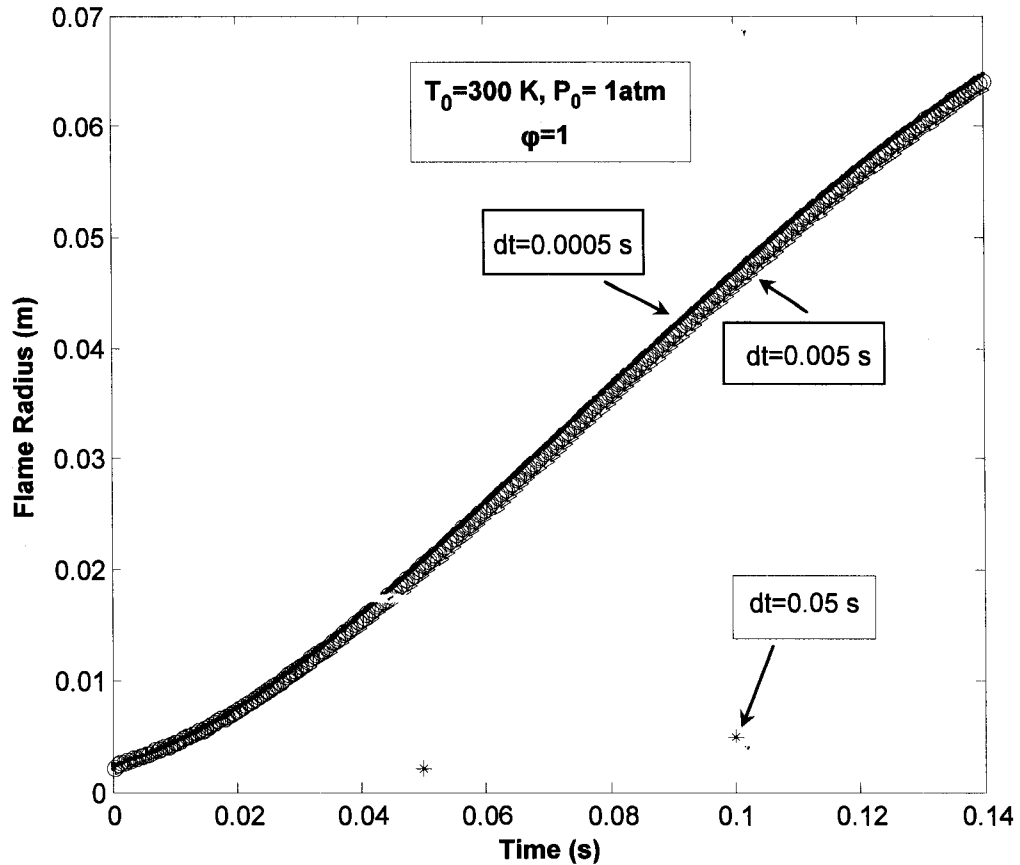


Figure 5.37: Effect of time step changes on the simulation results of flame propagation inside the chamber at $T_0=300$ K, $P_0=1$ atm

5.3. Comparison of the Simulation Results with the Experiment

In this section some of the simulation results are compared with the experiment. The experiment was performed by Ting at the University of Alberta [1995]. The combustion chamber used was a 125mm cubical chamber with an equivalent cell radius of 76.6 mm. The spark gap was 5mm located at the centre of the chamber. Simulations are conducted to provide, among other parameters, unburned gas temperature and chamber pressure as functions of relative flame radius. These results are comparable with the semi-empirical unburned gas temperature and measured chamber pressure obtained by Ting [1995] as shown in Figures 5.38 and 5.39.

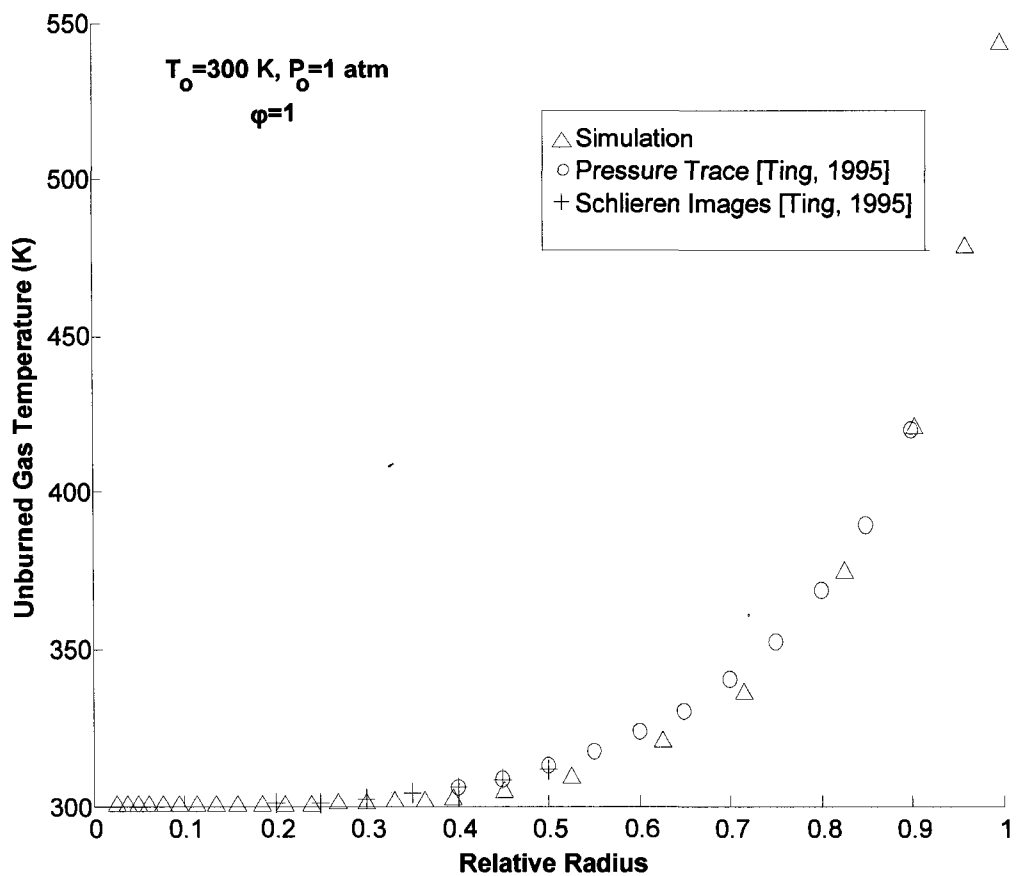


Figure 5.38: Comparison of temperature profile inside the chamber with experiment for the stoichiometric mixture

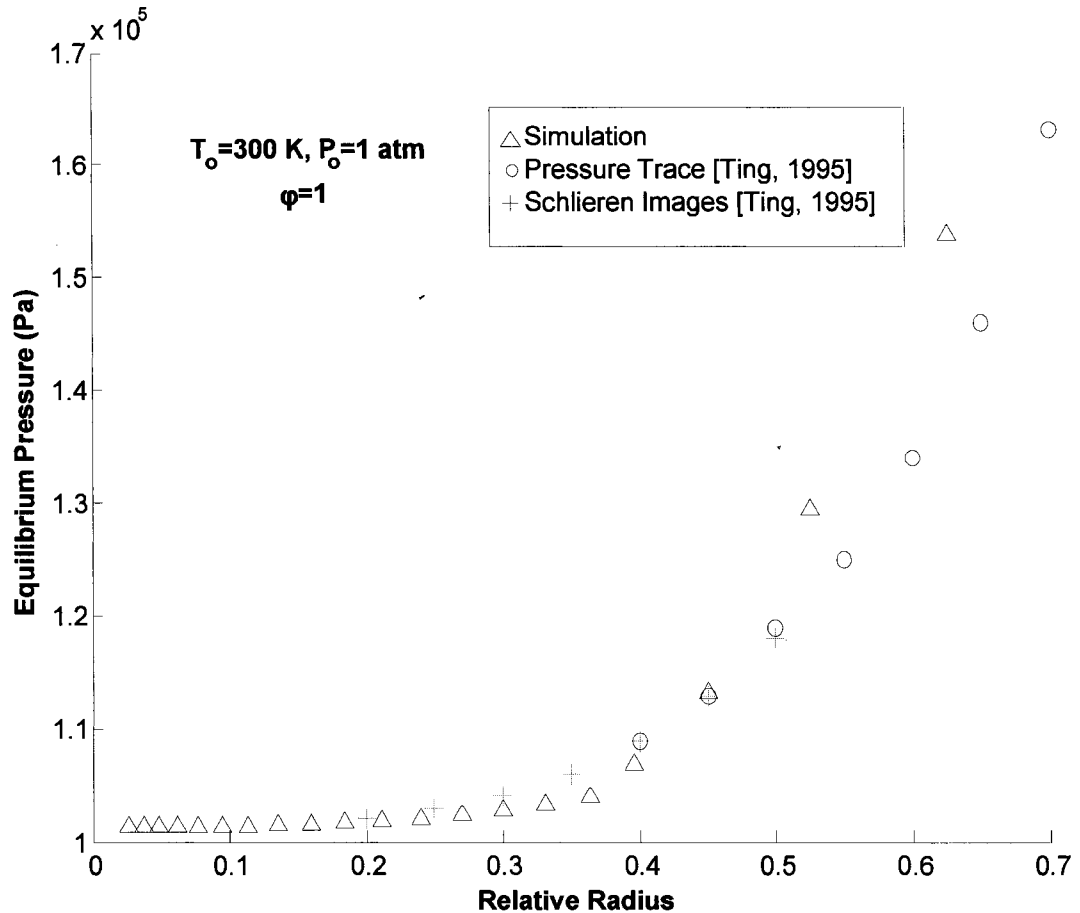


Figure 5.39: Comparison of the pressure profile inside the chamber with experiment for the stoichiometric mixture

Figure 5.40 shows the comparison of the experimental and numerical results of the stretched flame speed. There are some sources of uncertainty in the experimental results such as heat losses especially when some part of the flame touches the walls, the uncertainty in the equipments and the measurements and genuine fluctuations of pressure and temperature inside the chamber. Due to relatively large noise to signal ratio in the early pressure trace (when the pressure rise is very small), the laminar flame speed results fluctuate significantly. As the flame grows, this ratio becomes progressively smaller [Ting, 1995].

Note that the experimental spark kernel was about 5 mm (gap of spark electrode) in radius and the time step between two consequent schlieren images was 0.0005 second. No experimental flame speed could be deduced below a relative flame radius of

approximately 0.2. In other words, engine spark plugs produce a spark kernel which is typically larger than relative flame radius of 0.05 according to Figure 5.40. Therefore, the very slow combustion which takes place as portrayed by the simulated stretched flame speed for relative flame radius of less than 0.05 does not exist in practice. The results further suggest the advantage of using a more powerful spark plug for generating a larger spark kernel, enhancing burning and reducing cycle to cycle variation in spark ignition engine.

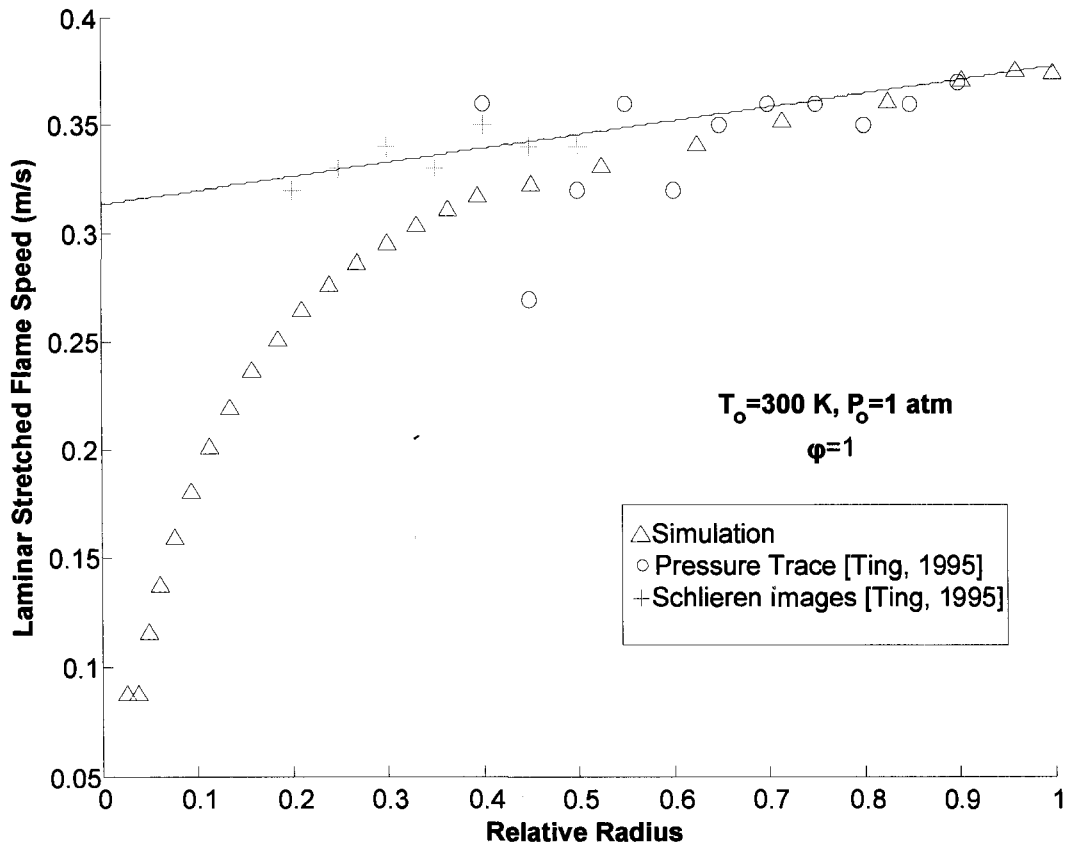


Figure 5.40: Comparison of stretched flame speed inside the chamber with experiment for the stoichiometric mixture

CHAPTER 6

CONCLUSIONS AND RECOMMENDATIONS

This chapter draws all major conclusions on stretched, premixed, adiabatic, laminar, spherical methane-air flame propagating either freely or confined in a chamber. In addition some recommendations are suggested for possible future work.

6.1. Conclusions

It has been shown in this study that a freely expanding flame ball may be modeled via the stretched flame approach. It is found that stretch always decreases the flame speed of a methane-air flame from its unstretched value. In other words, the Markstein length and/or number are always positive over the range of conditions considered. The reduction in flame speed is largest when the flame is small, that is, right after ignition. Increase in temperature tends to diminish the stretch effect. Changes in pressure from 1 to 3 atm did not result in noticeable alteration in stretch sensitivity, though the underlying unstretched laminar flame speed is slightly reduced. The stoichiometric mixture is least sensitive to stretch and the stretch effect is enhanced moving away toward the lean or rich flammability limit. This is very important in engine performance because stretch sensitive mixture can lead to increased cycle to cycle variations and misfire.

It is also noted that the effective Lewis number is rather sensitive to temperature change and hence, unity Lewis number assumption is not viable for accurate stretched flame modeling. Lewis number which is a key parameter in calculating Markstein number is taken as the weighted average of excess and deficient reactants.

In the confined case, the highest equilibrium temperature and pressure at each flame size corresponds to near stoichiometric mixture and decreases as we move away from the stoichiometric condition. Initial mixture temperature has more influence on the flame speed than the pressure. Increasing initial unburned mixture temperature from 300 K to 500 K results in a flame speed of three times faster while decreasing the pressure from 3 atm to 1 atm leads to a maximum of 1.8 times increase in flame speed. The effect of

stretch on flame propagation is very important at initial flame growth stage and is lessened as the flame grows large. For the same mixture stoichiometry, increasing the initial temperature leads to stretch rate increment up to two times. This effect shows the significant effect of temperature changes on flame growth.

Another interesting result is that there is not a significant difference in the laminar flame speed of freely propagating and stretched confined flames. Maybe one reason is due to the effect of confinement in increasing the temperature inside the chamber which enhances the flame speed. However, there is much difference between the stretched and unstretched flame speed in the confined chamber especially at the initial flame propagation stage. For a specific initial condition the stoichiometric mixture has the largest flame speed among all mixture compositions studied under the same initial condition.

6.2. Recommendations

This study has been carried out for limited ranges of pressure and temperature. The simulation can be extended to elevated pressures to better represent the engine environment. A detailed sensitivity analysis can be performed to evaluate the effect of changes in key parameters on flame propagation; recall that there are still significant discrepancies in the open literature concerning unstretched flame speed, flame thickness, Markstein length and Markstein number. Considering heat losses during the flame growth can lead to more accurate results. This laminar flame model can be further extended to a turbulent flame model using the laminar flamelet concept. In this turbulent case, the flame front is considered as composed of elements of laminar stretched flamelets, each of which is similar to a segment of the laminar flame modeled in this thesis.

REFERENCES

K. T. Aung, L. K. Tseng, M. A. Ismail, and G. M. Feath, "Response to comment by S. C. Taylor and D. B. Smith on laminar burning velocities and Markstein numbers of hydrocarbon/air flames", *Combustion and Flame* 102:526-530, 1995.

J. K. Bechtold and M. Matalon, "The dependence of Markstein length on stoichiometry", *Combustion and Flame* 127: 1906-1913, 2001.

G. L. Borman and K. W. Ragland, *Combustion Engineering*, McGraw-Hill Inc., New York, USA, 1998.

D. Bradley, P. H. Gaskell and X. J. Gu, "Burning velocities, Markstein lengths and flame quenching for spherical methane-air flames: A computational study", *Combustion and Flame* 104: 176-198, 1996.

D. Bradley and C. M. Harper, "The development of instabilities in laminar explosion flames", *Combustion and Flame* 99: 562-572, 1994.

CHEMKIN Collection, User manual, Reaction Design, USA, 1998.

P. Clavin, "Dynamic behavior of premixed flame fronts in laminar and turbulent flow", *Progress in Energy and Combustion Science* 11: 1-59, 1985.

P. Clavin and F. A. Williams, "Effects of molecular diffusion and of thermal expansion on the structure and dynamics of premixed flames in turbulent flows of large scale and low intensity", *Journal of Fluid Mechanics* 116: 251-282, 1982.

S. G. Davis, J. Quinard and G. Searby, "Determination of Markstein numbers in counterflow premixed flames", *Combustion and Flame* 130: 112-122, 2002.

A. De, D. S-K. Ting, M. D. Checkel, "The effects of temperature and pressure on stretched, freely propagating, premixed, laminar methane-air flame", *SAE Paper* 2006-01-0494, 2006.

B. Deshaies and P. Cambray, "The velocity of a premixed flame as a function of the flame stretch: An experimental study", *Combustion and Flame* 92: 361-375, 1990.

D. R. Dowdy, D. B. Smith, S. C. Taylor and A. Williams, "The use of expanding spherical flames to determine burning velocities and stretch effects in hydrogen/air mixtures", *Twenty-Third Symposium (International) on Combustion, The combustion Institute* 23: 325-332, 1991.

B. Emami, R. Liu, D. S-K Ting, M. D. Checkel, "A numerical study on the burning velocity of a spherical, premixed methane-air flame", *SAE Paper* 2005-01-1124, 2005.

M. L. Frankel and G. Sivashinsky, "On effects due to thermal expansion and Lewis number in spherical flame propagation", *Combustion Science and Technology* 31: 131-138, 1983.

M. L. Frankel, P. Gordon, G. I. Sivashinsky, "A stretch-temperature model for flame-flow interaction", *Physics Letters A* 361: 356–359, 2007.

R. M. Fristrom and A. A. Westerberg, *Flame Structure*, McGraw-Hill Inc., New York, USA, 1965.

J. Gatowski, J. B. Heywood and C. Deleplace, "Flames photographs in a spark ignition engines", *Combustion and Flame* 56: 71-81, 1984.

J. Gottgens, F. Mauss and N. Peters, "Analytic approximations of burning velocities and flame thickness of lean hydrogen, methane, ethylene, ethane, acetylene, and propane flames", *The Twenty Fourth International Symposium on Combustion*, The Combustion Institute, 129-135, 1992.

X. J. Gu, M.Z. Haq, M. Lawes and R. Woolley, "Laminar flame speed and Markstein lengths of methane-air mixtures", *Combustion and Flame* 121:41-58, 2000.

J. B. Heywood, *Internal Combustion Engine Fundamental*, McGraw-Hill Inc., New York, USA, 1988.

B. Karlovitz, D. W. Denniston, D. H. Knapschaefer and F. E. Wells, "Studies on turbulent flames", Fourth International Symposium on Combustion, The Combustion Institute, 613-620, 1953.

R. J. Kee, F. M. Rupley, J. A. Miller, M. E. Coltrin, J. F. Grcar, E. Meeks, H. K. Moffat, A. E. Lutz, G. Dixon-Lewis, M. D. Smooke, J. Warnatz, G. H. Evans, R. S. Larson, R. E. Mitchell, L. R. Petzold, W. C. Reynolds, M. Caracotsios, W. E. Stewart, P. Glarborg, CHEMKIN Collection, Release 4.1, Reaction Design, Inc., San Diego, CA, USA, 2006.

K. K. Kuo, Principles of Combustion, John Wiley and Sons Inc., New Jersey, USA, 2005.

S. Kwon, L. K. Tseng and G.M. Feath, "Laminar burning velocities and transition to unstable flames in H₂/ O₂/ N₂ and C₃H₈/ O₂/ N₂ mixtures", Combustion and Flame 90: 230-246, 1992.

C. K. Law, "Dynamics of stretched flames", Twenty-Second Symposium (International) on Combustion, The Combustion Institute, Pittsburgh, PA., 1381-1402, 1989.

S. Y. Liao, D. M. Jiang and Q. Cheng, "Determination of laminar burning velocities for natural gas", Fuel 83: 1247-1250, 2004.

A. Lipatnikov, "Some issues of using Markstein number for modeling premixed turbulent combustion", *Combustion Science and Technology* 119: 131-154, 1996.

M. Matalon and B. J. Matkowsky, "Flames as gas dynamic discontinuities" *Journal of Fluid Mechanics* 124: 239-259, 1982.

G. H. Markstein, *Non-Steady Flame Propagation*, Pergamon Press, Oxford, 1964.

M. Metghalchi and J. C. Keck, "Burning velocities of mixtures of air with methanol, isooctane and indolene at high pressures and temperatures," *Combustion and Flame* 48: 191-210, 1982.

A. F. Mills, *Heat and Mass Transfer*, CRC Press, Irwin, USA, 1995.

U. C. Muller, M. Bollig and N. Peters, "Approximations for burning velocities and Markstein numbers for lean hydrocarbon and methanol flames", *Combustion and Flame* 108: 349-356, 1997.

G. Rozenchan, D.L. Zhu, C. K. Law and S. D. Tse, "Outward propagation, burning velocity, and chemical effects of methane flames up to 60 atm", *Proceedings of the Combustion Institute* 29: 1461-1469, 2002.

G. Searby and J. Quinard, "Direct and indirect measurements of Markstein numbers of premixed flames", *Combustion and Flame* 82: 298-311, 1990.

Y. Shoshin and J. Jarosinski, "Stretch rates and local burning velocities measured along limit methane-air flame propagating upward in half-opened tube", 21st ICDERS July 23-27, Poitiers, France, 2007

G. P. Smith, D. M. Golden, M. Frenklach, N. W. Moriarty, B. Eiteneer, M. Goldenberg, C. T. Bowman, R.A. R. K. Hanson, S. Song, W. C. Gardiner, V. V. Lissianski and Z. Qin, GRI Mech 3.0, http://www.me.berkeley.edu/gri_mech/, 2004.

R. A. Strehlow and L. D. Savage, "The concept of flame stretch (Non strictly one dimensional premixed flame propagation modes)", *Combustion and Flame* 31: 209-211, 1978.

C. J. Sun, C. J. Sung, J. He and C. K. Law, "Dynamics of weakly stretched flames: quantitative description and extraction of global flame parameters", *Combustion and Flame* 118:108-128, 1999.

S. C. Taylor, "Burning velocity and the influence of flame stretch", Ph.D. dissertation, University of Leeds, Department of Fuel and Energy, Leeds, 1991.

D. S-K. Ting, "Modeling turbulent flame growth in a cubical chamber", PhD Thesis, Department of Mechanical Engineering, University Of Alberta, 1995.

L. K., Tseng, L. A. Ismail and G. M. Feath, "Laminar burning velocities and Markstein numbers of hydrocarbon/air flames", *Combustion and Flame* 95: 410-426, 1993.

S.R. Turns, *An Introduction to Combustion - Concepts and Application*, McGraw-Hill series in mechanical engineering, US, 1996.

C.N. Vagelopoulos, F.N. Egolfopoulos, "Direct experimental determination of laminar flame speeds", *Twenty-Seventh Symposiums (International) on Combustion*, 513, 1998.

A. van Maaren, D. S. Thung and L. P. H. De Goey, "Measurement of flame temperature and adiabatic burning velocity of methane/air mixtures", *Combustion Science and Technology* 96: 327-344, 1994.

Appendix A: Stretched Freely Propagating Flame Calculations

This appendix details the stretched freely propagating flame calculations. The program is in MATLAB format. The whole program calculates the stretched flame speed, stretch rate and flame growth of a laminar premixed methane-air flame based on user specified mixture stoichiometry, spark kernel size and initial pressure and temperature. Flame starts to burn from the specified spark kernel and the stretched flame speed and the corresponding stretch rate is calculated.

```

% This program is used to find the stretched flame speed of the freely
% propagating flame
% mixture stoichiometry, initial pressure, initial temperature, pressure
% exponent, temperature exponent, time step and spark kernel size.

T=input('T=');P=input('P=');fi=input('i=');Rspark=input('Rspark=')
%;Vtot=input('Vtot=') %;

%Required information for each mixture condition are imported from excel
%files.

%Data for fi=0.6, T=300-500 K, P=1-3 atm
Load('fi6T300P1','Sl_inf','Tb','sigma','LeD','LeE','alpha');
Load('fi6T300P2','Sl_inf','Tb','sigma','LeD','LeE','alpha');
Load('fi6T300P3','Sl_inf','Tb','sigma','LeD','LeE','alpha');

Load('fi6T400P1','Sl_inf','Tb','sigma','LeD','LeE','alpha');
Load('fi6T400P2','Sl_inf','Tb','sigma','LeD','LeE','alpha');
Load('fi6T400P3','Sl_inf','Tb','sigma','LeD','LeE','alpha');

Load('fi6T500P1','Sl_inf','Tb','sigma','LeD','LeE','alpha');
Load('fi6T500P2','Sl_inf','Tb','sigma','LeD','LeE','alpha');
Load('fi6T500P3','Sl_inf','Tb','sigma','LeD','LeE','alpha');
%*****

%Data for fi=0.8, T=300-500 K, P=1-3 atm
Load('fi8T300P1','Sl_inf','Tb','sigma','LeD','LeE','alpha');
Load('fi8T300P2','Sl_inf','Tb','sigma','LeD','LeE','alpha');
Load('fi8T300P3','Sl_inf','Tb','sigma','LeD','LeE','alpha');

Load('fi8T400P1','Sl_inf','Tb','sigma','LeD','LeE','alpha');
Load('fi8T400P2','Sl_inf','Tb','sigma','LeD','LeE','alpha');
Load('fi8T400P3','Sl_inf','Tb','sigma','LeD','LeE','alpha');

Load('fi8T500P1','Sl_inf','Tb','sigma','LeD','LeE','alpha');
Load('fi8T500P2','Sl_inf','Tb','sigma','LeD','LeE','alpha');
Load('fi8T500P3','Sl_inf','Tb','sigma','LeD','LeE','alpha');
%*****

%Data for fi=1, T=300-500 K, P=1-3 atm
Load('fi1T300P1','Sl_inf','Tb','sigma','LeD','LeE','alpha');
Load('fi1T300P2','Sl_inf','Tb','sigma','LeD','LeE','alpha');
Load('fi1T300P3','Sl_inf','Tb','sigma','LeD','LeE','alpha');

Load('fi1T400P1','Sl_inf','Tb','sigma','LeD','LeE','alpha');
Load('fi1T400P2','Sl_inf','Tb','sigma','LeD','LeE','alpha');

```



```

Load('fi1T400P3','Sl_inf','Tb','sigma','LeD','LeE','alpha');

Load('fi1T500P1','Sl_inf','Tb','sigma','LeD','LeE','alpha');
Load('fi1T500P2','Sl_inf','Tb','sigma','LeD','LeE','alpha');
Load('fi1T500P3','Sl_inf','Tb','sigma','LeD','LeE','alpha');
%*****

%Data for fi=1.2, T=300-500 K, P=1-3 atm
Load('fi12T300P1','Sl_inf','Tb','sigma','LeD','LeE','alpha');
Load('fi12T300P2','Sl_inf','Tb','sigma','LeD','LeE','alpha');
Load('fi12T300P3','Sl_inf','Tb','sigma','LeD','LeE','alpha');

Load('fi12T400P1','Sl_inf','Tb','sigma','LeD','LeE','alpha');
Load('fi12T400P2','Sl_inf','Tb','sigma','LeD','LeE','alpha');
Load('fi12T400P3','Sl_inf','Tb','sigma','LeD','LeE','alpha');

Load('fi12T500P1','Sl_inf','Tb','sigma','LeD','LeE','alpha');
Load('fi12T500P2','Sl_inf','Tb','sigma','LeD','LeE','alpha');
Load('fi12T500P3','Sl_inf','Tb','sigma','LeD','LeE','alpha');
%*****

%Data for fi=1.4, T=300-500 K, P=1-3 atm
Load('fi14T300P1','Sl_inf','Tb','sigma','LeD','LeE','alpha');
Load('fi14T300P2','Sl_inf','Tb','sigma','LeD','LeE','alpha');
Load('fi14T300P3','Sl_inf','Tb','sigma','LeD','LeE','alpha');

Load('fi14T400P1','Sl_inf','Tb','sigma','LeD','LeE','alpha');
Load('fi14T400P2','Sl_inf','Tb','sigma','LeD','LeE','alpha');
Load('fi14T400P3','Sl_inf','Tb','sigma','LeD','LeE','alpha');

Load('fi14T500P1','Sl_inf','Tb','sigma','LeD','LeE','alpha');
Load('fi14T500P2','Sl_inf','Tb','sigma','LeD','LeE','alpha');
Load('fi14T500P3','Sl_inf','Tb','sigma','LeD','LeE','alpha');
%*****

beta=198468*(Tb-300)/(8.314*(Tb^2)) %Zeldovich number
gama1=2*sigma/(sqrt(sigma)+1) % A Costant
gama2=(4/(sigma-1))*(sqrt(sigma)-1-log(0.5*(sqrt(sigma)+1))) %A Constant
C=1+beta*(ffi-1) %A Constant
Le_eff=1+(((LeE-1)+(LeD-1)*C)/(1+C)) %Effective Lewis number
alfap=gama1+0.5*beta*(Le_eff-1)*gama2; %A Constant
delta=alfap/Sl_inf; % Flame thickness
L=delta*(alfap-(sigma-1)*(gama1/sigma)) % Markstein length
Ma=L/delta % Markstein number

```

```
%#####  
####
```

```
gama1=2*sigma/(sqrt(sigma)+1)  
gama2=(4/(sigma-1))*(sqrt(sigma)-1-log(0.5*(sqrt(sigma)+1)))  
beta=198468*(Tb-300)/(8.314*(Tb^2)) %Zeldovich number  
C=1+beta*(ffi-1)  
Le_eff=1+(((LeE-1)+(LeD-1)*C)/(1+C))  
alfa=gama1+0.5*beta*(Le_eff-1)*gama2;  
delta=alfap/Sl8;  
L=delta*(alfa-(sigma-1)*(gama1/sigma)) % Ma length  
Ma=L/delta
```

```
%#####  
####
```

```
r(1)=Rspark;  
dr=0.0001;  
t(1)=0;  
a=2*L*sigma;
```

```
for i=1:1000
```

```
    r(i+1)=r(i)+dr; %New Radius
```

```
    Sl_s(i)=Sl_inf./(1+a./r(ii)); %Stretched flame speed
```

```
    t(i+1)=(1/sigma)*(r(i+1)-r(i))*(1/Slun(i))+t(i); %Corresponding Time
```

```
    k(i)=(2/r(i))*(dr/(t(i+1)-t(i))); %Stratch rate
```

```
end
```

Appendix B: Thermodynamic Equilibrium Flame Growth Model in Confinement

This appendix details the thermodynamic equilibrium flame growth model. The program is in MATLAB format. The whole program simulates a pressure trace of a laminar methane-air flame based on user specified mixture stoichiometry, spark kernel size, initial pressure and temperature, pressure and temperature effects in terms of pressure and temperature exponents.

Flame starts to burn from the specified spark kernel accounting effects of pressure and temperature changes during the flame growth. Unstretched flame data are gotten from CHEMKN.

```

% This program simulates a pressure trace of a laminar premixed flame
% propagation in confinement from known
% mixture stoichiometry, initial pressure, initial temperature,
% pressure exponent, temperature exponent, time step and spark kernel %size.

T=input('T=');P=input('P=');fi=input('i=');dt=input('dt=');Rspark=input('Rspark=')

% Required information for each mixture condition are imported from %excel files.

% Data for fi=0.6, T=300-500 K, P=1-3 atm
Load('fi6T300P1','Sl_inf','Tb','sigma','LeD','LeE','alpha');
Load('fi6T300P2','Sl_inf','Tb','sigma','LeD','LeE','alpha');
Load('fi6T300P3','Sl_inf','Tb','sigma','LeD','LeE','alpha');

Load('fi6T400P1','Sl_inf','Tb','sigma','LeD','LeE','alpha');
Load('fi6T400P2','Sl_inf','Tb','sigma','LeD','LeE','alpha');
Load('fi6T400P3','Sl_inf','Tb','sigma','LeD','LeE','alpha');

Load('fi6T500P1','Sl_inf','Tb','sigma','LeD','LeE','alpha');
Load('fi6T500P2','Sl_inf','Tb','sigma','LeD','LeE','alpha');
Load('fi6T500P3','Sl_inf','Tb','sigma','LeD','LeE','alpha');
%*****

% Data for fi=0.8, T=300-500 K, P=1-3 atm
Load('fi8T300P1','Sl_inf','Tb','sigma','LeD','LeE','alpha');
Load('fi8T300P2','Sl_inf','Tb','sigma','LeD','LeE','alpha');
Load('fi8T300P3','Sl_inf','Tb','sigma','LeD','LeE','alpha');

Load('fi8T400P1','Sl_inf','Tb','sigma','LeD','LeE','alpha');
Load('fi8T400P2','Sl_inf','Tb','sigma','LeD','LeE','alpha');
Load('fi8T400P3','Sl_inf','Tb','sigma','LeD','LeE','alpha');

Load('fi8T500P1','Sl_inf','Tb','sigma','LeD','LeE','alpha');
Load('fi8T500P2','Sl_inf','Tb','sigma','LeD','LeE','alpha');
Load('fi8T500P3','Sl_inf','Tb','sigma','LeD','LeE','alpha');
%*****

% Data for fi=1, T=300-500 K, P=1-3 atm
Load('fi1T300P1','Sl_inf','Tb','sigma','LeD','LeE','alpha');
Load('fi1T300P2','Sl_inf','Tb','sigma','LeD','LeE','alpha');
Load('fi1T300P3','Sl_inf','Tb','sigma','LeD','LeE','alpha');

Load('fi1T400P1','Sl_inf','Tb','sigma','LeD','LeE','alpha');
Load('fi1T400P2','Sl_inf','Tb','sigma','LeD','LeE','alpha');
Load('fi1T400P3','Sl_inf','Tb','sigma','LeD','LeE','alpha');

```

```

Load('fi1T500P1','Sl_inf','Tb','sigma','LeD','LeE','alpha');
Load('fi1T500P2','Sl_inf','Tb','sigma','LeD','LeE','alpha');
Load('fi1T500P3','Sl_inf','Tb','sigma','LeD','LeE','alpha');
%*****

```

```

% Data for fi=1.2, T=300-500 K, P=1-3 atm
Load('fi12T300P1','Sl_inf','Tb','sigma','LeD','LeE','alpha');
Load('fi12T300P2','Sl_inf','Tb','sigma','LeD','LeE','alpha');
Load('fi12T300P3','Sl_inf','Tb','sigma','LeD','LeE','alpha');

```

```

Load('fi12T400P1','Sl_inf','Tb','sigma','LeD','LeE','alpha');
Load('fi12T400P2','Sl_inf','Tb','sigma','LeD','LeE','alpha');
Load('fi12T400P3','Sl_inf','Tb','sigma','LeD','LeE','alpha');

```

```

Load('fi12T500P1','Sl_inf','Tb','sigma','LeD','LeE','alpha');
Load('fi12T500P2','Sl_inf','Tb','sigma','LeD','LeE','alpha');
Load('fi12T500P3','Sl_inf','Tb','sigma','LeD','LeE','alpha');
%*****

```

```

% Data for fi=1.4, T=300-500 K, P=1-3 atm
Load('fi14T300P1','Sl_inf','Tb','sigma','LeD','LeE','alpha');
Load('fi14T300P2','Sl_inf','Tb','sigma','LeD','LeE','alpha');
Load('fi14T300P3','Sl_inf','Tb','sigma','LeD','LeE','alpha');

```

```

Load('fi14T400P1','Sl_inf','Tb','sigma','LeD','LeE','alpha');
Load('fi14T400P2','Sl_inf','Tb','sigma','LeD','LeE','alpha');
Load('fi14T400P3','Sl_inf','Tb','sigma','LeD','LeE','alpha');

```

```

Load('fi14T500P1','Sl_inf','Tb','sigma','LeD','LeE','alpha');
Load('fi14T500P2','Sl_inf','Tb','sigma','LeD','LeE','alpha');
Load('fi14T500P3','Sl_inf','Tb','sigma','LeD','LeE','alpha');
%*****

```

```

beta=198468*(Tb-300)/(8.314*(Tb^2)) %Zeldovich number
gama1=2*sigma/(sqrt(sigma)+1) % A Costant
gama2=(4/(sigma-1))*(sqrt(sigma)-1-log(0.5*(sqrt(sigma)+1))) %A Constant
C=1+beta*(ffi-1) %A Constant
Le_eff=1+(((LeE-1)+(LeD-1)*C)/(1+C)) %Effective Lewis number
alfap=gama1+0.5*beta*(Le_eff-1)*gama2; %A Constant
delta=alfa/Sl_inf; % Flame thickness
L=delta*(alfap-(sigma-1)*(gama1/sigma)) % Markstein length
Ma=L/delta % Markstein number

```

```

%*****INITIAL VALUES

```

```

%Initial values are set here:
Rmol= 83143; %Gas universal constant [j/kmol.K]
Vtot=0.001882; %Total volume of the chamber %m3
P0=101325; %Reference Pressure [Pa]
T0=300.15; %Reference Temperature [K]

Texp=5.75*fi^2-12.15*fi+7.98; % Temperature Exponent
Pexp=-0.925*fi^2+2*fi-1.473; % Pressure Exponent
Tinit= 300.15; % Initial Temperature
Pinit= 101325; % Initial Pressure

PE=Pinit; %Initial Set
Tr=Tinit; %Initial Set
Rbomb=(0.75* Vtot/ 3.141592654)^(1/3) % Chamber Radius
Vspark=(4/3)*3.141592654*((Rspark)^3); %Spark Volume

MWR=(1/(1+4.76*(2/fi)))*(16.043+(2/fi)*32+(2/fi)*3.76*28); %Reactant Molecular
Weight
Mass=(MWR*Pinit*Vtot)/(Rmol*Tinit); %Total mass which remains constant
Rbnow=Rspark; %Initial Set
Mb=0; %Burned Mass

t=0;
mm=Rspark;
%#####Volume Correction
%After burning the an specified element the new pressure is guessed and
%corrected based on the equality of the volumes.

while (abs(Mb-Mass)>1e-4) %Procedure is continued until the whole mass burns.

Pi=PE;

%Cp Of each reactant
CP_CH4=(4.184/8.314)*(-0.29149+26.327*(Tr/1000)-
10.61*(Tr/1000)^2+1.5656*(Tr/1000)^3+0.16573*(Tr/1000)^( 2));

CP_O2=0.03212936e2+0.1127486e-2*Tr+0.057561e-5*Tr^2+0.1313877e-8*Tr^3-
0.0876855e-11*Tr^4;

CP_N2=0.03298677e2+0.14082404e-2*Tr-0.0396322e-4*Tr^2+0.056415e-7*Tr^3-
0.0244485e-10*Tr^4;

CP_H2=0.032981e2+0.0824294e-2*Tr-0.08143e-5*Tr^2-0.094754e-
9*Tr^3+0.0413487e-11*Tr^4;

```

```
CP_H2O=0.0338684e2+0.0347498e-1*Tr-0.0635469e-4*Tr^2+0.0696858e-7*Tr^3-
0.02506588e-10*Tr^4;
```

```
CP_CO2=0.022757e2+0.099221e-1*Tr-0.10409e-4*Tr^2+0.0686668e-7*Tr^3-
0.0211728e-10*Tr^4;
```

```
%Cp of reactants mixture
```

```
CP_R=(1/(1+4.76*(2/fi)))*(CP_CH4+(2/fi)*CP_O2+(2/fi)*3.76*CP_N2);
```

```
% Heat specific ratio (Gamma) for the reactants
```

```
GMR=CP_R/(CP_R-1);
```

```
% It is assumed that each element goes through an isentropic process. %Here the
corresponding temperature is calculated. Pi is the pressure %before the element burn.
mass changes is not considered here.
```

```
% Estimate PE, the end pressure after this element burns ( it is just a guess)
```

```
Tr= Tinit*(Pi/Pinit)^((GMR-1)/GMR);
```

```
% Unstretched flame speed according to the new pressure and temperature
```

```
Sl2= Sl8*((Pi/P0)^Pexp)*((Tr/T0)^Texp);
```

```
% New flame thickness
```

```
delta=alfap/Sl2;
```

```
L=delta*(alfa-(sigma-1)*(gama1/sigma));
```

```
a=2*L*sigma;
```

```
Sl=Sl2/(1+(a/Rbnow));
```

```
if Mb==0
```

```
    dVbg=Vspark;
```

```
else
```

```
    dVbg= Sl*dt*4*3.141593*Rbnow^2;    % Volume burnt in the next time step
```

```
end
```

```
dMbg= dVbg*MWR*Pi/(Rmol*Tr); %Burning mass
```

```
molR=dMbg/MWR; %Mole number of the reactants [kmol]
```

```
if fi<1
```

```
    MWP=(1/(1+9.52/fi))*(1*44.01+2*18+(2/fi)*3.76*28+(2/fi-2)*32);
```

```
    CP_P=(1/(1+4.76*(2/fi)))*(CP_CO2+(2/fi-
```

```
2)*CP_O2+(2/fi)*3.76*CP_N2+2*CP_H2O);%Cp of reactant
```

```
    GMP=CP_P/(CP_P-1); %Heat specific ratio of the products
```

```
else
```

```
    MWP=(1/(3+7.52/fi))*(1*44.01+(4/fi-2)*18+(2/fi)*3.76*28+(4-4/fi)*2);
```

```

CP_P=(1/(1+4.76*(2/fi)))*(CP_CO2+(2/fi)*3.76*CP_N2+(4/fi-2)*CP_H2O+(4-
4/fi)*CP_H2);%Cp of reactant
GMP=CP_P/(CP_P-1);
end

```

```

molP=dMbg/MWP; %Mole number of the reactants [kmol]

```

```

Mb=Mb+dMbg; % new value for the burned mass. Burning mass ia added to the burned
mass

```

```

PE=Pi+fi*(dMbg/Mass)*Pinit; % New guess for the equilibrium pressure

```

```

%#####Unburnt Side

```

```

%VUB: Volume of the unburned side before the mass element burns
%VUA: Volume of the unburned side after the mass element burns
%VBB: Volume of the burned side before the mass element burns
%VBA: Volume of the burned side after the mass element burns

```

```

if dVbg==Vspark
VUB=((Mass-Mb)/Mass)*Vtot*(Pinit/Pi)^(1/GMR);
VBB=Vtot-VUB;
VBA=VBB*(Pi/PE)^(1/GMP);
else
VUB=((Mass-Mb-dMbg)/Mass)*Vtot*(Pinit/Pi)^(1/GMR);
end

```

```

VUA=VUB*((Pi/PE)^(1/GMR)); %mass changes is not considered

```

```

%#####Burned Side

```

```

VBB=Vtot-VUB;
VBA=VBB*(Pi/PE)^(1/GMP);
SumV=VBA+VUA; %the volume of all the burned and unburned elements together
Rbnow=((3*VBA)/(4*3.141592654))^(1/3); %New radius based on the new volume

```

```

VE=dVbg*(Pi/PE)*(Tb/Tr)*(molP/molR); % Equilibrium volume for the burning
elemnt

```

```

Rratio=Rbnow/Rbomb; %Relative radius
ERV=VE-(Vtot-SumV); %Error which is related to the guessed pressure

```

```

%If the error is greater than 0.01%, then make a new estimate of pressure
%and go back and recalculate the volume with this new pressure

```

```

while (ERV> 0.0001)
VUB=((Mass-Mb-dMbg)/Mass)*Vtot*(Pinit/Pi)^(1/GMR);

```



```
VUA=VUB*((Pi/PE)^(1/GMR)); %mass changes is not cosidered
VBB=Vtot-VUB;
VBA=VBB*(Pi/PE)^(1/GMP);
```

```
SumV=VBA+VUA;
Rbnow=((3*VBA)/(4*3.141592654))^(1/3);
VE=dVbg*(Pi/PE)*(Tb/Tr)*(molP/molR);
```

```
ERV=VE-(Vtot-SumV); %Error in the volume
```

% New pressure is guessed based on the overestimation or underestimation %of the previous guess

```
if (ERV)>0
    PE=Pi+1.2*(PE-Pi)
else
    PE=PE+(PE-Pi)/1.2;
end
```

```
end
```

```
% Stretch calculation based on the new radius
k=(2/Rbnow)*((Rbnow-mm)/dt); %Stretch rate
mm=Rbnow;
t=t+dt;
```

```
end
```

```
*****
```

Gamma= specific heat ratio, molP= moles of products/ mole of fuel, molR= moles of reactants/ mole of fuel, MWR= molar mass of the reactants, P= pressure, PE= pressure at thermodynamic equilibrium, Pexp= pressure exponent, Texp= temperature exponent, Pi= pressure before the element burns, Tr= corresponding temperature to Pi, Tb= temperature corresponding to PE, P₀= initial pressure before ignition, T₀= initial temperature before ignition, Rspark= spark radius, R_{bnow}= radius of the burning element, Sl_∞ = Sl at 300 K and 1 atm, Sl₀= unstretched laminar burning velocity Sl= stretched laminar burning velocity, dVu=element volume before it burns, SumV= total volume of

all other elements, V_E = volume element at equilibrium, V_{tot} = total cell volume, V_{ua} = volume of the unburned side after the element burns, V_{ub} = volume of the unburned side before the element burns, V_{ba} = volume of the burned side after the element burns, V_{bb} = volume of the burned side before the element burns, dV_{bg} = volume of the burning element, dM_{bg} = mass of the burning element, M_b = Burned mass, $Mass$ = total mass, dt =time step, R = ideal gas constant, $\pi= 3.1416$

VITA AUCTORIS

NAME: Pegah Ghanbari-Bavarsad

PLACE OF BIRTH: Khuzestan- Iran

YEAR OF BIRTH: 1982

EDUCATION: Nikan High School, Khuzestan, Iran
1996-2000

Amir Kabir University of Technology, Tehran, Iran
2000-2004 B.Sc.

Sharif University of Technology, Tehran, Iran
2004-2006 M.Sc.

University of Windsor, Windsor, Ontario
2007-2008 M.Sc